ARGONNE NATIONAL LABORATORY
P. O. Box 299
Lemont, Illinois

SOME PROBLEMS IN HORIZONTAL TWO-PHASE TWO-COMPONENT FLOW

by

Bobbie L. Richardson

A Thesis
Submitted to the Faculty
of
Purdue University
In Partial Fulfillment of the
Requirements for the Degree
of
Doctor of Philosophy

December, 1958

Operated by The University of Chicago
under
Contract W-31-109-eng-38

DISCLAIMER

DISCLAIMER

Portions of this document may be illegible in electronic image products. Images are produced from the best available original document.

ACKNOWLEDGMENT

The author gratefully acknowledges the assistance given to him by his graduate committee and in particular by Professor E. A. Trabant in preparing for and performing this work. He also wishes to express his sincere appreciation to the members of the Heat Engineering Section at Argonne National Laboratory. In particular, he is indebted to Dr. P. A. Lottes for suggesting the problem and consultations, and to P. L. Zaleski, and Wm. Brewer for their help in constructing the equipment, and taking and reducing the data.

To Miss M. Jean Radcliff he extends his thanks for typing his thesis.

To the Graphic Arts Group he is indebted for the photographic work and reproduction of the thesis.

TABLE OF CONTENTS

TABLE OF CONTENTS

TABLE OF CONTENTS

vi

LIST OF TABLES

LIST OF TABLES

LIST OF FIGURES

LIST OF FIGURES

LIST OF FIGURES

LIST OF FIGURES

LIST OF FIGURES

LIST OF FIGURES

LIST OF FIGURES

NOMENCLATURE

Symbol	Quantity	Units
A	Area	ft^2
De	Equivalent diameter	ft
f	Fannings friction factor	
G	Mass flow rate	$lb_{mass}/sec\ in^2$
ΔKE	Change in kinetic energy due to change in flow area	ft liquid
N_{Re}	Reynolds number $\left(\dfrac{G\ De}{\mu}\right)$	
ΔP_{TP}	Two-phase pressure drop	lb_{force}/ft^2
ΔP_ℓ	Pressure drop due to liquid flowing at a rate $(1-x)$ times the total flow rate	lb_{force}/ft^2
ΔP_g	Pressure drop due to gas flowing at a rate x times the total flow rate	lb_{force}/ft^2
R_ℓ	Liquid volume fraction	
S	Slip ratio (V_g/V_ℓ)	
V	Velocity	ft/sec
W	Flow rate	lb_{mass}/sec
x	Quality W_g/W_{total}	
α	Vapor volume fraction	
μ	Viscosity	$lb_{force}\ sec/ft^2$
ρ	Density	lb_{mass}/ft^3
ϕ	$(\Delta P_{TP}/\Delta P_{SP})^{1/2}$	
χ	$(\Delta P_\ell/\Delta P_g)^{1/2}$	

NOMENCLATURE

Subscripts

A, B, C, D	Refer to position along channel
e	Equivalent
g	Gas phase
ℓ	Liquid
m	Mean
s	Static

A number of special terms not included in this list are defined where they are used.

ABSTRACT

An experimental investigation was conducted on the flow of air-water mixtures in a number of horizontal rectangular Lucite test sections, whose aspect ratios varied from two to sixteen. These test sections were assembled in various combinations to permit the study of the effect of a sudden change in flow area on the significant flow parameters.

A technique was developed for measuring the volume fraction of each phase, making use of the difference of the attenuation characteristics of the liquid and the vapor for gamma radiation. This technique was evaluated making use of a number of Lucite mockups with known void distributions.

Information is presented on the factors influencing the volume fractions, flow patterns and slip ratios in the channels studied. The two-phase pressure drop is compared with existing correlations, and a relationship predicting this pressure drop, in terms of the liquid volume fraction, is derived.

The energy losses associated with an abrupt expansion or contraction were studied. A correlation based on the experimental results is presented to permit the prediction of these losses.

SOME PROBLEMS IN HORIZONTAL
TWO-PHASE TWO-COMPONENT FLOW

Chapter I
INTRODUCTION

1. Importance of Two-Phase Flow Studies

It is difficult to over-emphasize the importance of the study of two-phase flow. The simultaneous flow of a liquid and a gas or vapor is a common occurrence in boilers, evaporators, heat exchangers, condensers, and chemical reaction equipment. This type of flow occurs in the chemical process industry, refrigeration, petroleum, and electrical power systems. The recent demands for increased thermal power from smaller volumes, in particular in rockets and nuclear reactors, have led to the utilization of nucleate boiling heat transfer, because of the high heat fluxes which can be obtained. This has also led to an increase in the demand for knowledge of the behavior of liquid-vapor systems under a variety of conditions.

2. Historical

Although the application of knowledge in this area has taken place for a long time, the organized study of the problem has only recently been undertaken. One of the first investigations reported was that of Rateau[1]* on the flow of boiling water through nozzles. Attempts were made to relate the pressure drop for two-phase flow to a friction factor by Benjamin and Miller[2] and by McAdams[3] et al.

Martinelli[4,5,6] and his co-workers at the University of California studied the pressure drop and the volume fraction of each phase present for a number of two-phase, two-component systems. The tests were performed with air as the gas phase and water, oils, kerosene or benzene as the liquid phase.

*Supercripts refer to references in the Bibliography.

The correlations for the pressure drop were based on two postulates:

(a) the static pressure drop for the gaseous phase is equal to that of the liquid phase regardless of the flow pattern present;

(b) the liquid volume plus the vapor volume equals the total volume of the pipe.

Although theoretically these postulates restrict the application of the correlation obtained, it has been extended to those cases where transverse pressure gradients exist and for pulsating flows.

In this work it was found that the data could be correlated in terms of two parameters ϕ and χ, and these were defined by the relationships:

$$\phi_{\ell}^2 = \frac{\Delta P_{TP}}{\Delta P_{\ell}} \tag{1.1}$$

$$\phi_g^2 = \frac{\Delta P_{TP}}{\Delta P_g} \tag{1.2}$$

and

$$\chi^2 = \frac{\Delta P_{\ell}}{\Delta P_g} \tag{1.3}$$

The single phase pressure drops were determined on the basis of each phase flowing alone in the channel at its own weight flow rate. In a later paper Martinelli[7] and Nelson extended this correlation to include the pressure drop due to flow with vaporization, where the steam quality was a linear function of position along the pipe.

A study of the non-isothermal flow was reported by Johnson[8] and Abou-Sabe, and they suggested that the pressure drops depend upon the gas-liquid interfacial conditions.

In a report of an investigation of two-phase flow in a pipe line contactor, Alves[9] states that the Martinelli-Lockhart correlation is

within $\pm$ 40 per cent of the experimental pressure drop values. He indicates that there is a dependence on the type of flow pattern present.

An extensive investigation was conducted by Bergelin[10] and Gazely[11] which concentrated on stratified flows and interfacial shears. A friction factor relationship is presented for the pressure drop in the vapor phase.

An analytical study by Levy[12] has verified the parameters of Lockhart and Martinelli for annular flow. In Levy's analysis, a reduced Navier-Stokes equation for laminar flow, and the seventh-power law for the turbulent flow was assumed to determine the velocity distribution. He also assumed zero velocity of the wall and equal liquid and vapor velocities at the interface.

In a study of evaporation of fluids in pipes, Linning[13] proposed that one of three flow patterns must exist; annular, separated, or frothing. A mathematical model is developed for the first two assuming a uniform velocity for each phase, and taking into account interphase effects and wall effects. Momentum and energy equations are developed for the flow models mentioned.

A modification of the Lockhart-Martinelli parameters is proposed to correlate the behavior of two-phase flow in rough pipes in a report presented by Chisholm[14] and Laird.

A recent study presented by Petrick[15] reports on the effect of changes in flow area on the void fraction in vertical two-phase flow.

This discussion of the background of the study of two-phase flow problems does not include reference to all of the work which has been done in the field. Two recent bibliographies presented by Isbin[16] et al., and by Masnovi[17] may be referred to for a more complete coverage of the work in this area.

4

3. Purpose

The purpose of this investigation was to provide information on the behavior of air-water mixtures in horizontal rectangular channels, and in particular to investigate the effect of a sudden enlargement or contraction in the flow area on the distribution and velocity of each phase, and upon the static pressure in the channel. In line with these objectives, the flow channels were formed of transparent lucite to facilitate the visual and photographic recording of the type of flow pattern present. A gamma-ray attenuation technique was developed and evaluated to measure the phase distribution in the test section, and a system was provided for metering and measuring the flow of each phase and of determining the static pressure in the test section.

Chapter II

EXPERIMENTAL EVALUATION OF GAMMA-RAY
ATTENUATION VOID MEASURING TECHNIQUES

1. Introduction

In the study of two-phase flow phenomena a knowledge of the fraction of each phase present is necessary for the determination of the relative velocity of the individual phases and the average density of the mixture.

Many different techniques have been used to determine the vapor volume fraction, or void fraction experimentally. Griffith,[18] et al., photographed the flow and based void calculations on the number and size of the bubbles photographed. McManus[19] made use of an insulated probe in the channel with a micrometer positioning system which could detect and locate the liquid-vapor interface in annular flow. Johnson and Abou-Sabe[8] used quick-acting valves at each end of the test section to trap the two-phase mixture and then determined the void fraction from measurements of the volume of each phase present.

A method which has been recently developed is the use of the difference in the attenuation of gamma radiation of the two phases to determine the vapor volume fraction.[15,20,21] Studies using lucite blocks to simulate the liquid phase were conducted by Cook.[22] This study demonstrated that the accuracy of the method is dependent upon the source geometry, and the void distribution for a preferential void distribution. Hooker and Popper[24] have considered the radiation attenuation technique and its dependence on instrumentation stability and other factors. This technique has also been used to measure the density and homogeneity of slurries,[25] and the uniformity of solid materials.[26]

In this study, to facilitate the comparison between the actual void values and those obtained from the radiation attenuation method,

lucite models were substituted for the actual liquid-vapor system. The attenuation characteristics of the lucite are approximately the same as those of water for the gamma radiation used.

Various distributions and magnitudes of voids were machined into the lucite mockups, and the actual voids present in the models were determined by weight loss and by physical measurement of the model. The void distributions were selected so as to include the extremes which are encountered in two-phase flow.

A comparison was made between two techniques for the void fraction measurement, i.e., the "one-shot" method and the traversing method. In the "one-shot" method a "window" in front of the scintillation counter is slightly larger than the flow channel, and admits a relatively large beam of gamma rays. A single value from the output of the instrumentation system is the basis for the calculation of an average value of the void fraction for the channel.

In the "traversing" technique a relatively small window (1/32-inch) admits a collimated beam of radiation to the counter. The beam and counter are moved across the channel and the output of the system is recorded as a function of beam position. From this record the dependence of the void fraction on the position in the channel was determined. The average value of the void fraction was found by integrating the void vs. position curve and dividing by the channel width.

2. Theoretical

In the determination of the void fraction, the gamma radiation was assumed to be monoenergetic, and the attenuation was assumed to be exponential. Thus the following equation was obtained

$$I = I_0 \, e^{-\mu x} \tag{2.1}$$

where I = intensity of the radiation at x   (photons/cm^2 sec)

I_0 = intensity of the beam at x = 0   (photons/cm^2 sec)

μ = linear absorption coefficient   (cm^{-1})

x = absorber thickness   (cm)

The linear absorption coefficient is related to the microscopic cross section by the equation

$$\mu = \frac{N_0 \rho \sigma}{A} \tag{2.2}$$

where

N_0 = Avogadro's number - 6.02×10^{23} nuclei/gram mole

A = atomic weight - grams/gram mole

σ = microscopic cross section - cm^2/nucleus

ρ = density of absorber - grams/cm^3 .

For a given liquid and its vapor, the absorption coefficient of each phase will therefore be proportional to the density of that phase.

For a two-phase mixture, from the standpoint of radiation attenuation, the flow will be between two extremes. In one case the vapor, liquid, and structure may be considered to exist in parallel lamina, perpendicular to the beam of radiation. The neutron intensity at the detector will be given by the following equation:

$$I = I_0 e^{-\mu_s t_s} e^{-\mu_\ell t_\ell} e^{-\mu_v t_v} \tag{2.3}$$

where

μ_s = linear absorption coefficient of the structure - cm^{-1}

μ_ℓ = linear absorption coefficient of the liquid - cm^{-1}

μ_v = linear absorption coefficient of the vapor - cm^{-1}

t_s = total structure thickness - cm

t_ℓ = total liquid thickness - cm

t_v = total vapor thickness - cm

If the channel were filled with a single phase the values of the radiation intensity for the liquid and vapor respectively are

$$I_\ell = I_0 \, e^{-\mu_s t_s} \, e^{-\mu_\ell t} \tag{2.4}$$

and

$$I_v = I_0 \, e^{-\mu_s t_s} \, e^{-\mu_v t} \tag{2.5}$$

where

t = total channel width

and

$$t = t_\ell + t_v \tag{2.6}$$

Dividing (2.3) by (2.4) and using (2.6) it follows that

$$I = e^{(\mu_\ell - \mu_v) \cdot t_v} \tag{2.7}$$

Similarly (2.5) divided by (2.4) yields

$$\frac{I_v}{I_\ell} = e^{(\mu_\ell - \mu_v) \, t} \tag{2.8}$$

Expressing (2.7) and (2.8) in logarithmic form and taking the ratio we obtain

$$\alpha = \frac{\ln (I/I_\ell)}{\ln (I_v/I_\ell)} \tag{2.9}$$

where $\alpha = t_v/t$ = vapor volume fraction.

If the response of the detecting and recording instrumentation is linear, the following must be true:

$$I = K R \tag{2.10}$$

where

I = radiation intensity

K = instrumentation constant

R = recording chart reading in arbitrary units

Equation (2.9) may then be expressed in terms of recording chart readings.

$$\alpha = \frac{\ln\left(R/R_f\right)}{\ln\left(R_e/R_f\right)} \tag{2.11}$$

where R = recording chart reading for two phase flow

R_f = recording chart reading for liquid phase only

R_e = recording chart reading for vapor or void only.

For the determination of the void fraction α, it is necessary to obtain three readings. The empty or vapor, reading, and the full, or liquid reading serve as calibrations for the system as a whole. No detailed information is needed on the source strength, absorption coefficients, or instrumentation constants as long as these quantities do not change during the measurements. Recalibration runs have to be made with a frequency which depends upon the stability of the source, and instrumentation.

In the second extreme case the two phases are assumed to exist in lamina parallel to the path of the radiation. For this case the radiation at the detector is

$$I = \frac{I_0}{A} e^{-\mu_s t_s} \left[A_v e^{-\mu_v t} + A_\ell e^{-\mu_\ell t} \right] \tag{2.12}$$

where

A = total area of beam

A_v = area of beam passing through vapor

A_ℓ = area of beam passing through liquid

For each phase singly,

$$I_\ell = I_0 e^{-\mu_\ell t} e^{-\mu_s t_s} \tag{2.13}$$

$$I_v = I_0 e^{-\mu_v t} e^{-\mu_s t_s} \tag{2.14}$$

Substitution of (2.13) and (2.14) into (2.12) yields

$$I = I_v \frac{A_v}{A} + I_\ell \frac{A_\ell}{A} \tag{2.15}$$

Noting that $\dfrac{A_v}{A} = \alpha$ and $\dfrac{A_\ell}{A} = 1 - \alpha$

equation (2.15) becomes

$$\alpha = \left(\frac{I - I_\ell}{I_v - I_\ell}\right) \tag{2.16}$$

and making use of (2.10) it follows that

$$\alpha = \left(\frac{R - R_\ell}{R_v - R_\ell}\right) \tag{2.17}$$

As has been noted by Petrick[15] and others, there is a much stronger tendency for two-phase mixture to behave according to the first case and this is the relationship which will be used in the calculation of voids in the following work.

It must also be noted, however, that large errors may result due to the use of relationship (2.11) in the determination of the void fraction where a strong parallel path effect does exist. This is shown in the results of some of the studies using the one-shot technique with the mockups. It is also seen that the narrow beam of the radiation used in the traversing technique makes this method nearly insensitive to parallel path effects in any flow pattern which may be encountered in two-phase flow.

3. Description of Equipment

   a. Source

   A thulium-170 source was used in the void measuring equipment. The thulium-170 has a half life of approximately 129 days and decays by beta emission to ytterbium-170. In 90 per cent of the decays a 0.97 Mev beta particle is emitted, followed by a 0.0522 Mev photon [23] In the remainder of the decays a 0.886 Mev beta particle is given off, leaving the ytterbium-170 in an excited state. The ytterbium then emits a 0.084 Mev gamma ray. A certain amount of Bremsstrahlung is present due to the decay betas. The decay scheme and energy spectrum for the thulium-170 are shown in Figure 2.1.
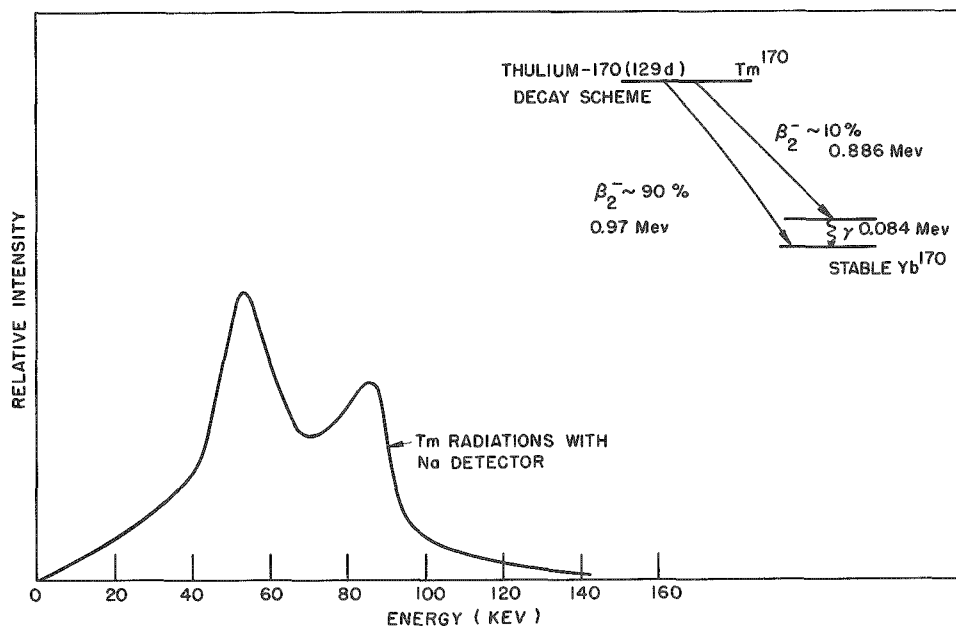
Figure 2.1 Energy Spectrum and Decay Scheme for Thulium-170
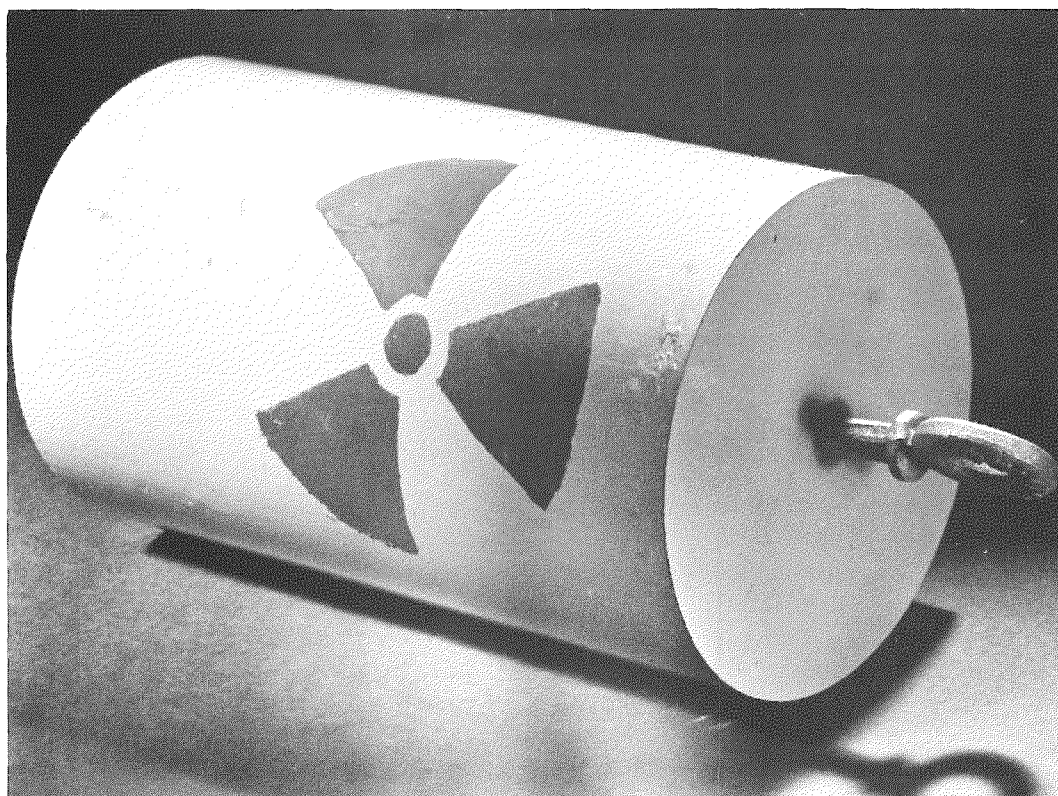
Figure 2.2 Thulium Source in Lead Cylinder

The source was a 0.2 inch pellet which was shielded in a lead cylinder 3.5 inches in diameter and 6 inches in length (Figure 2.2). In order to obtain a more nearly mono-energetic source, a 0.25 inch lead filter was placed over the end of the shield to eliminate most of the lower energy radiation. The source initially had a strength of approximately 9 roentgen per hour at a distance of 2 inches.

b.   Instrumentation

A one-inch thick thallium activated, sodium-iodide crystal was used to detect the gamma radiation which passed through the test section. The crystal was optically coupled to a photomultiplier tube (RCA 5819). The crystal and photomultiplier tube were then assembled in an aluminum shield as shown in Figure 2.3.

The voltage for the detector was provided by a combination high voltage supply and linear current amplifier into which the output of the detector was fed. The output of the current amplifier was recorded by a Brown Recording Potentiometer (Model S-153X16V-X-156).

The scintillation counter assembly was protected from stray radiation by a lead shield which was designed to accept lead windows of various dimensions (Figures 2.4 and 2.5).

c.   Void Traversing Mechanism

The void traversing mechanism made use of a stationary lower plate on which the mockup holders were fastened. A 4.1 rpm constant speed motor (Bodine model KC1-22RC) was mounted on this fixed plate. Four 0.25 inch diameter rods were bolted to this plate to serve as rails.

An upper plate was equipped with 12 grooved fiber wheels which rolled along these rails. This moving plate carried two sources, and two scintillation counter assemblies with their shields and windows as shown in Figures 2.6 and 2.7. The upper plate was moved with respect to the lower fixed plate by a 0.375-inch diameter lead screw
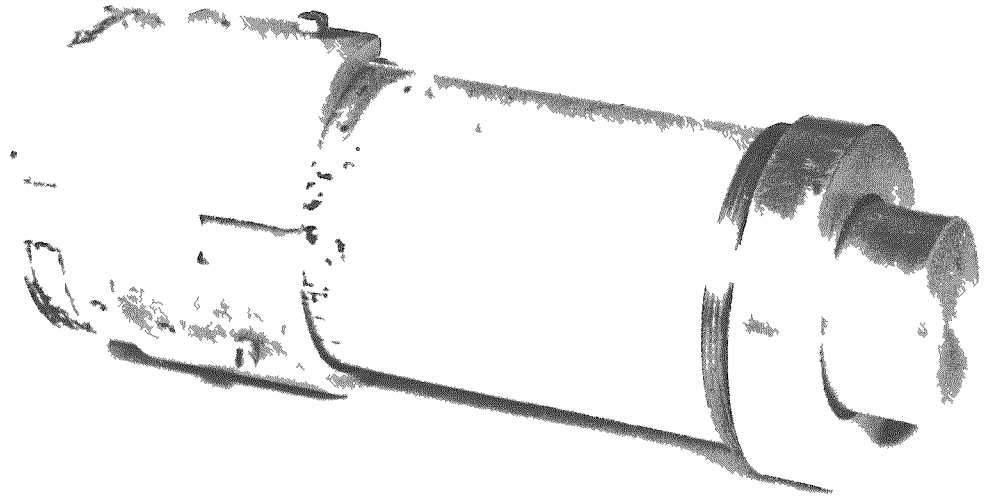
Figure 2.3 Scintillation Crystal Photomultiplier Tube Assembly
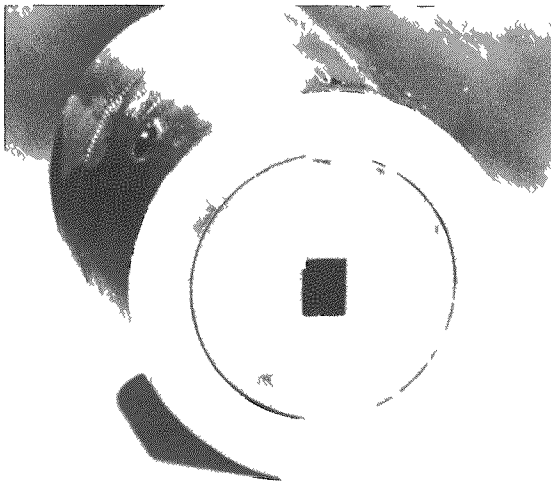
Figure 2.4 Lead Detector Shield
with 1/2 x 5/8 Window
in Place

Figure 2.5 Lead Window,
1/2 x 1/32 inch
Opening

14
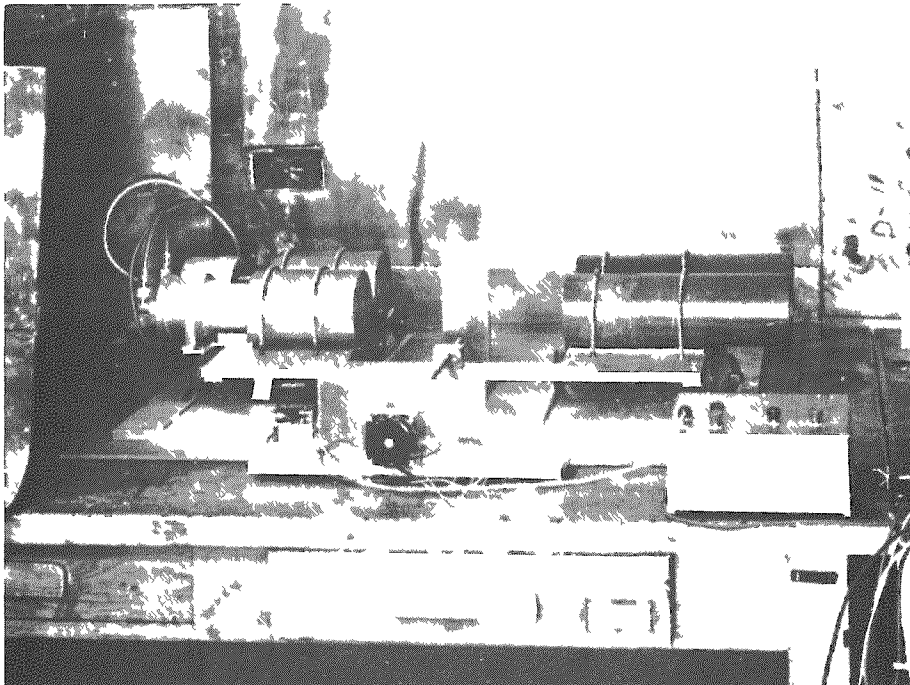
Figure 2.6   Void Traversing Mechanism with Rectangular
Mockup and Holder in Place
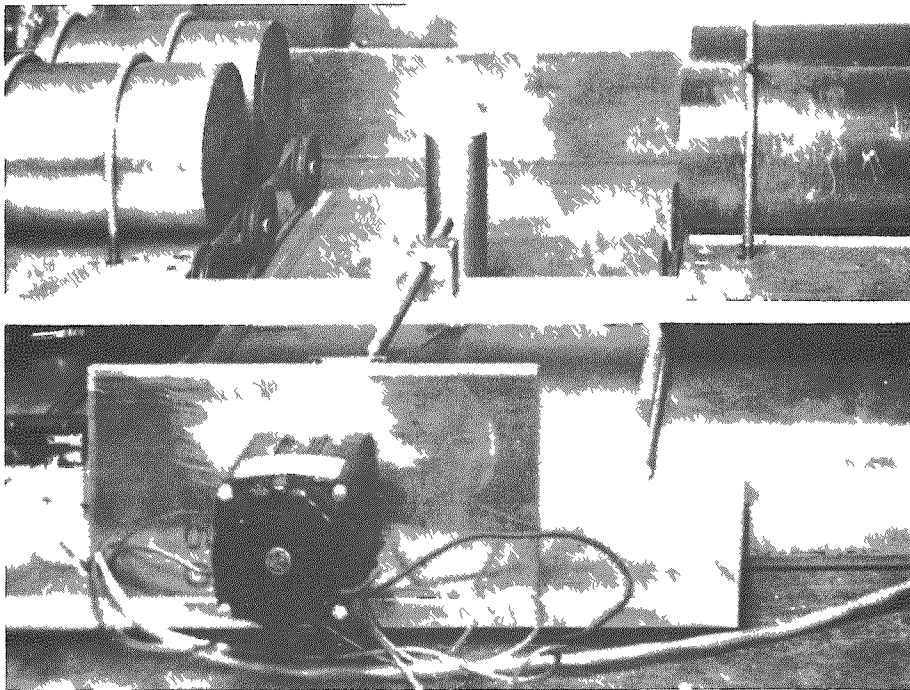
Figure 2.7   Closeup of Void Traversing Mechanism with
Cylindrical Mockup and Holder in Position

which was driven by the motor, and which turned in a threaded block on the moving plate. The pitch of the lead screw was 40 threads per inch.

The motor was used to position the source-detector pairs or to move them at a constant speed in either direction by means of a system of switches and relays mounted in the control box.

d.   Lucite Void Mockups

Lucite mockups were used to simulate the void distributions which are encountered in the simultaneous flow of a liquid and a gas or vapor.

Rectangular mockups were 6.5 inches long, and 2 inches wide. Thirteen of the mockups were 1 inch thick, and nine were 0.5 inch thick. Cylindrical mockups were 1 inch long and six had a 1/2-inch diameter, while ten had a 1-inch diameter. Representative mockups are shown in Figures 2.8 through 2.13. The void fractions for the mockups studied range from 0.09 to 0.81. The dimensions of these mockups were carefully checked after the machining, and the void fraction calculated. For those mockups where it was practical, the weight of the mockup was obtained on a balance, and the void fraction determined from the comparison with a solid block of lucite. The void fraction obtained by weight was taken as the correct value for comparison with the values obtained by radiation attenuation techniques, as the value of the weight was obtained to five significant figures.

An aluminum mockup holder with a wall thickness of 0.25 inch was obtained for each set of models. The full flow channel was simulated by a solid block of lucite.

4. Test and Calculation Procedures

a.   One-Shot Method

The source holder was aligned with respect to the detector by adjusting its position until a maximum output of the instrumentation
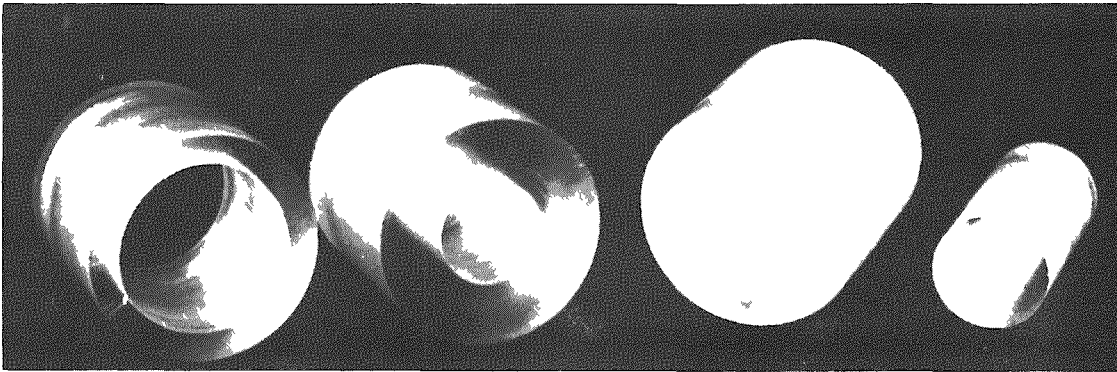
Figure 2.8 Cylindrical Lucite Mockups Used in Attenuation
Technique Evaluation

Figure 2.9 Additional Cylindrical Lucite Mockup
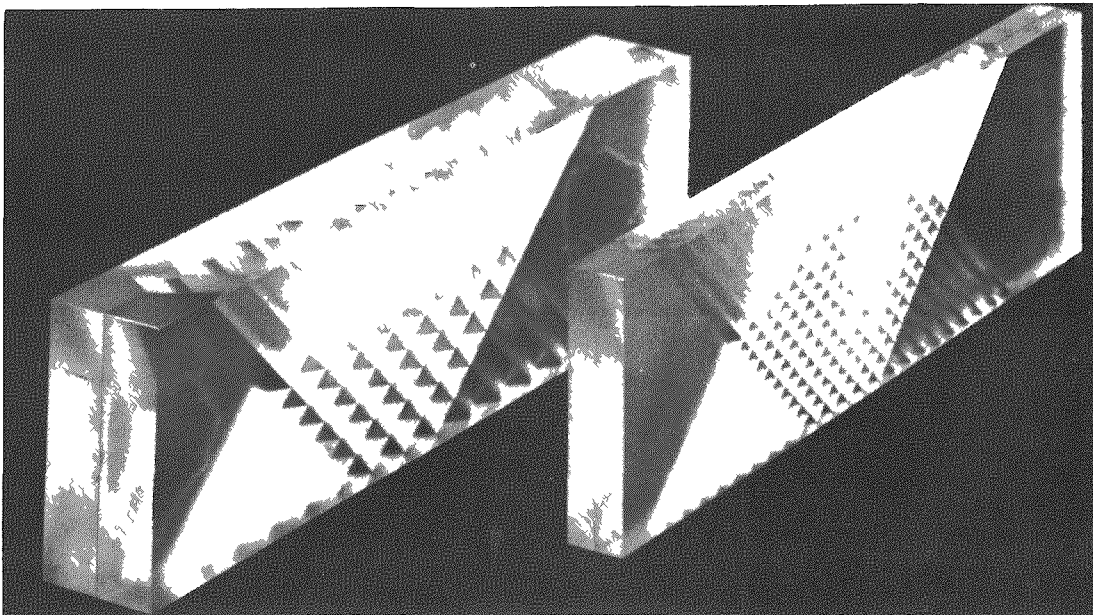
Figure 2.10 Rectangular Lucite Mockups
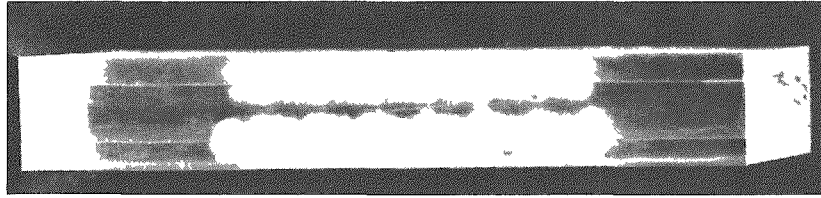
Figure 2.11 Rectangular Lucite
Mockup with Spheri-
cal Voids
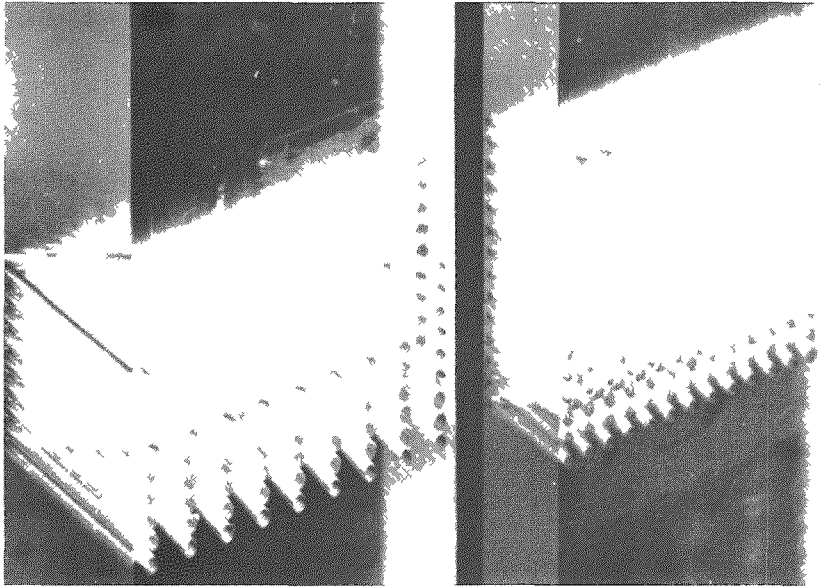
Figure 2.12 Lucite Mockup to
Simulate Homoge-
neous Flow
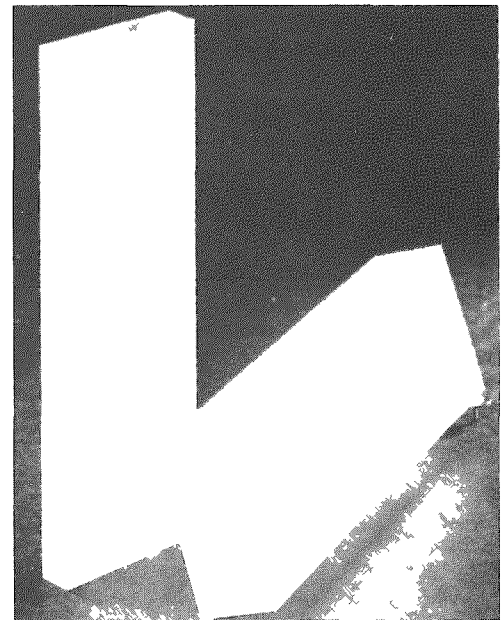
Figure 2.13 Lucite Mockup to Simulate Annular Flow

was noted. The movable plate was then centered with respect to the mockup and holder. Three readings were then obtained from the recording potentiometer. The values were noted with the test mockup in the holder, with the holder empty, and with a solid lucite block in the holder. These values were noted as the run, the empty, and the full readings respectively. The void fraction was then obtained by substituting the three values obtained into equation (2.11).

b. Traversing Method

The source holder was aligned with respect to the detector which was equipped with the narrow window (1/2 inch by 1/32 inch), as before. The movable plate was driven by the motor and lead screw so that the beam of gamma radiation traversed the mockup and holder. A record was obtained of the instrumentation output as a function position of the gamma beam. This operation was repeated with the holder empty, and with the solid block in place. Three strip chart records were then obtained which, as before, were the run, empty and full respectively. For a corresponding set of records, the traverses were always made in the same direction. A typical set of traverse records are shown in Figure 2.14.

The analysis of the traverse records required that values be taken from corresponding points on the three records to calculate a local value of the void fraction. The records were aligned and divided into a convenient number of equal lengths and the values obtained from the trace. For the rectangular mockups local values of α were all weighted equally in determining an average value for the cross section.

For cylindrical mockups, a weighting system was developed for the determination of the average value of the void fraction. The local void fraction values were weighted according to the chord length at the particular position of the radiation beam.
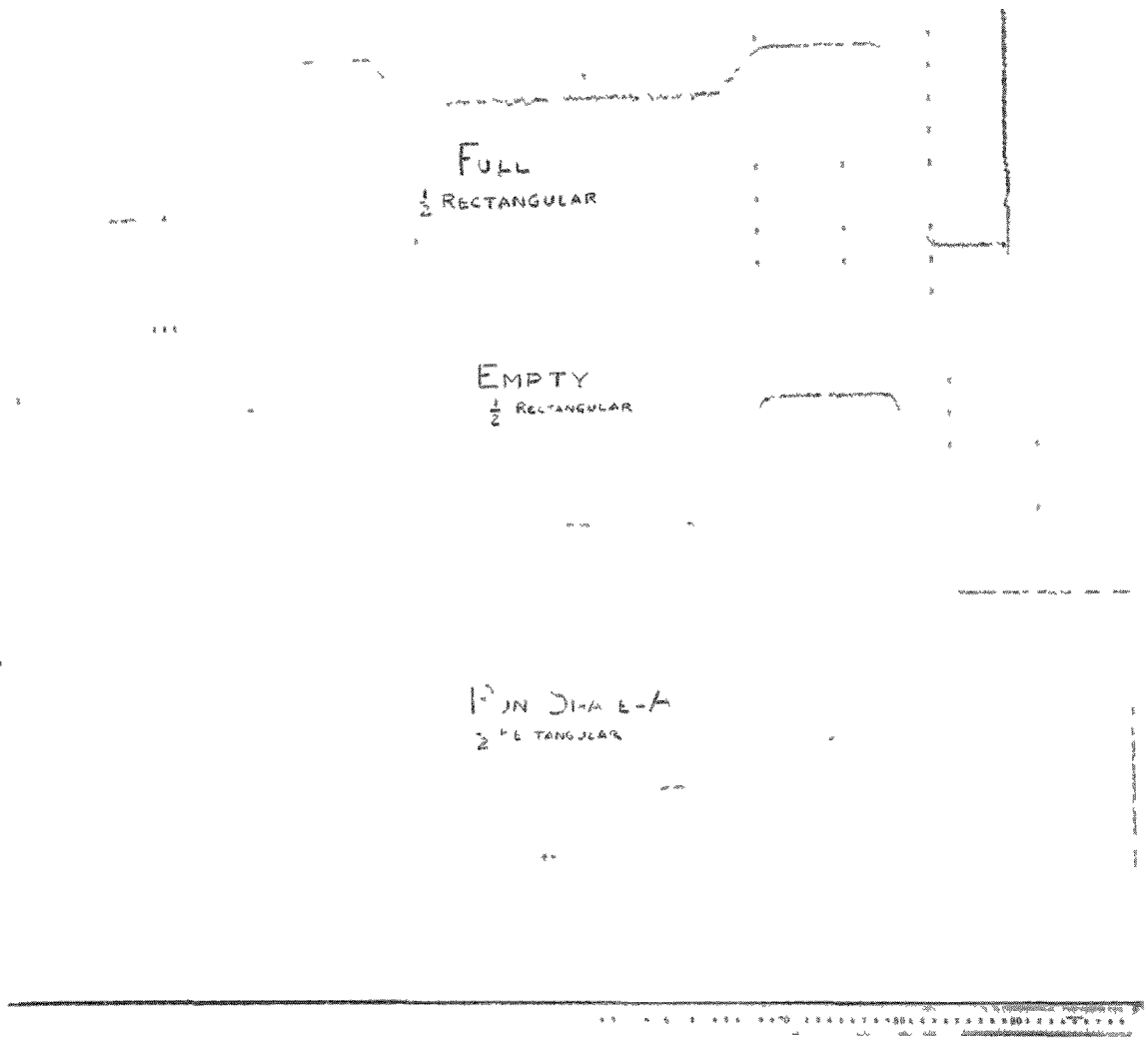
Figure 2.14 Typical Records Obtained from a Void Traverse

The void fraction is equal to the void area divided by total area assuming the void is equivalent to a single hole in the circular cross section

$$\bar{\alpha} = \text{actual void} = \frac{\text{area of void}}{\text{area of circle}} \quad .$$

For the area of the hole, the following is true from Figure 2.15.

$$\text{area of the void} = \int_{-R}^{R} C(x)\, dx \qquad (2.18)$$

From a definition of the local void fraction

$$\alpha(x) = \frac{C(x)}{f(x)} \qquad (2.19)$$

and

$$f(x) = 2\sqrt{R^2 - x^2} \qquad (2.20)$$

where R = radius of cross section.

Therefore

$$C(x) = 2\alpha(x)\sqrt{R^2 - x^2}$$

and

$$\bar{\alpha} = \frac{1}{\pi R^2} \int_{-R}^{R} 2\alpha(x)\sqrt{R^2 - x^2}\, dx \quad .$$

If the integration is replaced by a summation, then the average void fraction becomes

$$\alpha = \frac{2}{\pi R^2} \sum_{i=1}^{n} \alpha_i \sqrt{R^2 - x_i^2}\ \Delta x_i \quad .$$

For the calculations presented in this report, Δx_i was taken as one-sixteenth of the diameter and the corresponding values of x_i were taken. The values of α_i were found from a plot of α as a function of position. These plots were made from the traverse record data.
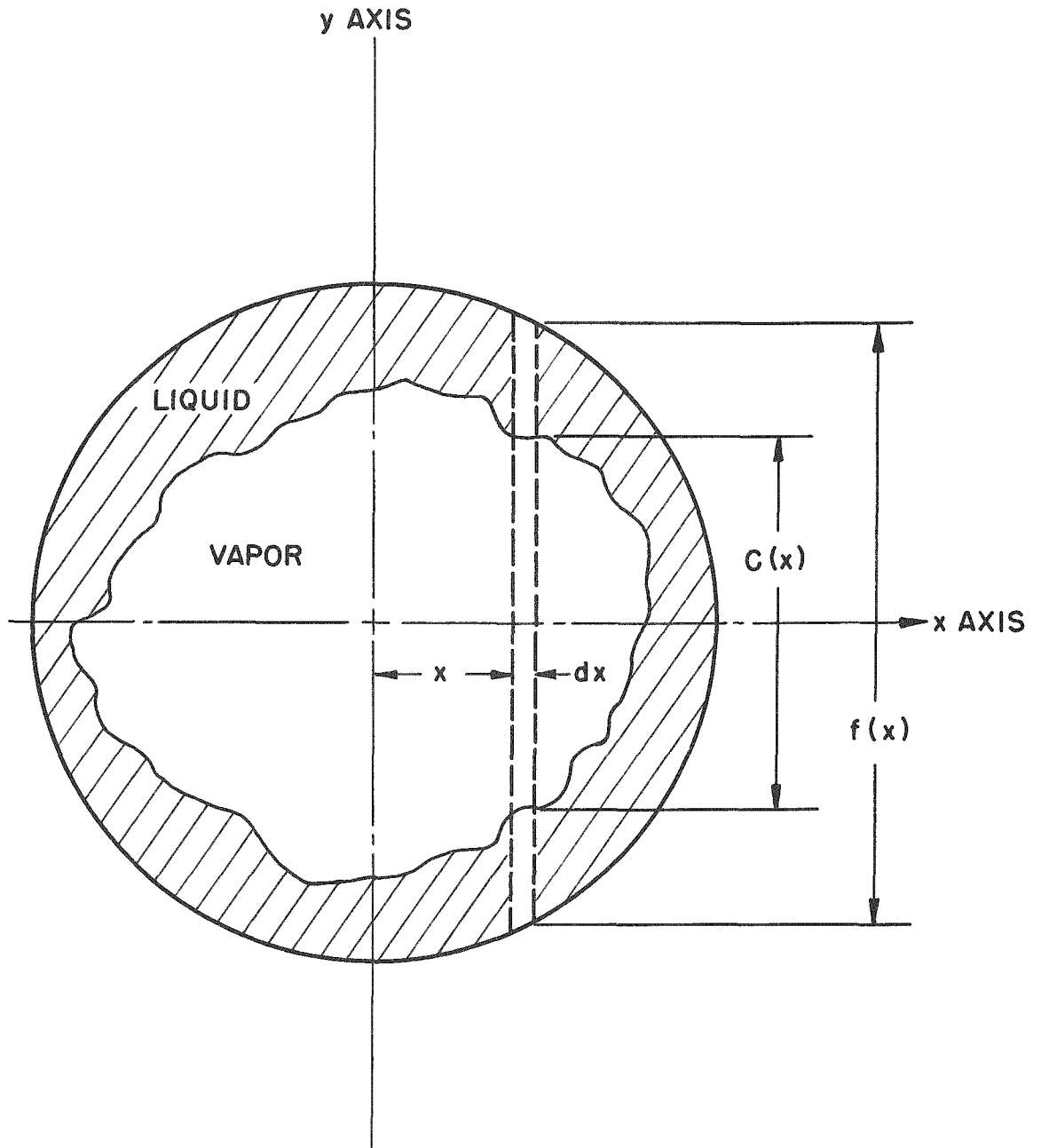
Figure 2.15 Representation of Cylindrical Void Distribution

5. Results

    a.   Rectangular

The results for the one-shot calculations for the rectangular mockups are shown in Tables 2.1 through 2.4. The reproducibility of this data is indicated by the relatively small value of average per cent deviation from the mean.

The local values of the void fraction as obtained from the traverse data are compared with the local values calculated from the dimensions and geometry of the mockups in Figures 2.16 through 2.22. The comparisons of the traverse and one-shot values with the void fraction by weight and by dimensions are shown in Tables 2.5 and 2.6. These data show that the traversing technique offers a definite advantage over the one-shot method for the strongly preferential void distributions. The advantage is greater for the larger test section. The plots of the local void fraction also show that the traversing technique yields at least qualitative information about the type of void distribution which is present.

The difference in the one-shot results for the different-size windows is a geometric effect, which is due to the fact that the radiation is not composed of parallel rays. This can be seen from considering Figure 2.23. For the narrow window the radiation weighs the void distribution in the center of the channel too heavily and thus gives an incorrect value. Increasing the window width gives a corresponding increase in the accuracy of the results obtained. This is strongly demonstrated in the data for the one-inch rectangular mockups A, B, and C, as shown in Table 2.6.

TABLE 2.1

VOID FRACTION RESULTS, ONE-SHOT METHOD

1/2 x 2 inch section, 5/8 inch window

Mockup	Run 1	Run 2	Run 3	Run 4	Run 5	Run 6	Run 7	Average Value	Average % Deviation
A	0.543	0.534	0.533	0.535	0.538	0.544	0.543	0.539	0.8
B	0.294	0.294	0.298	0.294	0.300	-	-	0.296	0.8
C	0.545	0.541	0.548	0.544	0.544	-	-	0.544	0.3
D	0.720	0.723	0.728	0.723	0.728	-	-	0.724	0.4
E	0.445	0.450	0.444	0.445	0.445	-	-	0.446	0.4
F	0.225	0.220	0.230	0.230	0.230	0.230	0.226	0.227	1.4
G	0.435	0.431	0.443	0.438	0.428	-	-	0.435	1.0
H	0.253	0.252	0.250	0.254	0.253	-	-	0.252	0.5
I	0.415	0.414	0.425	0.408	0.418	-	-	0.416	1.1

TABLE 2.2

VOID FRACTION RESULTS, ONE-SHOT METHOD

1/2 x 2 inch section, $1\frac{1}{8}$ inch window

Mockup	Run 1	Run 2	Run 3	Run 4	Run 5	Average Value	Average % Deviation
A	0.407	0.412	0.407	0,408	0.407	0.408	0.3
B	0.204	0.192	0.224	0.224	0.223	0.213	5.8
C	0.419	0.409	0.419	0.419	0.422	0.418	0.76
D	0.607	0.612	0.619	0.628	0.626	0.618	1.2
E	0.588	0.583	0.594	0.593	0.596	0.591	0.7
F	0.374	0.366	0.380	0.378	0.379	0.375	1.2
G	0.426	0.417	0.430	0.427	0.431	0.426	0.9
H	0.255	0.244	0.247	0.252	0.247	0.249	1.5
I	0.418	0.419	0.408	0.415	0.416	0.415	0.7

24

TABLE 2.3

VOID FRACTION RESULTS, ONE-SHOT METHOD
1 x 2 inch Section, 1⅛ inch Window

Mockup	Run 1	Run 2	Run 3	Run 4	Run 5	Average Value	Average % Deviation
A	0.135	0.136	0.136	0.133	0.146	0.137	2.5
B	0.595	0.609	0.591	0.594	0.598	0.597	0.8
C	0.311	0.317	0.312	0.308	0.314	0.312	0.8
D	0.588	0.592	0.593	0.594	0.597	0.593	0.4
E	0.740	0.746	0.754	0.750	0.745	0.747	0.5
F	0.176	0.176	0.184	0.176	0.186	0.180	2.4
G	0.307	0.310	0.306	0.309	0.310	0.308	0.5
H	0.160	0.158	0.159	0.156	0.156	0.158	0.9
I	0.240	0.243	0.235	0.245	0.250	0.243	1.6
J	0.397	0.399	0.405	0.405	0.406	0.402	0.9
K	0.785	0.784	0.785	0.780	0.786	0.784	0.2
L	0.498	0.503	0.510	0.509	0.507	0.505	0.8
M	0.431	0.433	0.440	0.425	0.418	0.429	1.5

TABLE 2.4

VOID FRACTION RESULTS, ONE-SHOT METHOD
1 x 2 inch Section, 1½ inch Window

Mockup	Run 1	Run 2	Run 3	Run 4	Run 5	Average Value	Average % Deviation
A	0.210	0.224	0.221	0.224	0.225	0.221	1.8
B	0.521	0.517	0.517	0.524	0.523	0.520	0.5
C	0.271	0.270	0.270	0.273	0.266	0.270	0.6
D	0.520	0.519	0.526	0.522	0.515	0.520	0.5
E	0.722	0.730	0.726	0.726	0.728	0.726	0.3
F	0.177	0.181	0.183	0.182	0.180	0.181	0.9
G	0.290	0.289	0.291	0.290	0.292	0.290	0.2
H	0.155	0.153	0.155	0.150	0.149	0.152	1.6
I	0.235	0.240	0.240	0.236	0.242	0.239	1.0
J	0.408	0.412	0.411	0.406	0.414	0.410	0.6
K	0.825	0.809	0.812	0.816	0.814	0.815	0.5
L	0.492	0.494	0.492	0.492	0.495	0.493	0.2
M	0.424	0.424	0.418	0.424	0.421	0.422	0.5
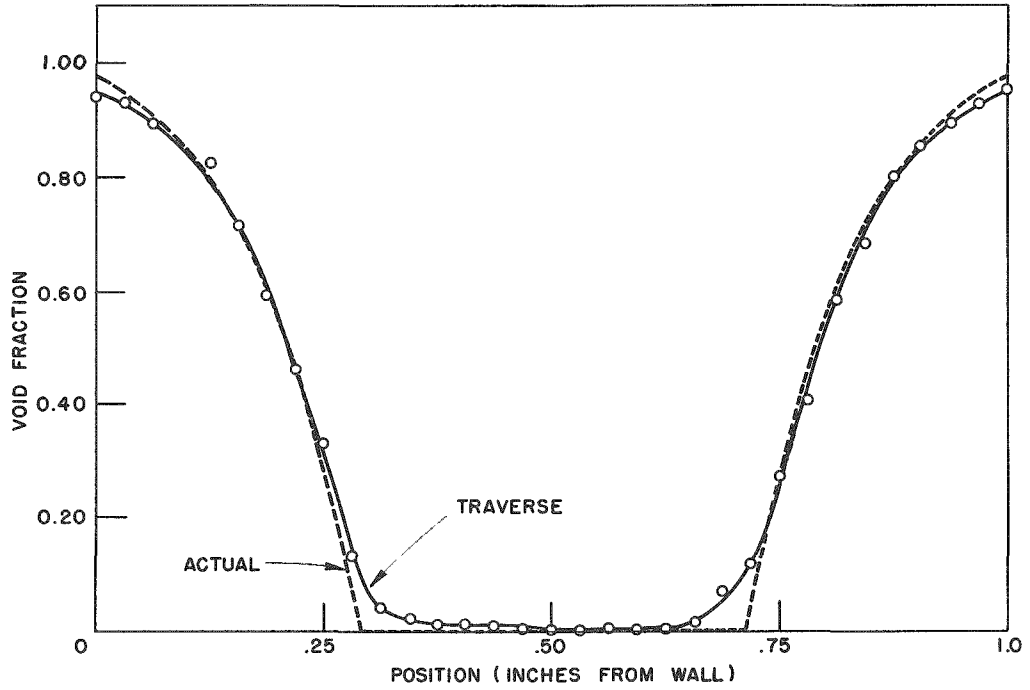
Figure 2.16 Local Void Fraction vs. Position,
One-inch Rectangular Mockup A
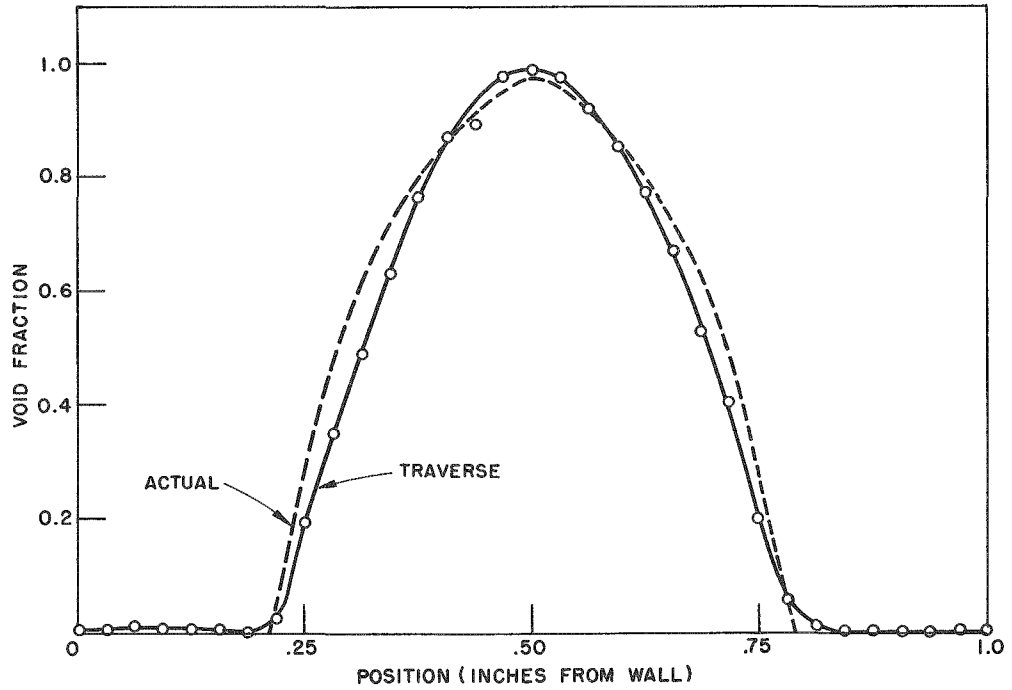
Figure 2.17 Local Void Fraction vs. Position,
One-inch Rectangular Mockup B
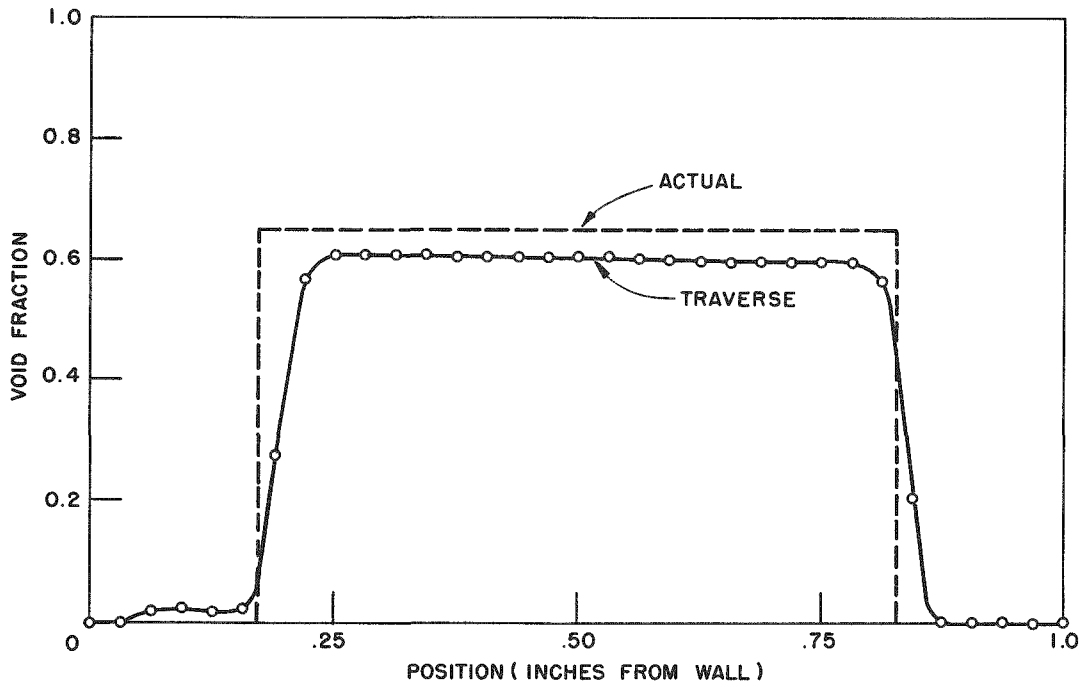
Figure 2.18 Local Void Fraction vs. Position,
One-inch Rectangular Mockup D
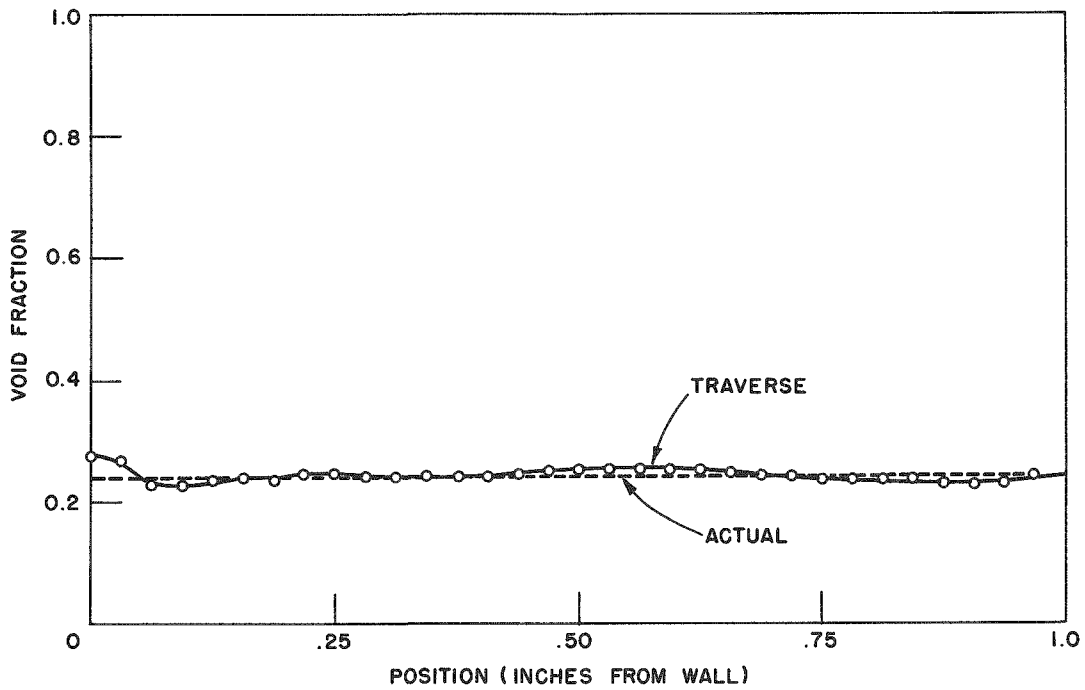
Figure 2.19 Local Void Fraction vs. Position,
One-inch Rectangular Mockup I
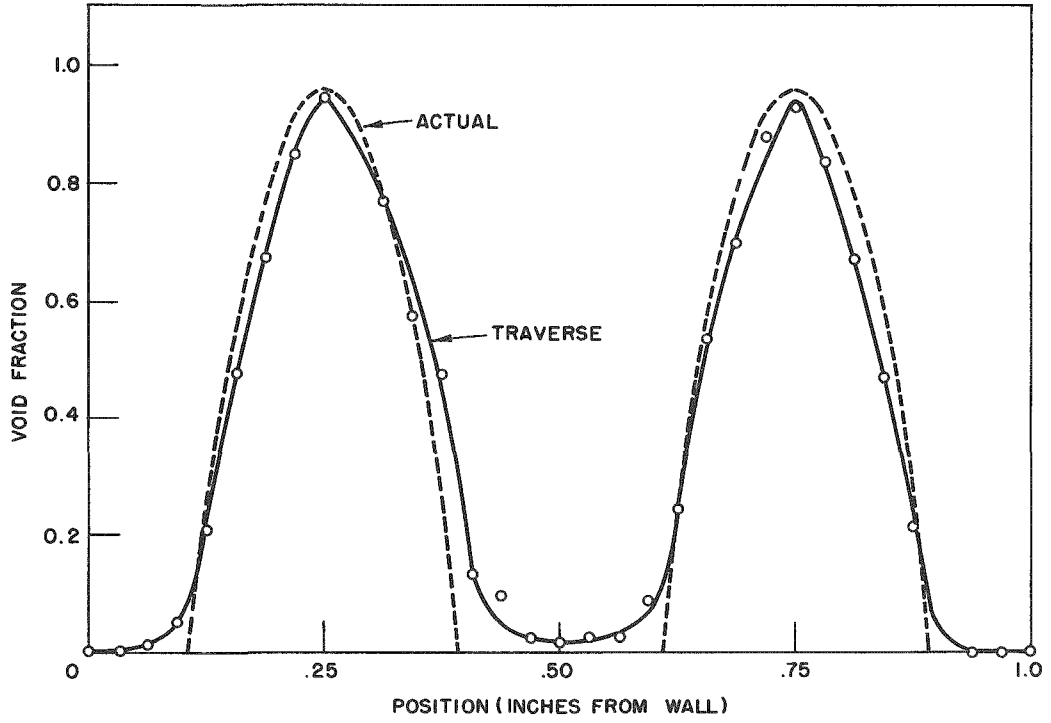
Figure 2.20 Local Void Fraction vs. Position,
One-inch Rectangular Mockup L
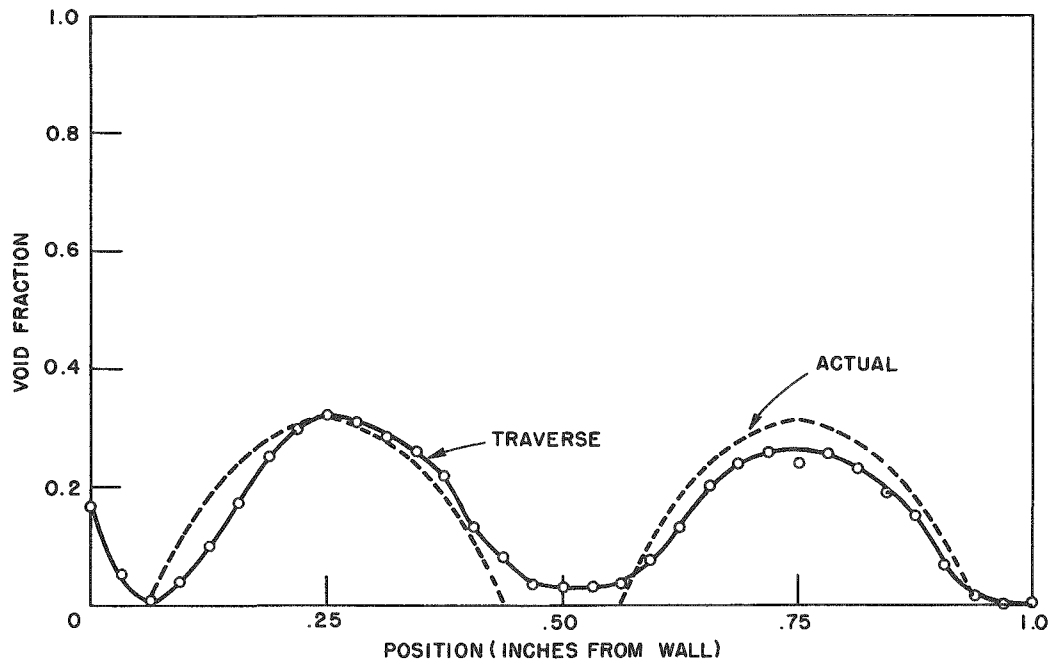
Figure 2.21 Local Void Fraction vs. Position,
One-inch Rectangular Mockup F
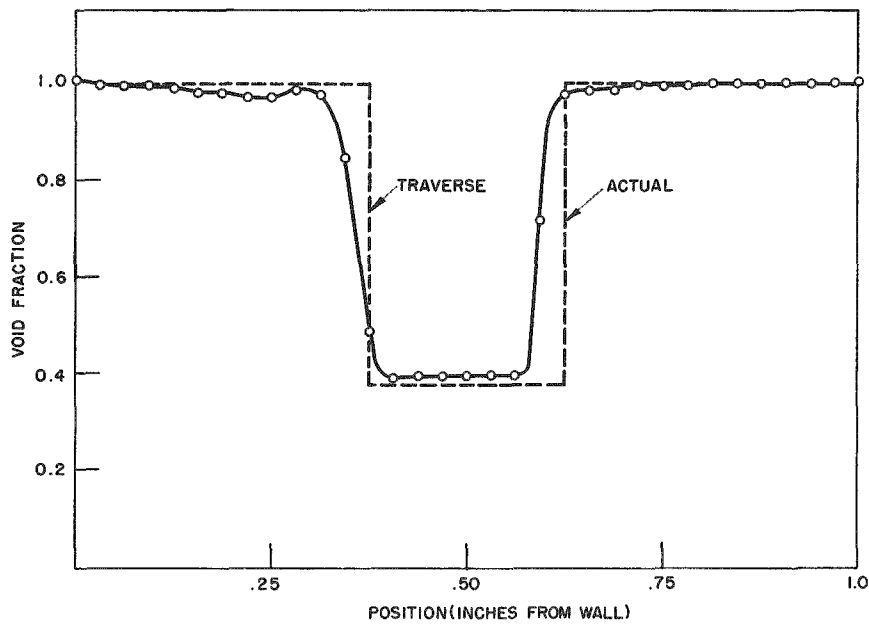
Figure 2.22 Local Void Fraction vs. Position,
One-inch Rectangular Mockup K
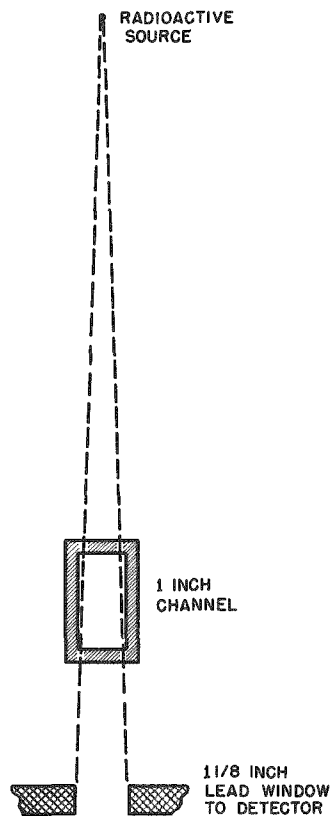
Figure 2.23 Effect of Window Size on One-Shot Results

TABLE 2.5

VOID FRACTION RESULTS, RECTANGULAR MOCKUPS

(1/2 inch x 2 inch)

Mock-up	Dimen-sion	Weight	Tra-verse	Percent Differ-ence	One Shot 5/8" window	Percent Differ-ence	One Shot $1\frac{1}{8}$" window	Percent Differ-ence
A	0.345	0.394	0.350	11.2	0.539	36.5	0.408	3.6
B	0.188	-	0.195	3.7	0.296	57.4	0.213	13.3
C	0.398	0.402	0.371	7.7	0.544	35.3	0.418	4.0
D	0.606	0.605	0.589	2.6	0.724	19.7	0.618	2.7
E	0.564	-	0.581	3.0	0.446	20.9	0.591	4.8
F	0.345	0.394	0.394	0	0.227	42.4	0.375	4.8
G	0.418	-	0.384	7.7	0.435	4.1	0.426	1.9
H	0.254	-	0.239	5.9	0.252	0.8	0.249	2.0
I	0.415	-	0.420	1.2	0.416	0.2	0.415	0
Average Percent Difference				4.8		24.1		4.1

Note: Weight values used in calculating percent difference where possible

TABLE 2.6

VOID FRACTION RESULTS, RECTANGULAR MOCKUPS

(1 inch x 2 inch)

Mock-up	Dimen-sion	Weight	Tra-verse	Percent Differ-ence	One Shot $1\frac{1}{8}$" window	Percent Differ-ence	One Shot $1\frac{1}{2}$" window	Percent Differ-ence
A	0.364	-	0.382	4.9	0.137	62.4	0.221	39.2
B	0.364	-	0.362	0.5	0.597	64	0.520	42.9
C	0.203	0.201	0.164	19.0	0.312	44.8	0.270	33.0
D	0.391	0.410	0.363	7.2	0.593	51.7	0.520	33.0
E	0.598	0.601	0.561	6.2	0.747	24.9	0.726	21.4
F	0.166	-	0.151	9.0	0.180	8.4	0.181	9.0
G	0.267	-	0.286	7.1	0.308	15.3	0.290	4.9
H	0.134	-	0.129	3.7	0.158	17.9	0.152	13.4
I	0.240	-	0.240	0	0.243	1.2	0.239	0.4
J	0.389	-	0.397	2.1	0.402	3.3	0.410	5.4
K	0.813	-	0.812	0.1	0.784	3.6	0.815	0.2
L	0.345	0.394	0.382	3.0	0.505	28.2	0.493	25.1
M	0.418	-	0.397	5.0	0.429	2.6	0.422	1.0
Average Percent Difference				5.2		25.3		17.6

b. Cylindrical

The cylindrical void mockup descriptions and dimensions are shown in Tables 2.7 and 2.8. The void fractions of the mockups were determined by weight loss and by dimensions. The weight values were more accurate, and were used as a basis for comparison with the void fractions determined from the attenuation techniques. This comparison is shown in Tables 2.9 and 2.10. As was the case for the rectangular mockups, the traverse results are better than the one-shot results. The maximum errors are greater in the case of the cylindrical mockups than they were in the case of the rectangular shapes. The comparison between void fractions determined by weight and attenuation methods are also shown in Figure 2.24.

6. <u>Conclusions</u>

The results of this series of tests indicates clearly that the radiation attenuation technique is an effective method for the determination of the void fraction in two-phase flow.

This technique is a powerful tool for the study of two-phase flow systems. It may be applied to any type of flow pattern, and it may be used with any type of flow conduit, for any pressure, temperature or conduit material.

The transit time of the radiation and the response time of the detection system are very short, and therefore with suitable recording instrumentation the technique may be used for the study of transient as well as steady-state flow phenomena.

The additional work necessary in the use of the traversing method, as compared to the one-shot method, is justified on the basis of the increase in accuracy and the information obtained on the distribution of each phase in the flow channel.

TABLE 2.7

VOID MOCKUP DESCRIPTION AND DIMENSIONS

One Inch Cylindrical Mockups

Shape	No. of holes	Diam. of holes	Void Fraction
A	1	0.453	0.205
B	1	0.3125	0.098
C	1	0.625	0.391
D	1	0.750	0.563
E	6	0.125	0.094
F	6	0.2031	0.248
G	6	0.250	0.375
H	7	0.230	0.370
I	7	0.190	0.253
J	9	0.102	0.094

TABLE 2.8

VOID MOCKUP DESCRIPTION AND DIMENSIONS

One-half Inch Cylindrical Mockups

Shape	No. of holes	Diam. of holes	Void Fraction
A	1	0.156	0.094
B	1	0.234	0.225
C	1	0.313	0.400
D	1	0.375	0.540
E	6	0.0625	0.089
F	6	0.094	0.203
G	6	0.125	0.360

TABLE 2.9

VOID FRACTION RESULTS, CYLINDRICAL MOCKUPS
ONE-INCH DIAMETER

Mockup	Dimension	Weight	Traverse	Per Cent Difference	One Shot	Per Cent Difference
A	0.205	0.207	0.182	12.1	0.293	41.5
B	0.098	0.094	0.086	8.5	0.137	45.7
C	0.391	0.393	0.383	2.5	0.508	29.3
D	0.563	0.556	0.502	9.7	0.687	23.6
E	0.094	0.097	0.104	7.2	0.100	3.1
F	0.248	0.243	0.226	7.0	0.274	12.8
G	0.375	0.370	0.250	32.4	0.414	11.9
H	0.370	0.353	0.301	15.0	0.417	18.1
I	0.253	0.247	0.250	1.2	0.296	19.8
J	0.094	0.094	0.104	10.6	0.128	25.5
Average Per Cent Difference				10.6		23.1

TABLE 2.10

VOID FRACTION RESULTS, CYLINDRICAL MOCKUPS
ONE-HALF INCH DIAMETER

Mockup	Dimension	Weight	Traverse	Per Cent Difference	One Shot	Per Cent Difference
A	0.094	0.095	0.112	17.9	0.103	8.4
B	0.225	0.192	0.190	1.0	0.253	31.8
C	0.400	0.378	0.407	7.7	0.446	18.0
D	0.540	0.545	0.513	5.9	0.601	10.3
E	0.089	0.093	0.109	17.2	0.082	11.8
F	0.203	0.203	0.157	22.7	0.217	6.9
G	0.360	0.359	0.379	5.6	0.439	22.3
Average Per Cent Difference				11.1		15.6

34
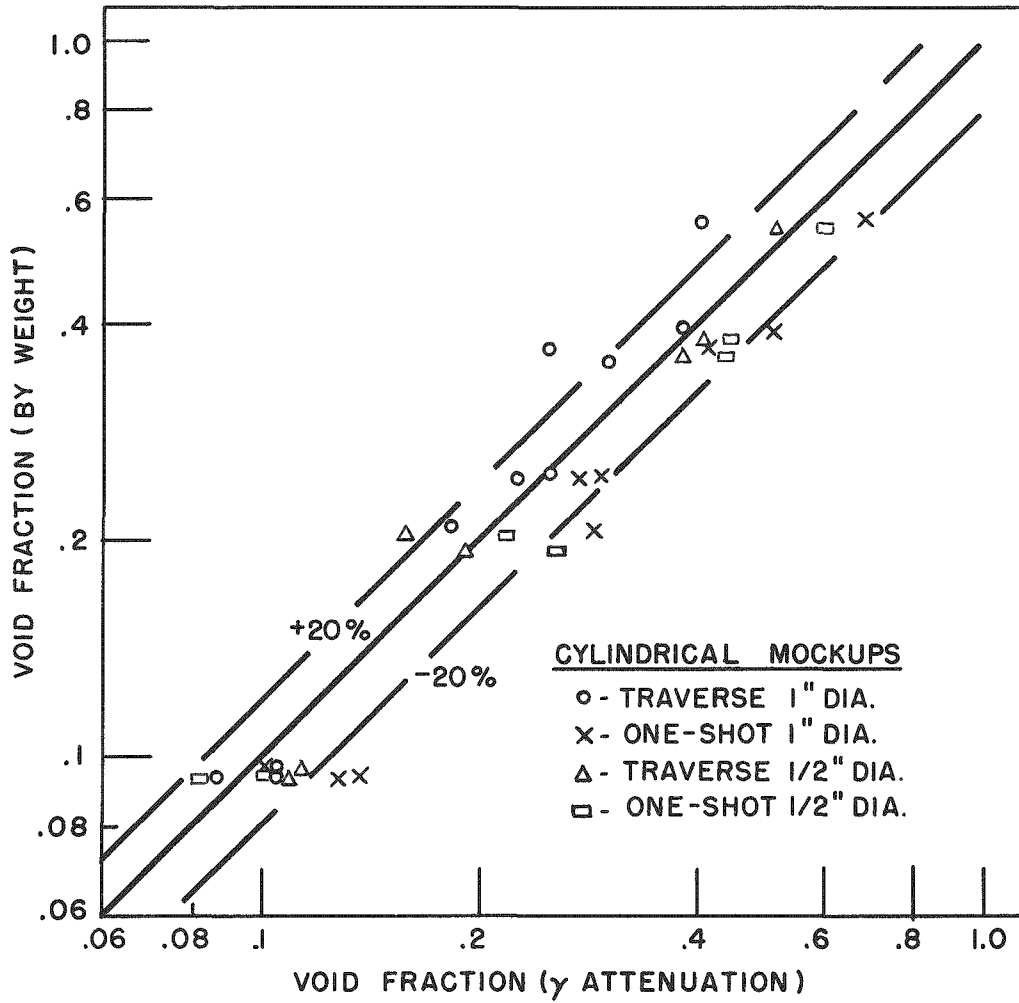
Figure 2.24 Comparison of Void Fraction by Weight and
by Radiation Attenuation Techniques

Chapter III

EXPERIMENTAL APPARATUS

1. Introduction

An experimental loop was designed and constructed to control and measure the significant test variables. Basically the loop was composed of a pump for the water, flow metering and measuring facilities for the air and water, a mixer for the two phases, the test section, a separator, and a tank. This was supplemented by apparatus for the measurement of pressure, voids, and fluid temperature. This system is shown in Figure 3.1 and is schematically shown in Figure 3.2.

2. Description of Equipment Components

a. Water System

The demineralized water used in the test program was circulated from the tank through the loop by means of a pump and motor. The flow was controlled by two valves in parallel, and a by-pass arrangement which made it possible to keep the pump operating in its most effective range. A system was arranged for flushing out the pump and the draining of the system. The flow of water was measured by an orifice-manometer system. The orifice, with a diameter of 0.5215 inch, was designed and installed according to the specifications of Grace and Lapple.[27] This orifice plate had been previously calibrated and was recalibrated in position in the loop.

b. Air System

The air supply was obtained from the 100 psi supply line of the laboratory. The air was filtered by a Norgren filter and was metered by one of a pair of orifices which were also installed in accordance with the specifications of Grace and Lapple.[27] The orifice diameters were 0.0961 and 0.2705 inches. The pressure upstream of the orifice plates was maintained at a constant 75 psig by a Norgren
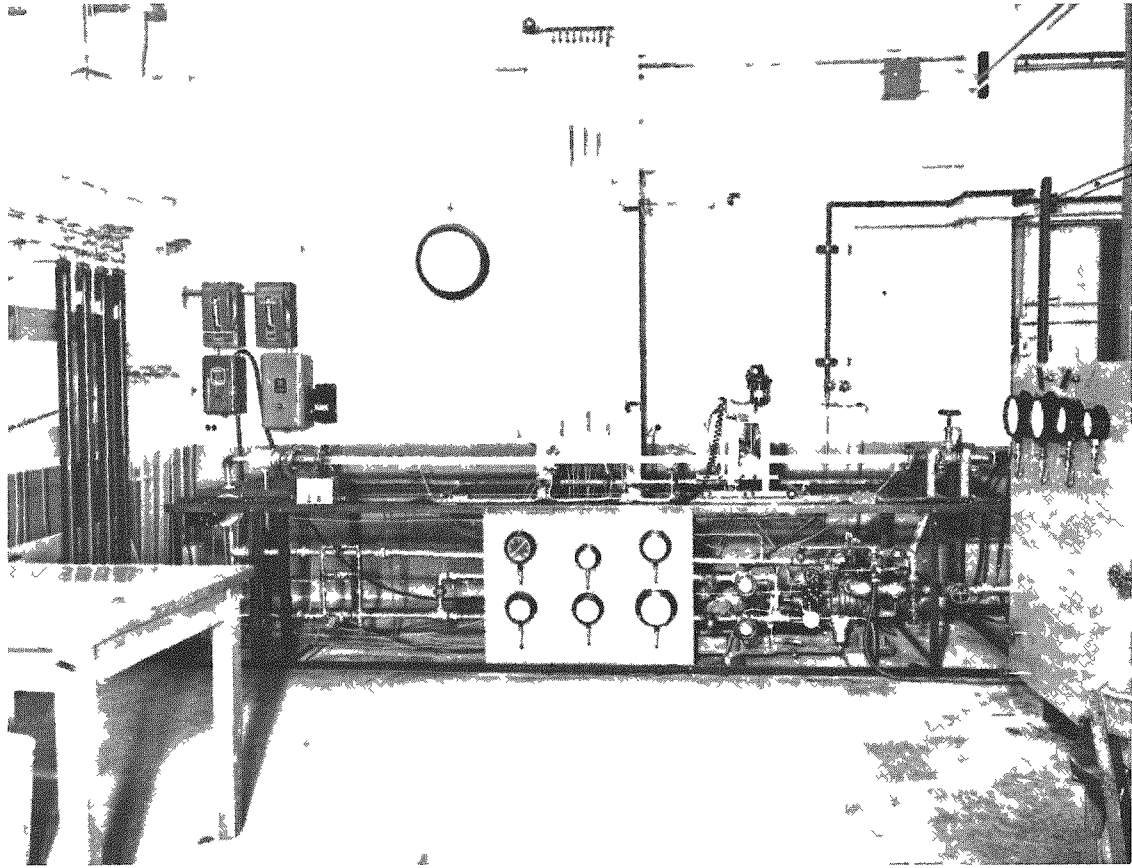
Figure 3.1 View of Experimental Loop
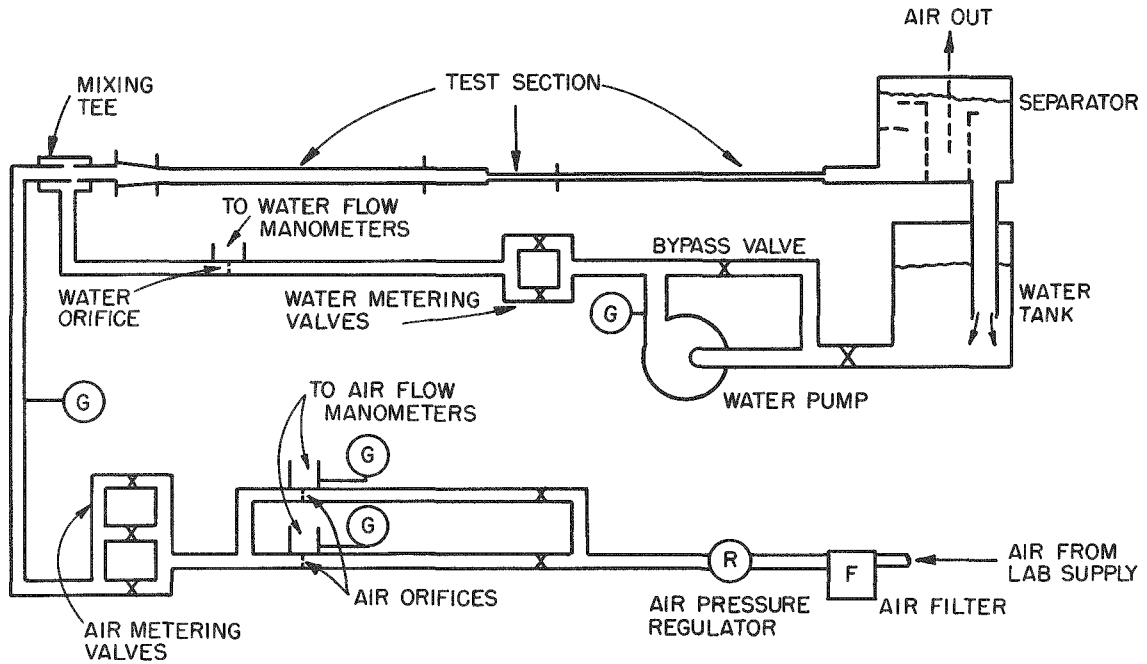
Figure 3.2 Schematic Drawing of Experimental Loop

air regulator. The pressure drop across the orifice was measured by manometers. The air flow was controlled by a parallel arrangement of three valves.

c. Liquid-Vapor Mixer

The mixer is shown in Figure 3.3. It was constructed from 3 x 3 x 1 inch pipe "tee." two 3-inch to 1-inch bushings and two pieces of one-inch pipe which were threaded for about two inches and are beveled at the ends. The details are shown in Figure 3.4. The ends of the pipe were adjusted until a suitable mixing is established. The air was introduced axially and the water was introduced into the stream in the tapered passage between the pipe ends.

d. Liquid-Vapor Separator

The separator was composed of a stainless steel rectangular tank which is fitted with a series of baffles. This device slowed the fluid down and allowed the vapor to escape from the liquid and pass into the room atmosphere.

e. Circular to Rectangular Transition Pieces

A set of four transition sections of stainless steel were constructed to change the flow channel from circular to rectangular. These were designed with flanges to permit their connection to the exit side of the mixer and to the test section. The exit ends of the transition sections matched the geometry of the test sections.

f. Test Sections

The test sections were constructed of lucite, with a wall thickness of 0.250 inch and flanges of 0.050 inch thick lucite. The test section was 10 ft long and was composed of three pieces. The two end pieces were each 4 ft long and were of constant cross section. The middle pieces for the uniform channel tests were also of constant cross section. For those tests where an abrupt change in cross section was desired, six sections, two feet in length were constructed with a change in cross section occurring at the middle of each. The two pieces of
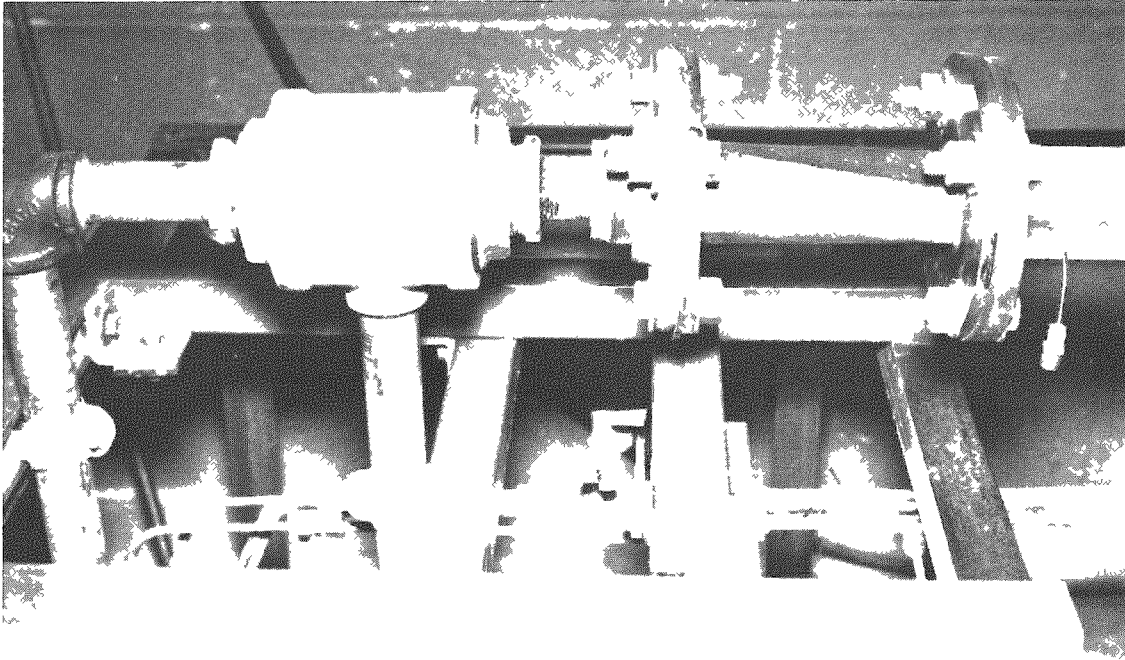
Figure 3.3 Liquid-Vapor Mixing Tee and Transition Piece
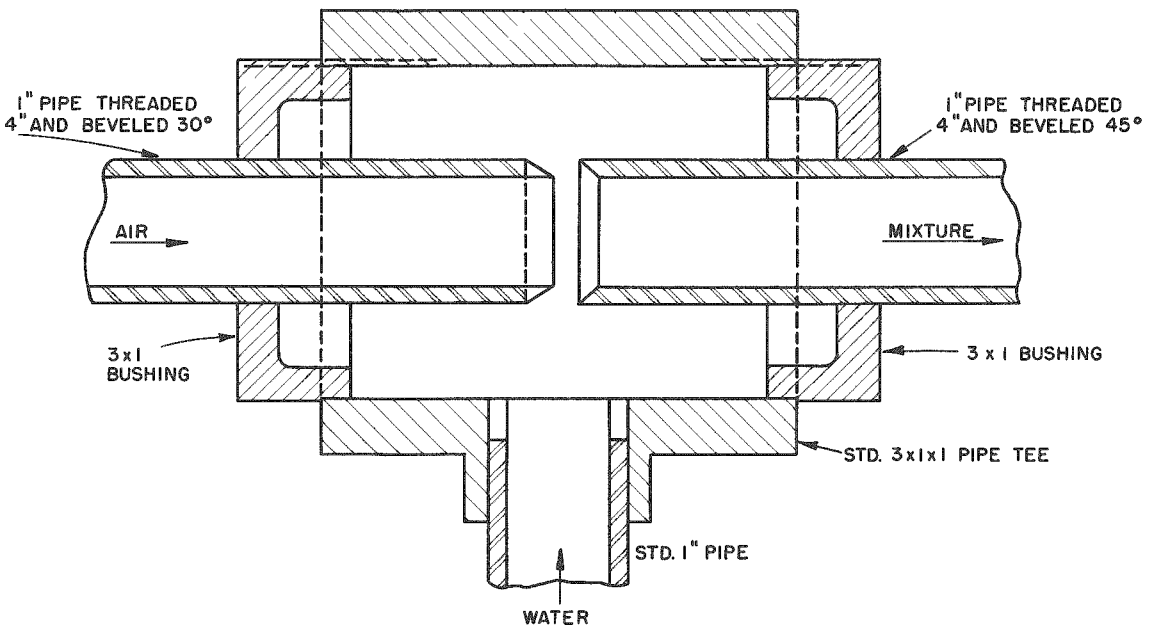
Figure 3.4 Details of Mixing Tee

constant cross section were connected to the ends of the two-foot transition sections by flanges and bolts. A cork gasket was used between the flanges. Care was taken during the assembly to maintain alignment of the test section components and to avoid any interference of the gaskets with the flow. Test section components are shown in Figure 3.5.

Pressure taps were located in the test sections as shown in Figure 3.6. They were placed in the bottom of the channel to eliminate the introduction of air into the manometer lines which would lead to incorrect readings. The pressure taps were pieces of one-eighth inch stainless steel tubing which were cemented into drilled holes in the test section wall with Minnesota Mining and Manufacturing Company EC801 Sealer.

3. Pressure Measurement

Initially an attempt was made to measure the pressure difference between pressure taps with a manometer system with the manometer fluid under water. A system of reservoirs was devised to trap the air which would enter the tubing. It was determined that the lack of reproducibility of the pressure drop data could be traced to the air which would enter the lines between the trap and the test section. The fluctuations in pressure were also too large to permit accurate readings of the pressure drop.

To eliminate this difficulty two steps were taken. Pieces of capillary tubing approximately 3.5 cm. in length with a bore of approximately 0.5 mm were inserted in the pressure line adjacent to the pressure tap. The viscous damping of the liquid in the capillary tube eliminated the undesirable fluctuations of the liquid level in the manometer tubing.

The copper tubing used with the manometers was replaced by clear Tygon tubing of 0.25 inch inside diameter. This tubing was fastened to a vertical panel and connected to a manifold at the top.
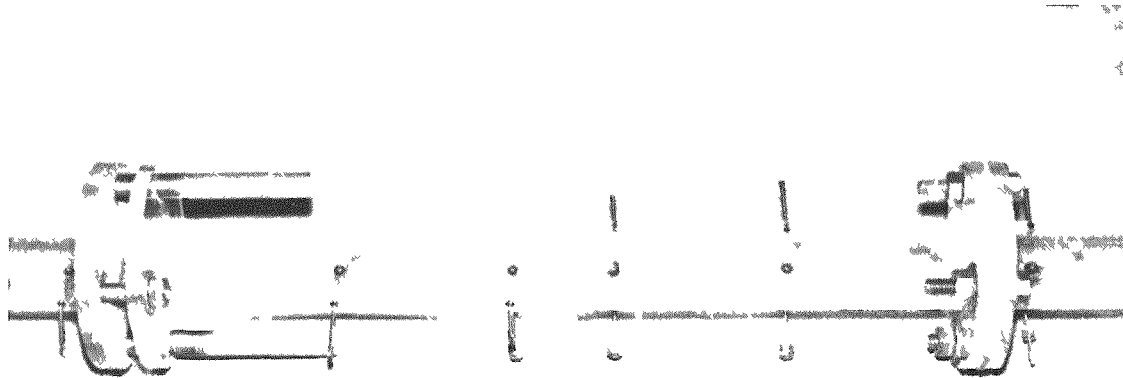
Figure 3.5 Test Section Components Showing
Assembly Process
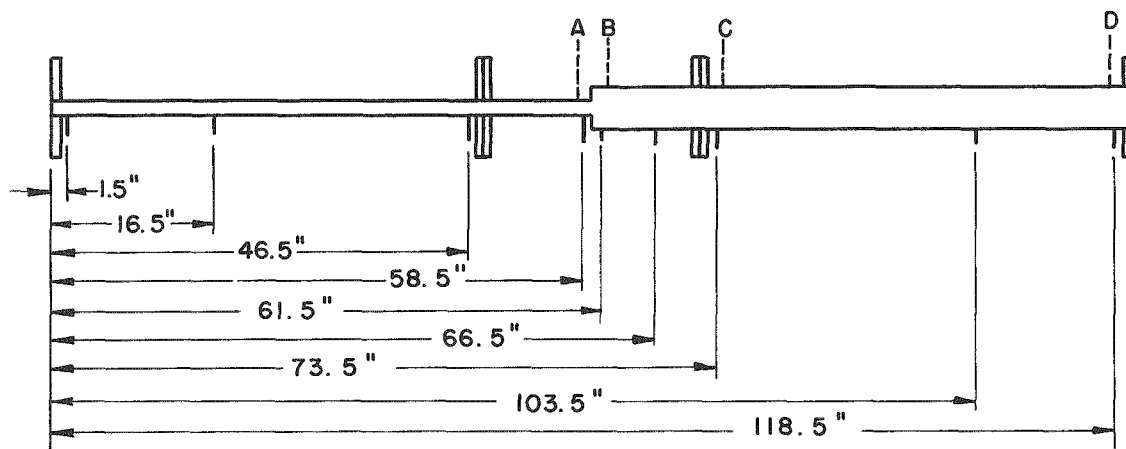
Figure 3.6 Pressure Tap Locations in Expansion
Test Section Assembly

This manifold was equipped with a valve to vent it to the atmosphere, and was connected by additional Tygon tubing to a regulated air supply. The air supply was connected to one leg of a manometer filled with mercury. The other leg of the manometer was open to the atmosphere. The difference in height of the two columns of this manometer indicated the difference in pressure between the air in the manifold and atmospheric pressure. This system is shown in Figure 3.1. In operation the water rose in the tubing until its height was sufficient to balance the pressure difference between the pressure tap and the air in the manifold. As the air in the manifold was static, the pressure above each water column in the tubing was constant. The difference between the heights of the water columns then indicated the difference in pressure between the corresponding pressure taps. The height of the water column, in terms of pressure, added to the pressure in the manifold was equal to the gage pressure at the pressure tap. This system combined the functions of the piezometer tube for measuring pressure with that of the manometer for measuring pressure difference.

4. Void Measuring Equipment

On the basis of the mockup study for the measurement of voids, the traversing technique was selected for the determination of the voids for the air-water mixtures. The equipment shown in Figures 3.7 and 3.8 was developed to perform this function.

The source and the detector with its lead shield and window were aligned and held rigidly in a "U" shaped frame which straddled the test section. This frame was raised or lowered by two cables which passed over fiber pulleys and were connected to a pair of threaded steel blocks. These blocks were threaded with opposite 1/2-NF-20 threads, were fitted on a common threaded shaft, and were restrained from rotating with the shaft by the main supporting frame. When the shaft, driven by a 4.1 rpm constant speed motor, was rotated the blocks
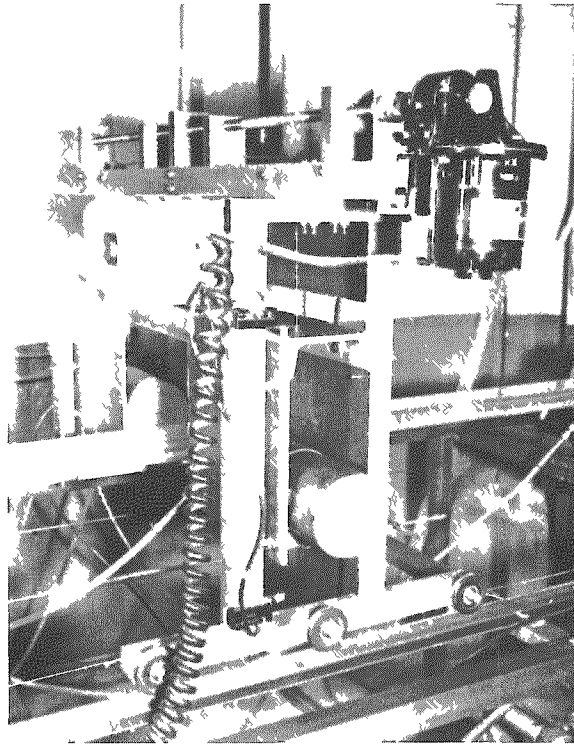
Figure 3.7 Side View of Traversing
Mechanism
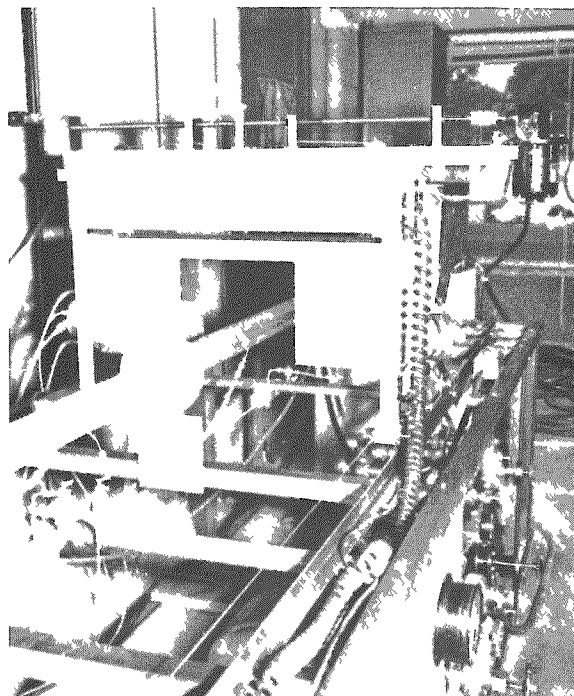
Figure 3.8 Front View of Traversing
Mechanism

were separated or moved closer together lowering or raising the
source-detector assembly at a uniform speed. The source detector
assembly was restrained from swinging or rotating by the frame,
and the two-point suspension resulted in uniform vertical translation
of this assembly. The vertical motion of this assembly was limited
by micro-switches which could be fixed at any desired position.

The void measuring system moved horizontally on grooved
fiber wheels which rolled on a rail. Horizontal motion was obtained
by means of a cable-pulley system, driven by a motor, which is
shown in Figure 3.9. The horizontal travel was limited by fixed
micro-switches.

Both the vertical and horizontal motions were controlled by
a single control box.

The power supply, amplifier, and recording system were the
same as those described in the mockup study in Chapter II, and are
shown in Figure 3.10. A Sola constant voltage transformer was in-
serted between the laboratory 110 V A.C. power supply and the
recording instrumentation to minimize the effect of line voltage
fluctuations.
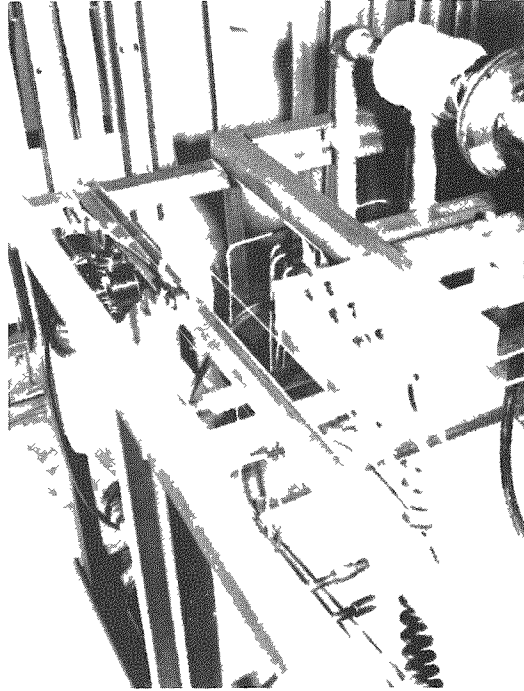
Figure 3.9 View of Horizontal Positioning
Drive System and Control Box
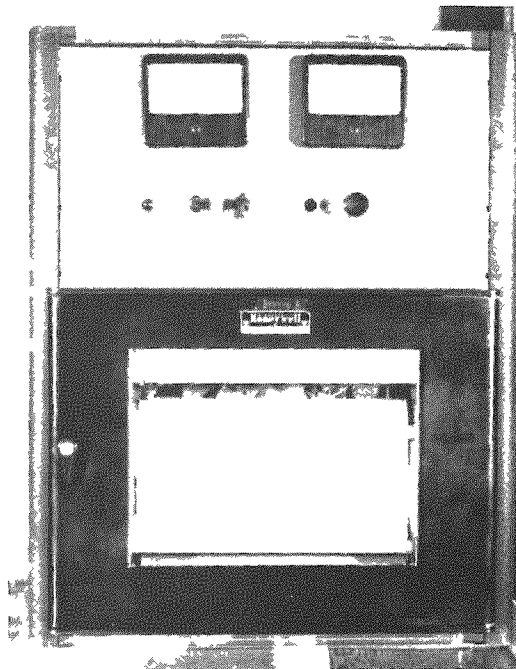
Figure 3.10 Amplifier, Power Supply
and Recorder

Chapter IV
OPERATING PROCEDURES

1. Preparation

The following procedures were adopted for the operation of the test equipment. It was felt that uniformity of procedure was necessary to minimize any error which might occur when different operators were using the equipment.

The test section components were flanged, and were bolted together with a cork gasket between the flanges. Positive alignment of the components was assured by the use of machined brass dowels which fitted snugly into the bolt holes in the flanges. A pair of these dowels were fitted diametrically opposite to each other through the flanges and held the flanges in alignment while the bolts were inserted and tightened in the other pair of holes. The dowels were then removed and the second pair of bolts were inserted and tightened. The alignment of the gasket was visually checked during this operation to make certain that it would seal the joint without obstructing the flow.

Both the end supports for the test section and the center supports were adjustable to facilitate the leveling and alignment of the test section. The longitudinal leveling of the test section was most easily accomplished by filling it partially full of water when the end flange and pressure tap connections were completed. The supports were adjusted until the position of the water level in the test section indicated that the section was level. A hand level was used to check the transverse level of the section. The section was rotated about its axis to level it in this plane.

2. Operation

At the start of each days operation the tube was empty and dry. The empty traverses were taken at this time. The recording

instruments were checked for zeroing and any necessary adjustments in voltage or current amplifier settings were made prior to the empty runs. These settings were unchanged during the days operation.

While the traverses of the empty tube were being made, the water in the pump was drained, and the pump flushed out with water from the tank. Stainless steel was used throughout the loop wherever possible, to minimize the water contamination by rust, but the pump casing and impeller were not stainless. Flushing the pump out before starting a days run minimized the contamination of the water. Demineralized water was used in all of the runs.

When the empty traverses had been completed, the water flow was started and, with the channel full of water, the full runs were taken. During this time the water flow manometer lines were bled to remove any air in the lines. The pressure measuring system was also purged of air in the lines. A visual check of the transparent Tygon tubing insured that the lines were free of air.

The proper air orifice was selected and the air flow regulator was adjusted until the pressure at the orifice was 75 psig. The air and water flow rates selected were established by adjusting the flow regulating valves until the flow manometers indicated the proper orifice pressure drop.

The void traverses for the two-phase flow run were then started. Care was taken to insure that the traverses were always made in the same direction at a given position along the channel. While the traverses were being made the pressure readings at the various taps were recorded, the temperature of the water in the tank noted and recorded, and the flow rates checked and recorded.

After the last run for a day the water in the test section was blown out. A flow of air was maintained through the section overnight in order to dry it out in preparation for the next set of empty traverses the following day.

The high voltage power supply and current amplifier were left on overnight to minimize any drift during the calibrating empty and full runs in the morning due to instability of the instrumentation while it was warming up. The empty and full traverses taken each day, or at the beginning of the runs on a new set of sections, served to calibrate the instrumentation, source, and channel, and eliminated the need for detailed knowledge of variation in source strength, long term changes in instrumentation characteristics or small variations in channel properties.

The pressure readings were taken by observing the height of the water column in the Tygon tubing. This height could be raised or lowered by changing the air pressure in the manifold connecting the tubing. If the total pressure drop were too great to be recorded at a single pressure setting, some of the tubes were closed off with tube clamps and the manifold pressure adjusted so that the pressure drop between the remaining taps could be determined. If necessary, the total pressure drop could be determined by separate measurements of the drop between each consecutive pair of taps. The air pressure in the manifold was indicated by a mercury filled manometer with one leg open to the atmosphere. This pressure was recorded for each run, and for each set of drops recorded.

Chapter V
FLOW PATTERNS

1. Introduction

The pattern of flow in a horizontal channel is dependent upon the complex interaction of the gravitational and hydrodynamic forces both interphase and intraphase, and the channel geometry. The study of these patterns has been carried out by various investigators. Their results are presented in the following paragraphs. They have attempted to distinguish the flow patterns primarily by visual observation, although reports have been made on the use of high-speed photography, motion pictures and stroboscopic techniques.

Alves[9] divided the flow pattern in horizontal pipes into the following seven categories based upon his observations of air-water and air-oil systems, and on the work of others. With a horizontal pipe flowing full of liquid, the types of flow patterns according to Alves which would result, with increasing gas flow rates are:

1. Bubble flow - flow in which bubbles of gas move along the upper part of the pipe at approximately the same speed as the liquid.

2. Plug flow - large plugs of gas are formed from the coalescence of many bubbles. They may be quite long and fill a large portion of the channel.

3. Stratified flow - the liquid flows along the bottom of the pipe and the gas moves along the top.

4. Wave flow - stratified flow in which the interface is disturbed by waves.

5. Slug flow - the crests of the waves seal the tubes and periodic frothy slugs pass down the tube.

6. Annular flow - the liquid moves in a film along the wall surrounding a core of relatively high velocity gas which has some vapor entrained in it.

7. Spray flow - the vapor phase is carried along dispersed in the gas.

Based on studies in a 1.042 inch inside diameter pipe 16 feet long with 18 inch glass pipe inserts at each end, Alves[9] divided the flow pattern regions according to the superficial velocity of each phase. This division is shown in Figure 5.1.

Huntington[28] et al. added semi-annular and cresting flows to those noted by Alves. These patterns are noted in the transition to annular flow at low and high liquid rates respectively. The investigations were performed in 1, 1-1/2, and 2 inch transparent tubes of 100 foot lengths for natural gas - kerosene mixtures. The correlation of flow patterns versus liquid and gas mass flow rates is shown in Figure 5.2.

Bergelin and Gazely[10] reported the results of their observations, and those of others, for air-water systems in one-inch tubes.

Kosterin[29] studied stratified, plug and spray flows in 1, 2, 3, and 4 inch pipes. Fried[30] used a stroboscopic technique and noted that the liquid moves in a helical path at the pipe wall. Johnson and Abou-Sabe[8] reported that their photographic and stroboscopic techniques were relatively unsuccessful.

The areas of the flow patterns, plotted with respect to flow rate of each phase from the data of Gazely and Abou-Sabe, are shown in Figures 5.3 and 5.4. Johnson and Abou-Sabe used somewhat different designations for the flow patterns noted. This includes flows which were described as pulsating bubble, sluggish annular, stratified slug and stratified bubble. This study was performed in a 0.870 inch inside diameter pipe 15.7 feet in length.

50
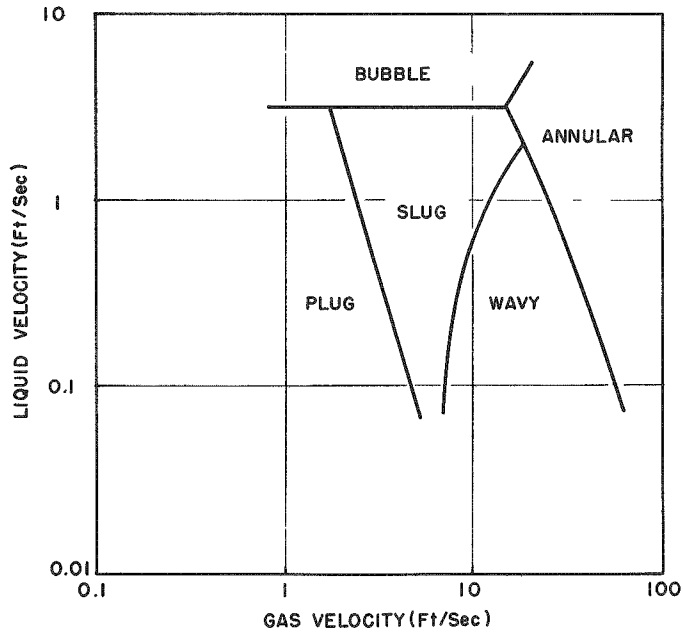
Figure 5.1 Flow Pattern Regions Proposed
by Alves
(1.042-inch i.d. pipe   air-water and air-oil mixtures)
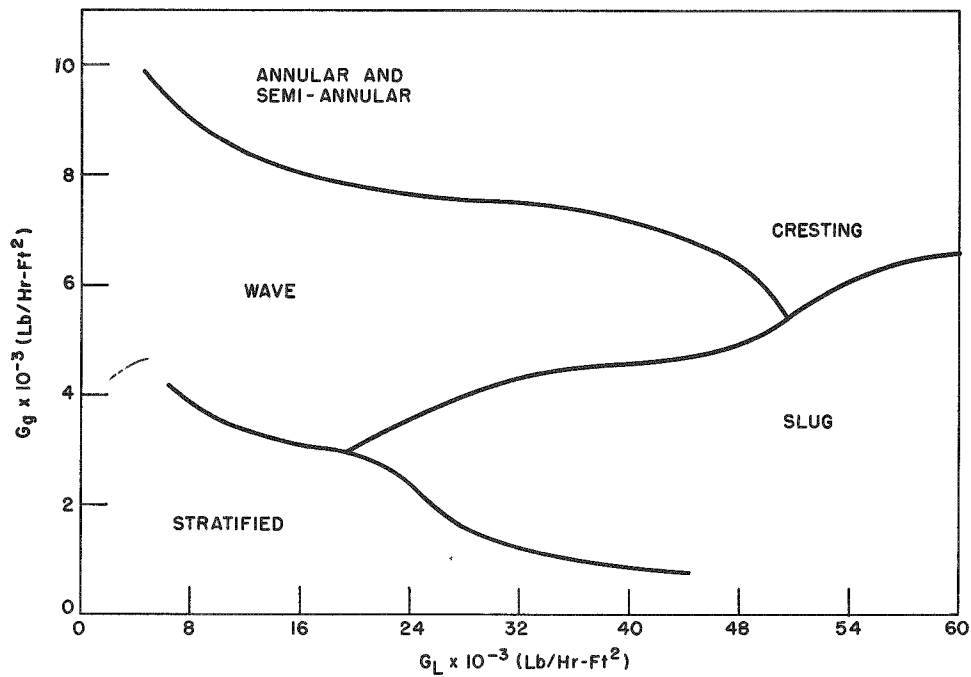
Figure 5.2 Flow Pattern Regions Suggested
by Huntington et al.
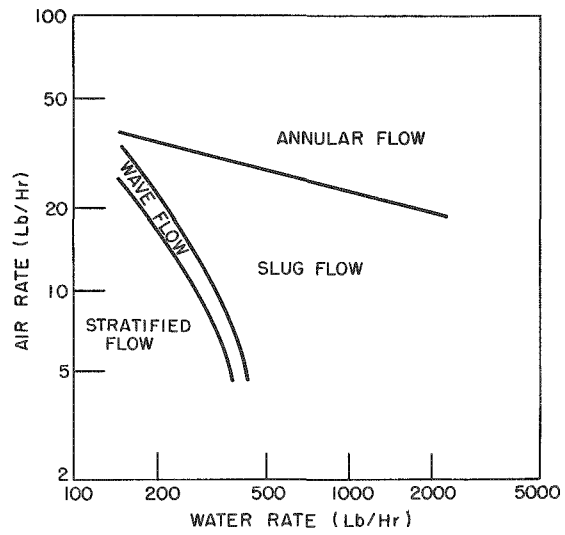
Figure 5.3 Limits of Various Types
of Flow by Gazely
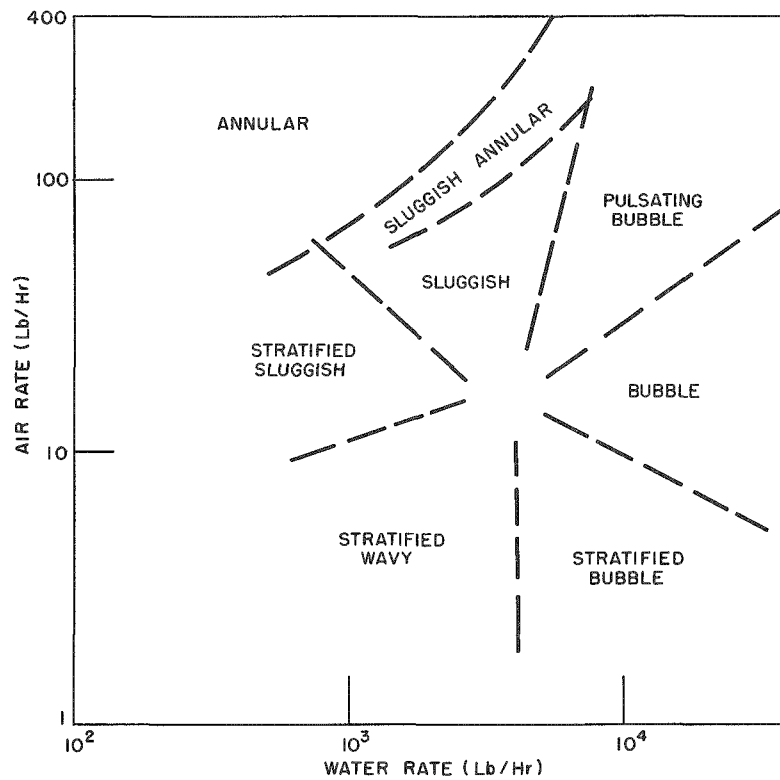
Figure 5.4 Areas of Flow Patterns for Flow
of Two-Phase Air-Water Mixture
in a 0.870 I.D. Horizontal Tube
from Abou-Sabe

Martinelli[4] and his associates made a visual study of the flow patterns resulting from the study of the flow of various hydrocarbons and air. They reported:

Liquid Rate	Gas Rate	Flow Pattern
Very low	Low and medium	Stratified or wavy
Very low	High	Annular
Low	Low	Plug, stratified, or wavy
Low	Medium	Plug, stratified, or wavy
Low	High	Annular
Medium	Low	Bubble
Medium	Medium and high	Special annular
High	Low, medium, and high	Froth

Special annular flow is described as annular flow, with waves moving with different velocities on the upper and lower surfaces of the pipe. Froth flow is a turbulent mixture of liquid and gas bubbles. These tests were performed in a one-inch diameter glass pipe over twenty feet in length.

Krasiakova[31] investigated the flow pattern problem for air-water systems in a 30 mm diameter pipe. The results of his observations are shown in Figure 5.5 where the flow pattern regimes are defined in terms of the superficial velocity of each phase. His descriptions of the flow patterns are somewhat different from those of other investigators.

Baker[32] obtained a correlation of the data of Gazely,[10] Jenkins,[33] Alves[9] and Kosterin[31] making use of parameters to take into account the variation of fluid properties for different systems. The various flow pattern regimes are plotted in terms of G/λ and $L\lambda\psi/G$, where G is the gas mass flow rate, L is the liquid flow rate,

$$\lambda = \left[\left(\frac{\rho_g}{0.075}\right)\left(\frac{\rho_\ell}{62.3}\right) \right]^{1/2} \quad \text{and} \quad \psi = \left[\left(\frac{73}{\nu}\right) \mu_\ell \left(\frac{62.3}{\rho_\ell}\right)^2 \right]^{1/3}$$
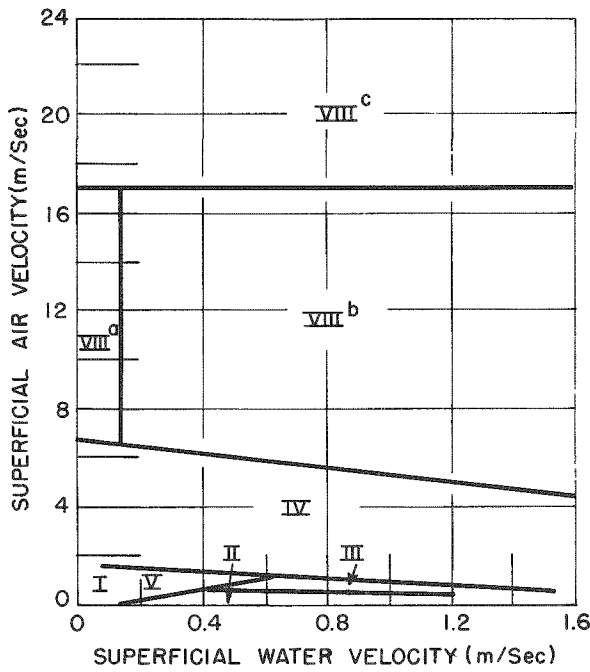
I. Primary Stratified Flow.
II. Bubble Flow (Bubble chains less than 500 mm - minimum bubble size 10 to 20 mm).
III. Bubble Flow (same except minimum size 2 - 3 mm).
IV. Bubble Flow (bubbles less than 500 mm without heads).
V. Bubble Flow (size greater than 500 mm).
VI. Splashing Flow.
VII. Secondary Stratified Flow.
VIII^a, VIII^b, VIII^c, Film Flow without spray, with some spray, and with more spray.

Figure 5.5 Krasiakova's Proposal for Boundaries of Characteristic Flow Regimes
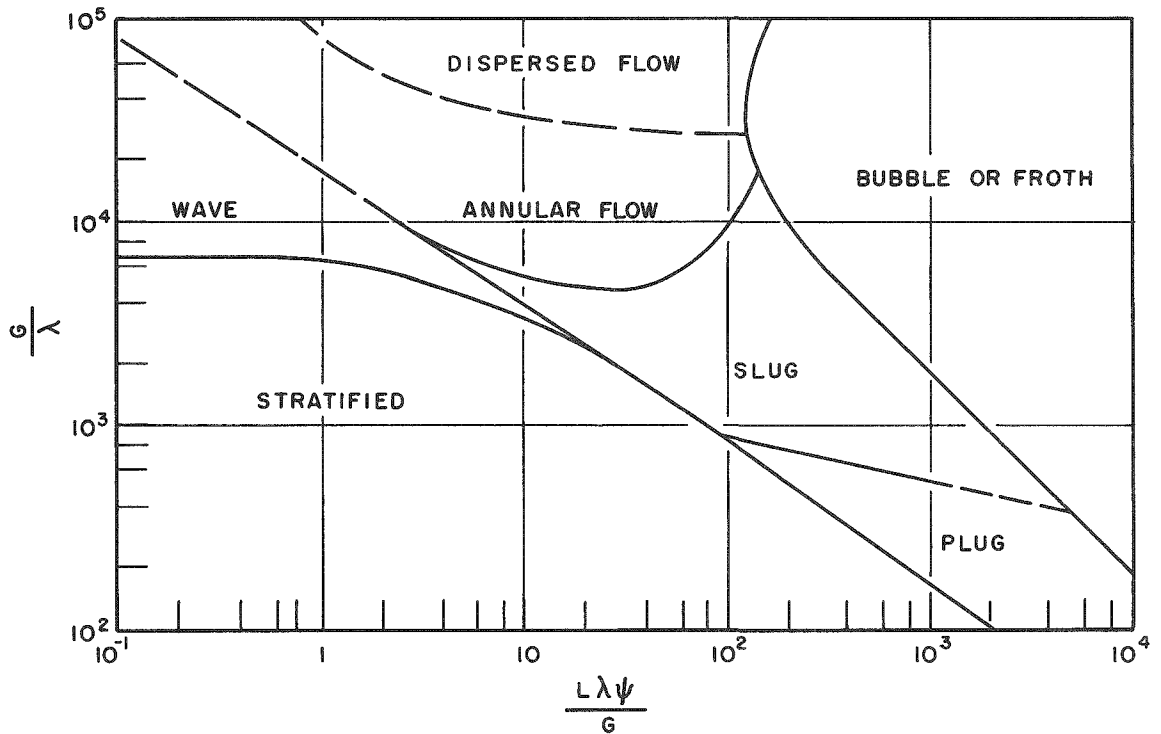
Figure 5.6 Flow Pattern Region Correlation of Baker

The density of the gas and liquid are in pounds per cubic foot, ν is the surface tension of the liquid in dynes per centimeter, and the liquid viscosity, μ_ℓ, is in centipoises. This correlation is reproduced in Figure 5.6.

The other investigations of flow patterns in horizontal pipes include those of Galegar[34] et al, Reichart[35] and Frazier.[36] From a comparison of the results reported by the various investigators it is evident that there is disagreement as to the bounds of the regions of each flow pattern and the types of flow observed.

2. Experimental Investigation

The previously mentioned studies were conducted in pipes of circular cross section. In this study the effect of the flow rate of each phase on the flow pattern was examined for three sections of rectangular cross section. The horizontal inside dimension was held constant at two inches. Vertical dimensions of 1-, 1/2-, and 1/4-inch were studied. The flows were normally run at a constant weight flow rate of water, and the air flow rate was increased gradually, with the values of the air rate at transitions of flow patterns being noted. Some additional data was taken with constant air weight flow rates with the water rate being varied and noted as the flow pattern changed.

3. Correlation of Results

While the results of this study are presented in terms of flow pattern regions bounded by lines, as in the case of the work of other investigators, it must be noted that the transitions are really bands rather than lines. Considerable hysteresis was noted in the study of this problem. With this limitation noted, the results of the flow pattern study are presented in Figures 5.7, 5.8 and 5.9.

It was noted that the decrease in channel spacing causes the region of stratified flow to be greatly decreased or entirely eliminated. The flow which would have been wave flow with a wider channel
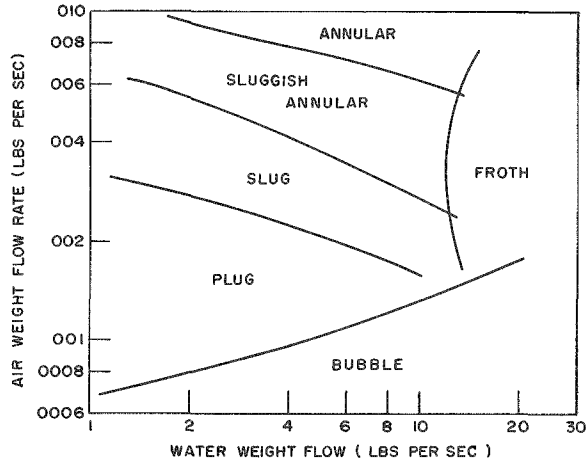
Figure 5.7 Flow Pattern Boundaries in 1/4 x 2 inch Channel
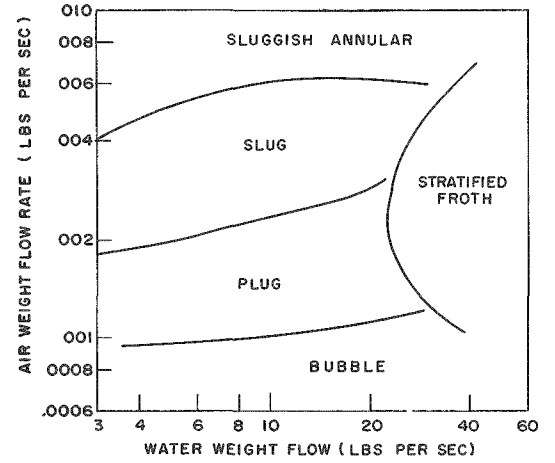
Figure 5.8 Flow Pattern Boundaries in 1/2 x 2 inch Channel
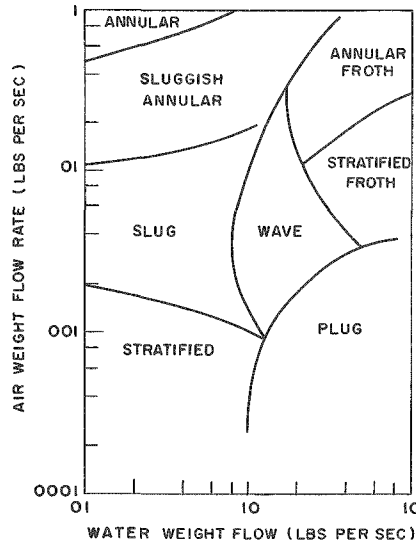
Figure 5.9 Flow Pattern Boundaries in 1 x 2 inch Channel

spacing is sluggish in channels of narrow spacing. When waves are formed, only small amplitudes are possible before they make contact with the top of the channel and the flow becomes slug flow. The flow patterns noted in the 1-inch by 2-inch section were photographed and are shown in Figures 5.10 to 5.17. The designations for the flow patterns are similar to those of Alves[9] and Abou-Sabe.[8] The region of froth flow was divided into stratified froth and annular froth. In the stratified froth region the liquid phase mixed with bubbles of gas moves along the bottom while the rest of the gas moves along the top. There is a froth interface between the lower liquid film and the gaseous core in the annular froth flow pattern. This flow pattern was also noted by Krasiakova[31] in round tubes.

In the sluggish annular flow pattern the flow was essentially annular, but was periodically disturbed by frothy slugs passing down the tube. The region of this pattern was too large to permit it to be considered as a transition region.

The type of flow pattern present is dependent to a certain extent on the length of the flow channel. In particular flows which may initially be bubble flow, with many small bubbles moving along the top surface tend to become plug flow as the many bubbles coalesce to form plugs of gas.

Information on the type of flow pattern to be expected is useful to the designer because the pressure drop accompanying certain flows is very unsteady with large pulsations of pressure. This is particularly true of slug and plug flow patterns.

Figure 5.10   Stratified Flow Pattern

Figure 5.11   Plug Flow Pattern

Figure 5.12   Wave Flow Pattern

Figure 5.13   Slug Flow Pattern
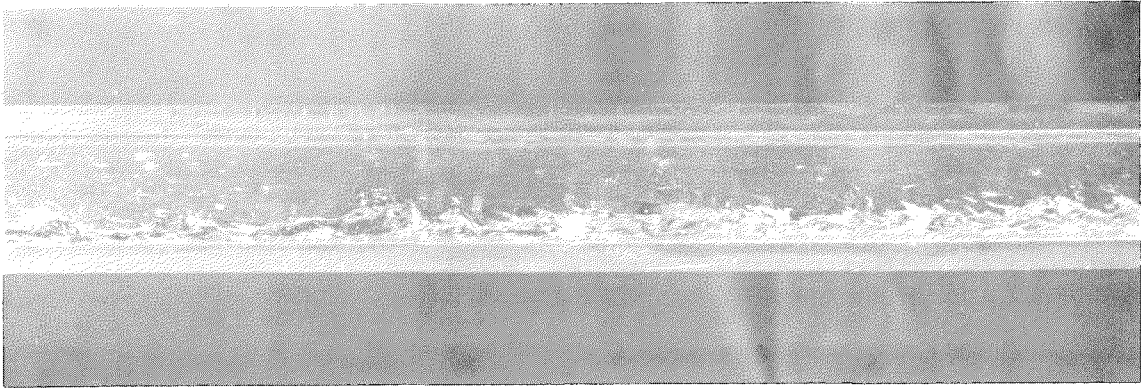
Figure 5.14 Sluggish Annular Flow
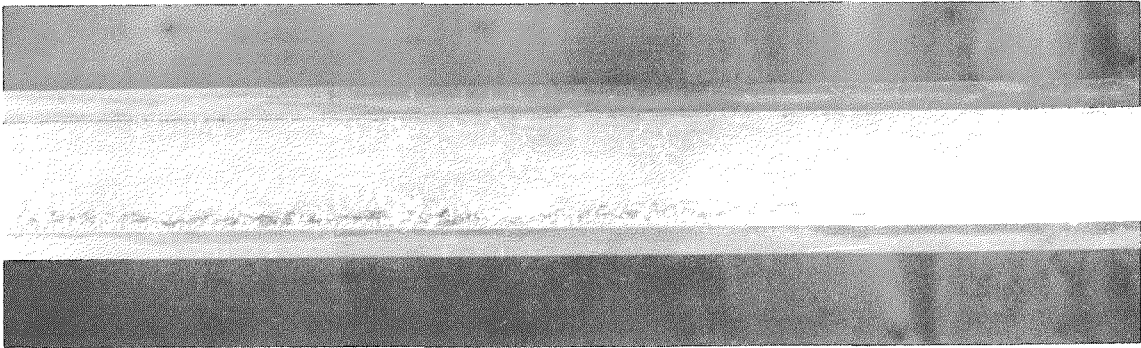
Figure 5.15 Annular Flow Pattern
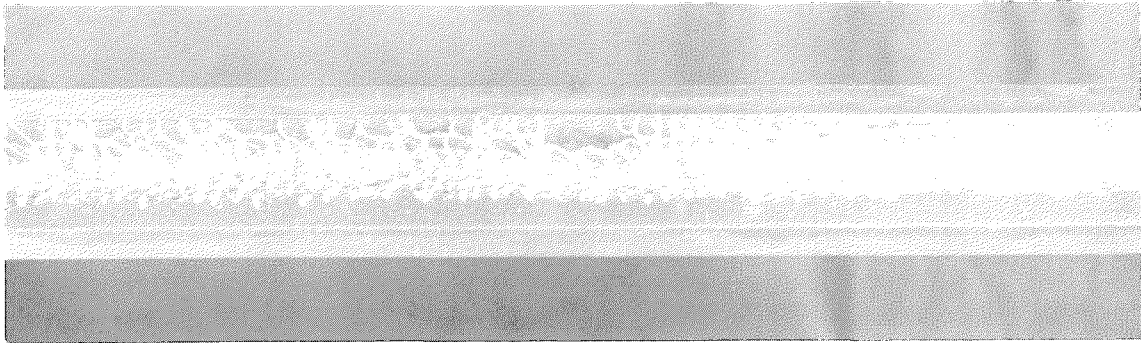
Figure 5.16 Stratified Froth Flow
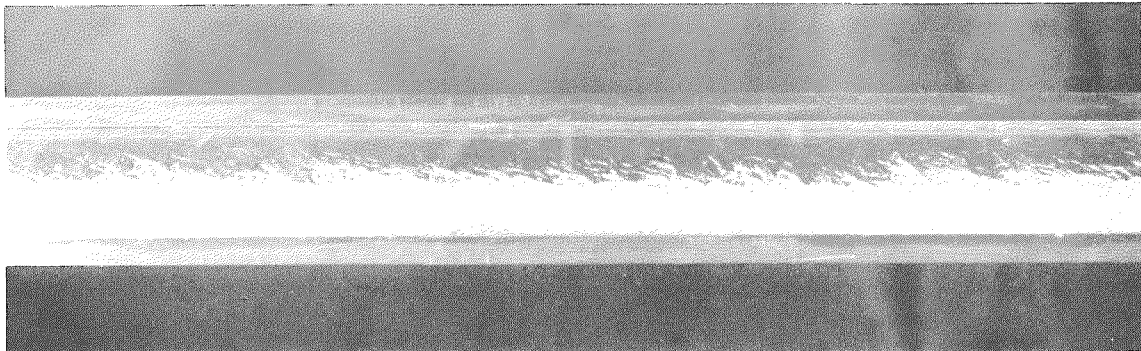
Figure 5.17 Annular Froth Flow

Chapter VI
VAPOR VOLUME FRACTIONS

1. Introduction

A knowledge of the fraction of each phase present in a channel is a prerequisite for the understanding of two-phase flow phenomena. As has been noted in Chapter II, this problem has been studied by many investigators, and by various techniques. A report is presented here of the results of a study of void fractions or vapor volume fractions in horizontal rectangular channels of various dimensions, with, and without, abrupt changes in their cross sectional areas. A comparison of the results of this study with those of other investigators is also presented.

Lockhart and Martinelli[6] present a correlation of the liquid volume fraction, R_ℓ against the parameter χ for various flow mechanisms and for the flow of air and various liquids including water and a number of hydrocarbons. The parameter χ is defined as the square root of the ratio of the pressure drop of the liquid phase to the pressure drop of the gas phase when each flows in the channel separately at its own weight flow rate. The results of correlation of their data with this parameter is shown in Figure 6.1. The correlation is based on the data of Thomsen,[37] Taylor,[38] and that of Lockhart.[39, 40]

The data of Thomsen and Taylor were obtained by trapping the flowing mixture between quick acting valves, blowing down the pipe and measuring the liquid content obtained. The results so obtained would be low because some of the liquid would be left on the walls. Lockhart also used quick acting valves, but used a volatile solvent to wash out the tube, and then evaporated the solvent. His values are probably high because of solvent remaining in the liquid. The results of the correlation based on both sets of data indicate that the errors involved are not large.
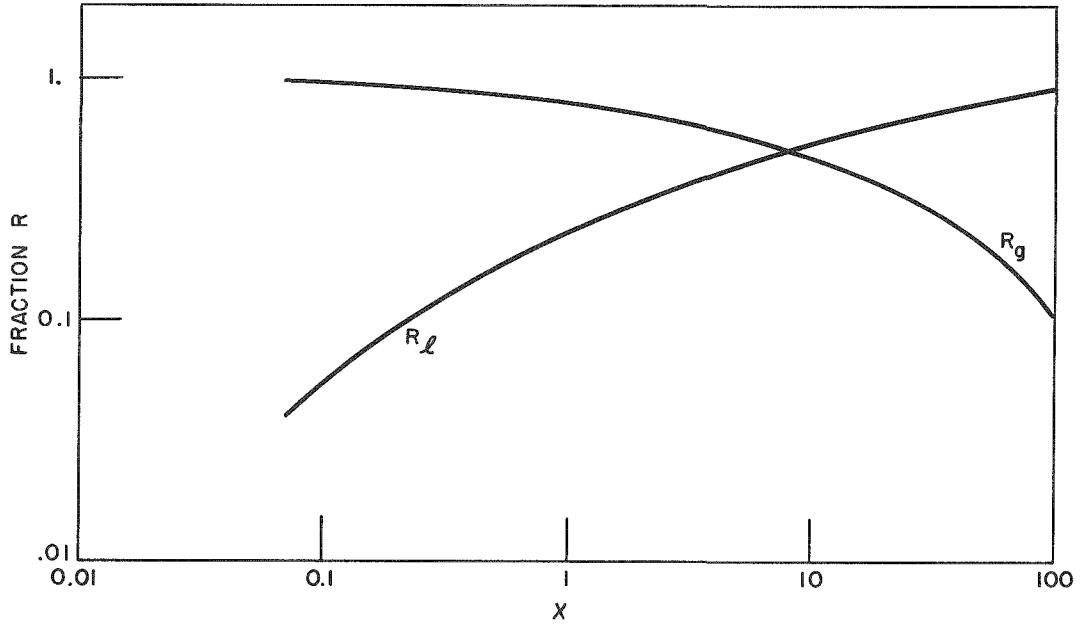
Figure 6.1 Relationship between $R\ell$, R_g and
χ from Lockhart and Martinelli
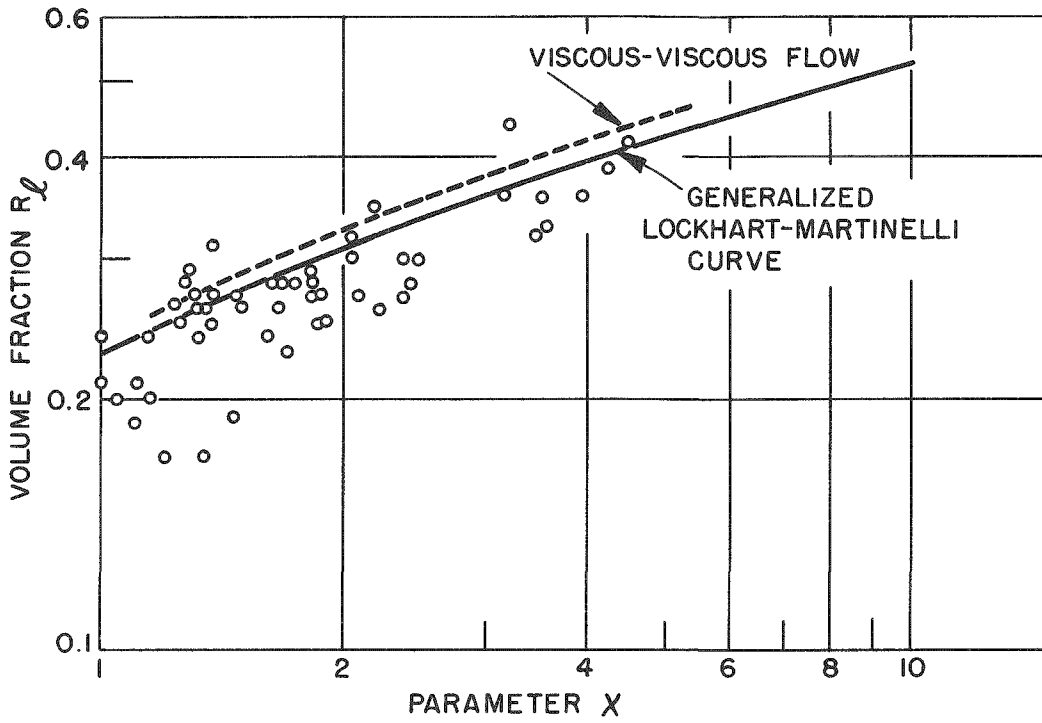
Figure 6.2 Liquid Volume Fraction vs. χ,
McElwee's Data

In a discussion of the Lockhart and Martinelli paper Putnam presents the results of a study in vertical tubes by McElwee[41] for liquid holdup, or volume fraction. McElwee's data are compared with the Lockhart-Martinelli curve in Figure 6.2. In the discussion following the Lockhart-Martinelli paper, there is disagreement as to whether the data of Lockhart are high for the liquid volume fraction, or that of McElwee too low.

The study of volume fractions in stratified flows was conducted by Bergelin and Gazely.[10] The volume fractions were determined from the measurements of the interfacial position of the two phases. The results of this investigation are shown in Figure 6.3. For this data, a strong dependence is seen to exist between the flow-type and the volume fraction of each phase. This same flow-type dependence was not noted in the data presented by Lockhart and Martinelli.[6] In their investigation of non-isothermal volume fraction relationships, Johnson and Abou-Sabe[8] made use of quick acting valves at each end of a horizontal pipe to trap the two phase mixture. The volume of air present was determined by filling the test section with water from a graduated container. The liquid volume fraction data is compared with the isothermal correlation of Lockhart and Martinelli in Figure 6.4, where it is seen that the results are lower than the Lockhart curve. It is also noted that there is some separation due to flow pattern.

Alves[9] also made use of a pair of valves to trap the two-phase mixtures in a pipe-line contactor to determine the liquid volume fraction. These data were taken for the entire contactor including bends. Tests were conducted for air-water and air-oil mixtures, and the results are shown in Figures 6.5 and 6.6. These data for the liquid volume fraction also tend to be below the Lockhart-Martinelli curve.
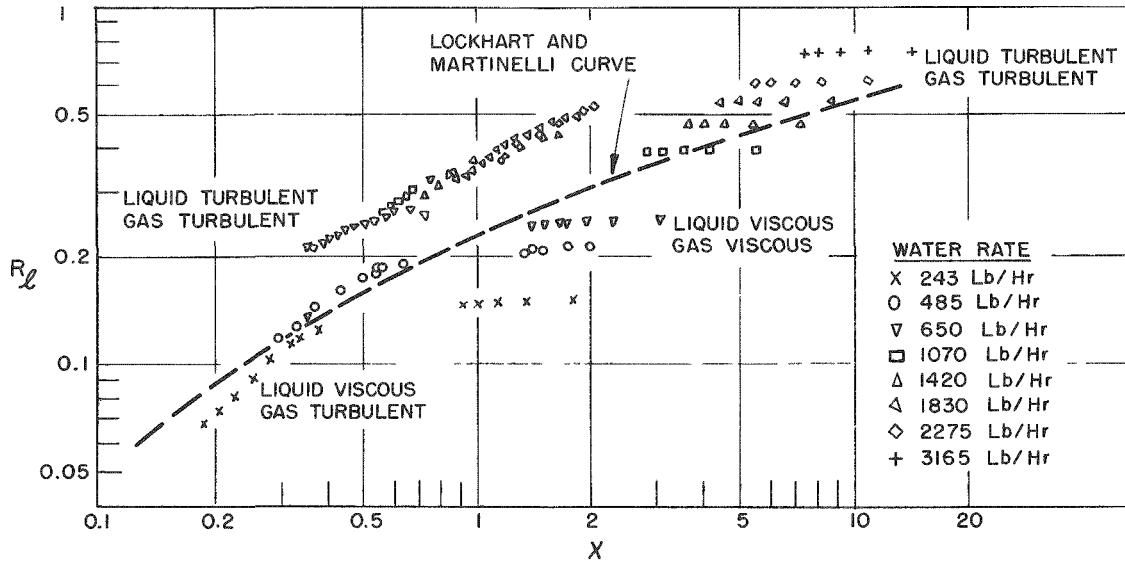
Figure 6.3 Comparison of Liquid Holdup Data of Bergelin
and Gazely for Air-Water Mixtures with
Lockhart-Martinelli Correlation
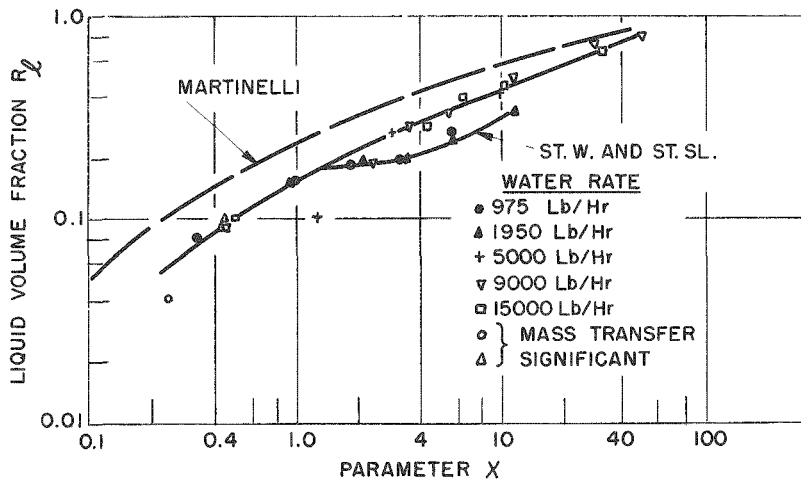
Figure 6.4 Correlation of Liquid Volume Fraction
by Johnson and Abou-Sabe
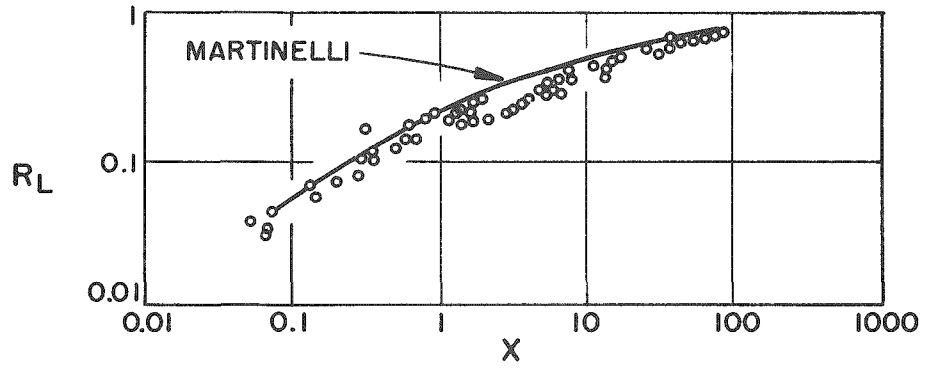
Figure 6.5 Liquid Holdup Correlation of Alves for
Air-Water Mixtures
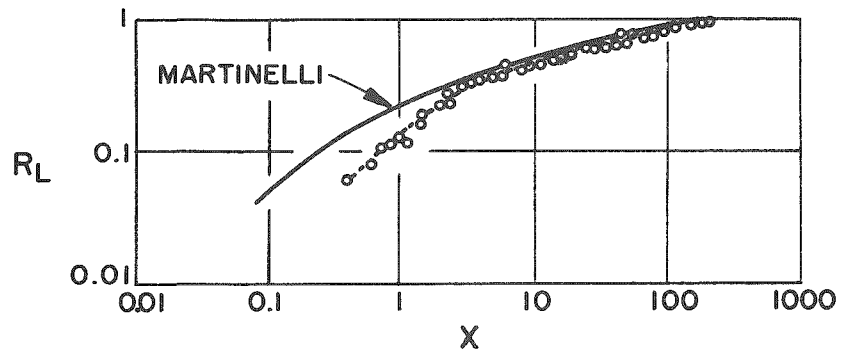
Figure 6.6 Liquid Holdup Correlation of Alves for
Oil-Air Mixtures

Chisholm and Laird[14] investigated the isothermal two-phase flow of air-water mixtures in smooth and in artificially roughened tubes. They also made use of quick closing cocks to trap the two-phase mixture in the test section to determine the liquid volume fraction. The results of this investigation were presented in terms of a modified Martinelli parameter $\bar{\chi}$ which is defined by

$$\bar{\chi} = \left(\frac{G_\ell}{G_g}\right)^{0.875} \left(\frac{\mu_\ell}{\mu_g}\right)^{0.125} \left(\frac{\rho_g}{\rho_\ell}\right)^{0.5} \tag{6.1}$$

This parameter reduces to the Martinelli parameter χ if the exponent n in the Blasius equation for the friction factor

$$f = \frac{C}{N_{Re}{}^n} \tag{6.2}$$

is equal to 0.25, which is the value usually taken for a smooth pipe.

The results of their investigation are shown in Figure 6.7 for smooth tubes and in Figure 6.8 for a tube with uniform sand roughness. The Lockhart-Martinelli curve is presented in Figure 6.7 for comparison. It is seen that the smooth tube data is below the Lockhart-Martinelli curve for liquid volume fraction. Chisholm and Laird also present two equations which are shown in these figures, which represent the data to within ± 25%.

Dengler[42] employed a soluble radioactive tracer to investigate the void fraction in the vertical flow of vaporizing water in heated tubes. His results are in general agreement with those of the other investigators.

An investigation making use of the attenuation of gamma-radiation from a selenium-75 source is reported by Isbin[43] et al. This technique was used to study the void fraction or vapor volume fraction in a vertical tube for the natural circulation of boiling water at various pressures. Their values for R_g, shown as a function of quality are consistently higher than the curve of Lockhart and Martinelli.
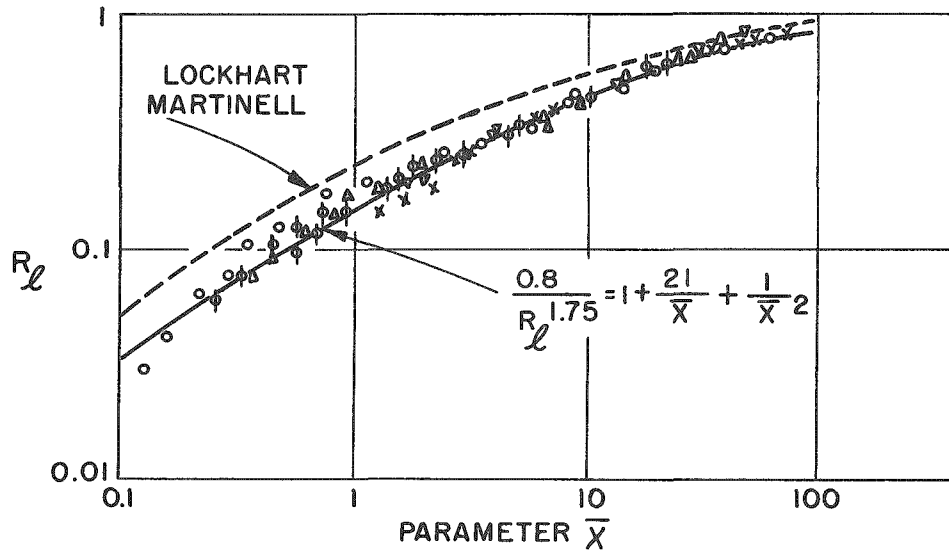
Figure 6.7 R_ℓ as a Function of $\bar{\chi}$ for a Smooth Tube from Chisholm and Laird
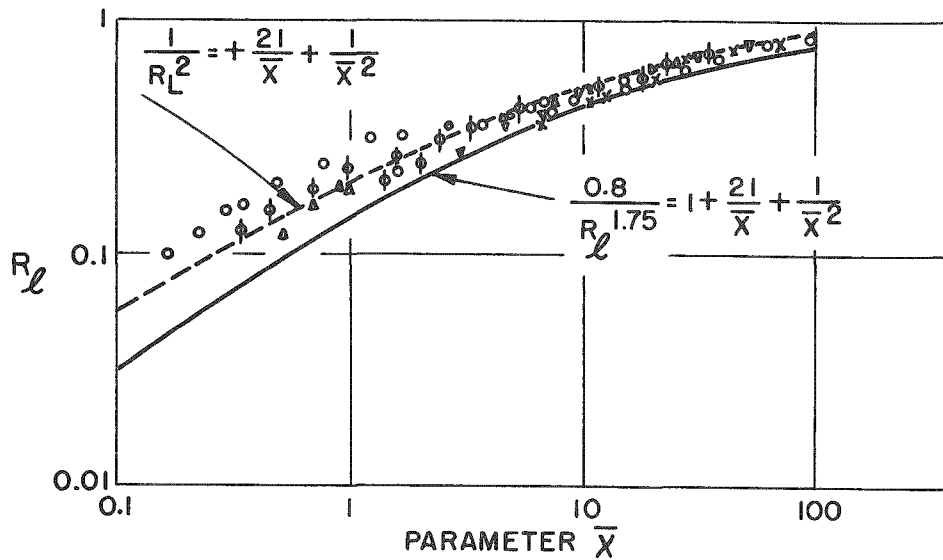
Figure 6.8 R_ℓ as a Function of $\bar{\chi}$ for a Uniform Sand-Roughness Tube from Chisholm and Laird

Gamma attenuation techniques were also used by Marchaterre,[44] Egen[21] et al; Cook[23] and Petrick[15] to determine the vapor volume fraction. McManus[19] studied annular flow only and reported measurements of film thickness on the walls and its dependence on angular position and flow parameters.

2. Experimental Program

Experimental data were taken for flow in the horizontal channels described in Chapter III. The following range of variables was included in the experimental void fraction study:

Quality	0.0005 to 0.0517
Areas	0.25 to 2.00 sq. in.
Area ratios	2:1 to 8:1
Water weight flow rates	0.30 to 3.66 lb per sec
Air weight flow rates	0.001 to 0.06 lb per sec.

For the expansion and contraction runs the void fraction was determined at four positions along the channel, located 2 inches before the change in area and 2, 14 and 58 inches after it. For the tests on channels of uniform cross section two determinations of the void fraction were noted 58 and 118 inches from the inlet end to the test section. The values of the void fraction results are shown in Tables 6.1 through 6.6.

In the determination of the phase distribution across the cross section the value of the local void fraction α, was determined at eleven equally spaced points using the relationships indicated in Chapter II. The average value of α was then determined by numerical integration using Simpson's rule.

Typical plots of the void distribution over the cross section are shown in Figures 6.9 through 6.20. (Position A is two inches before the flow area change and Position B is two inches after it.) These may be compared with the photographs of the corresponding flow conditions

TABLE 6.1

VOID FRACTION DATA, UNIFORM SECTIONS

1/2 inch section			1/4 inch section			1/8 inch section		
Quality	χ_{tt}	α	Quality	χ_{tt}	α	Quality	χ_{tt}	α
.0319	1.03	.75	.00224	12.6	.46	.00271	1.06	.52
.0113	2.92	.68	.00448	6.7	.56	.00382	7.8	.57
.00146	18.3	.48	.0153	2.23	.76	.00540	5.7	.63
.00232	12.2	.45	.00116	22.2	.39	.00151	17.8	.40
.0167	2.08	.70	.00170	16.0	.42	.00214	13.0	.42
.0517	.74	.84	.00604	5.1	.60	.00267	10.8	.50
.0348	1.07	.77	.00073	33.2	.26	.00113	22.8	.33
.00224	12.6	.46	.00138	19.0	.36	.00224	12.6	.47
.0120	2.78	.70	.00204	13.6	.44	.00387	7.7	.50
.00103	24.3	.58	.000635	37.2	.25	.0064	4.9	.61
.0127	2.65	.70	.00108	23.5	.36	.0116	2.9	.68
.00563	5.4	.64	.000518	45.	.20	.0164	2.1	.71
			.000978	25.7	.31			
			.00145	18.3	.38			

TABLE 6.2

VOID FRACTION 2.0 INCHES BEFORE EXPANSION

.125-E-1				.125-E-5				.125-E-.25		
Quality	χ_{tt}	α		Quality	χ_{tt}	α		Quality	χ_{tt}	α
.01639	2.1	.78		.01639	2.1	.74		.01639	2.1	.73
.01159	2.9	.70		.01159	2.9	.71		.01159	2.9	.68
.00662	4.7	.64		.00662	4.7	.64		.00662	4.7	.63
.00540	5.7	.59		.00540	5.7	.63		.00540	5.7	.65
.00382	7.8	.57		.00382	7.8	.56		.00382	7.8	.58
.00271	10.6	.54		.00271	10.6	.53		.00271	10.6	.52
.00266	10.8	.52		.00266	10.8	.53		.00266	10.8	.53
.00214	13.0	.47		.00214	13.0	.48		.00214	13.0	.49
.00152	17.5	.41		.00152	17.5	.42		.00152	17.5	.48

.25-E-1.0				.25-E-.5				.5-E-1.0		
Quality	χ_{tt}	α		Quality	χ_{tt}	α		Quality	χ_{tt}	α
.00222	12.7	.47		.00222	12.7	.49		.0403	.93	.84
.0151	2.27	.68		.0151	2.27	.769		.0164	2.1	.74
.0345	1.24	.79		.0345	1.24	.84		.0567	.69	.87
.00116	22.6	.45		.00116	22.0	.38		.00245	11.6	.55
.00169	16.0	.47		.00169	16.0	.43		.00103	24.5	.45
.00619	5.0	.69		.00619	5.0	.63		.0129	2.6	.70
.00073	33.0	.37		.00073	33.0	.31		.00564	5.5	.67
.00138	19.0	.47		.00138	19.0	.446		.0114	2.9	.70
.00205	13.6	.53		.00205	13.6	.50		.00147	18.	.49
				.00443	6.8	.575		.0330	1.12	.81

TABLE 6.3

VOID FRACTION 58 INCHES AFTER EXPANSION

.125-E-.5			.125-E-.25			.25-E-.5		
Quality	χ_{tt}	α	Quality	χ_{tt}	α	Quality	χ_{tt}	α
.01639	2.1	.68	.01639	2.1	.71	.00222	12.7	.43
.01159	2.9	.68	.01159	2.9	.69	.0151	2.27	.69
.00662	4.7	.65	.00662	4.7	.60	.0345	1.24	.78
.00540	5.7	.59	.00540	5.7	.65	.00116	22.6	.36
.00382	7.8	.57	.00382	7.8	.60	.00169	16	.41
.00271	10.6	.52	.00271	10.6	.55	.00619	5.0	.60
.00266	10.8	.52	.00266	10.8	.51	.00073	33	.34
.00214	13.0	.49	.00214	13.6	.49	.00138	19	.45
.00152	17.5	.42	.00152	17.5	.44	.00205	13.6	.49
						.00443	6.8	.53

TABLE 6.4

VOID FRACTION 2.0 INCHES BEFORE CONTRACTION

.5-C-.125			.5-C-.25			.25-C-.125		
Quality	χ_{tt}	α	Quality	χ_{tt}	α	Quality	χ_{tt}	α
.00266	10.8	.48	.00222	12.5	.46	.0164	2.1	.72
.00214	13	.46	.0151	2.25	.73	.0116	2.9	.69
.00152	17.7	.39	.0344	1.08	.78	.00663	4.7	.59
.00271	10.6	.53	.00116	22	.42	.00541	5.7	.54
.00382	7.7	.57	.00170	16.0	.47	.00382	7.7	.49
.00540	5.7	.54	.00621	5.0	.62	.00272	10.6	.51
.00663	4.7	.48	.00733	33	.34	.0024	12.8	.43
.0116	2.9	.59	.00138	19	.46	.00193	14.3	.44
.0164	2.1	.61	.00204	13.6	.52	.00137	19.1	.42

TABLE 6.5

VOID FRACTION 58 INCHES AFTER CONTRACTION

1.0-C-.25				1.0-C-.25				1.0-C-.5		
Quality	χ_{tt}	α		Quality	χ_{tt}	α		Quality	χ_{tt}	α
.00266	10.8	.49		.00116	22.	.38		.00238	11.9	.52
.00214	13.	.45		.0017	16.	.46		.039	.96	.82
.00152	17.7	.43		.0062	5.0	.67		.0553	.71	.82
.00271	10.6	.50		.0022	12.8	.55		.0160	2.15	.76
.00382	7.7	.56		.0328	1.13	.82		.0127	2.63	.75
.00540	5.7	.60		.0151	2.25	.74		.00562	5.5	.67
.00663	4.7	.61		.0021	13.3	.49		.00103	24.5	.36
.0116	2.9	.70		.00073	33.	.24		.00146	18.1	.43
.0164	2.1	.72		.00138	19.	.38		.0327	1.13	.81
								.0113	2.9	.75

.5-C-.125				.5-C-.25				.25-C-.125		
Quality	χ_{tt}	α		Quality	χ_{tt}	α		Quality	χ_{tt}	α
.00266	10.8	.56		.00222	12.5	.51		.0164	2.1	.74
.00214	13.0	.50		.0151	2.25	.76		.0116	2.9	.67
.00152	17.7	.46		.0344	1.08	.85		.00663	4.7	.57
.00271	10.6	.53		.00116	22.0	.42		.00541	5.7	.55
.00382	7.7	.56		.00170	16.0	.47		.00382	7.7	.48
.00540	5.7	.57		.00621	5.0	.68		.00272	10.6	.49
.00663	4.7	.64		.000733	33.	.37		.0024	12.8	.43
.0116	2.9	.65		.00138	19.	.44		.00192	14.3	.36
.0164	2.1	.69		.00204	13.6	.51		.00137	19.1	.30

TABLE 6.6

VOID FRACTION DATA IN EXPANSION RUNS

$(\alpha_A$ - 2 inches before expansion)
$(\alpha_B$ - 2 inches after expansion)

.125-E-1				.125-E-.5				.125-E-.25		
χ	α_A	α_B		χ	α_A	α_B		χ	α_A	α_B
.01639	.78	.99		.01639	.74	.94		.01639	.73	.83
.01159	.70	.95		.01159	.71	.93		.01159	.68	.77
.00662	.64	.92		.00662	.64	.89		.00662	.63	.79
.00540	.59	.91		.00540	.63	.90		.00540	.65	.79
.00382	.57	.90		.00382	.56	.88		.00382	.58	.74
.00271	.54	.91		.00271	.53	.86		.00271	.52	.64
.00266	.52	.93		.00266	.53	.75		.00266	.53	.71
.00214	.47	.86		.00214	.48	.86		.00214	.49	.64
.00152	.41	.86		.00152	.42	.83		.00152	.48	.61

.25-E-1.0				.25-E-.5				.5-E-1.0		
χ	α_A	α_B		χ	α_A	α_B		χ	α_A	α_B
.00222	.47	.80		.00222	.49	.71		.0403	.84	.87
.0151	.68	.91		.0151	.77	.83		.0164	.74	.81
.0345	.79	.92		.0345	.84	.92		.0567	.87	.93
.00116	.45	.82		.00116	.38	.67		.00245	.55	.72
.00169	.47	.81		.00169	.43	.68		.00103	.45	.64
.00619	.69	.92		.00619	.63	.79		.0129	.70	.86
.00073	.37	.80		.00073	.31	.63		.00564	.67	.74
.00138	.45	.71		.00138	.45	.71		.00114	.70	.83
.00205	.50	.73		.00205	.50	.73		.00147	.49	.67
				.00443	.58	.76		.0330	.81	.90

Figure 6.9 Vertical Void Fraction
Distribution for Run
No. .5-E-1-1,
Position A

Figure 6.10 Vertical Void Fraction
Distribution for Run
No. .5-E-1-1,
Position B

Figure 6.11 Vertical Void Fraction
Distribution for Run
No. .5-E-1-4,
Position A
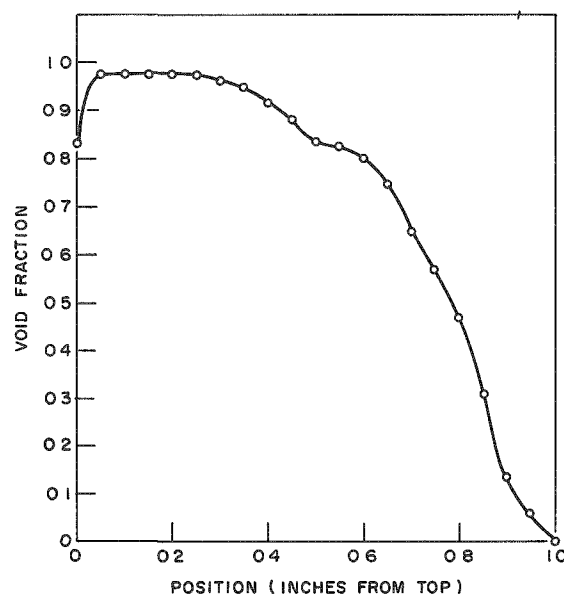
Figure 6.12 Vertical Void Fraction
Distribution for Run
No. .5-E-1-4,
Position B
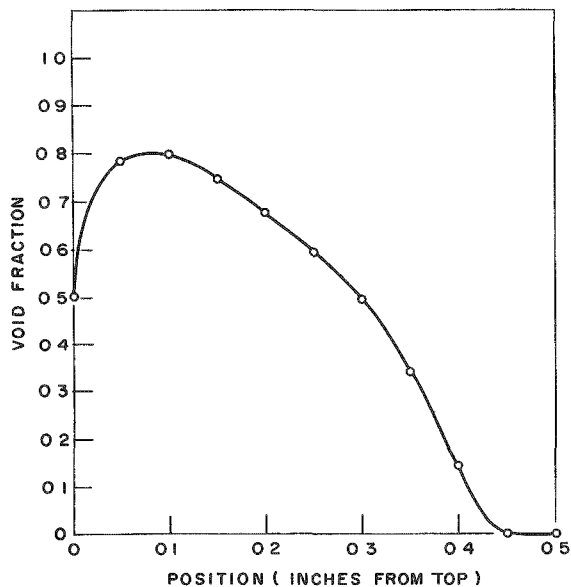
Figure 6.13 Vertical Void Fraction
Distribution for Run
No. .5-E-1-9,
Position A
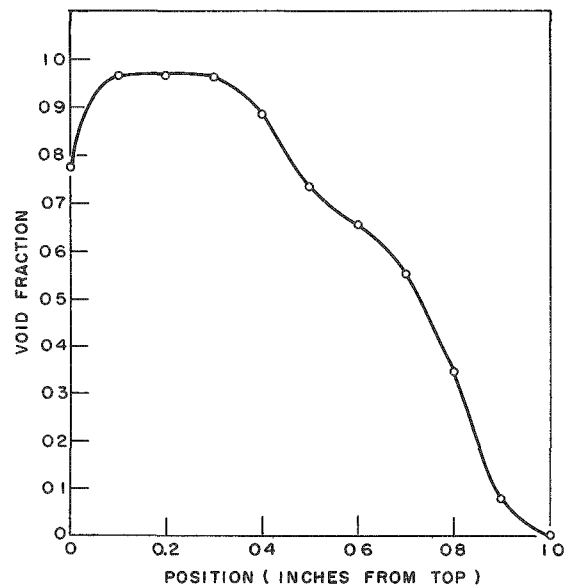
Figure 6.14 Vertical Void Fraction
Distribution for Run
No. .5-E-1-9,
Position B
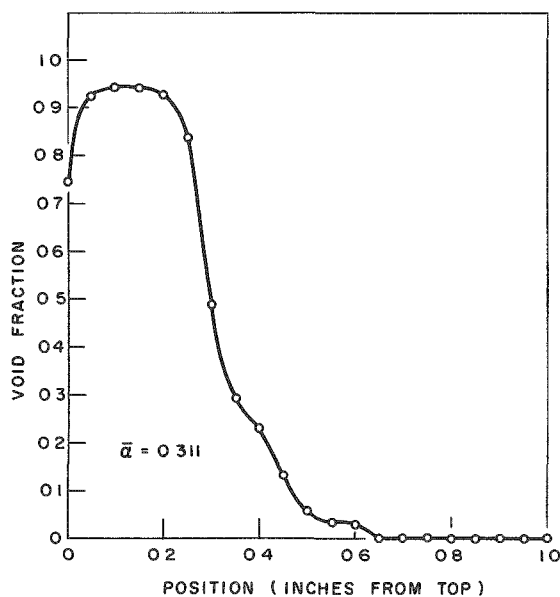
Figure 6.15 Vertical Void Fraction
Distribution for Run
No. 1-C-.5-1,
Position A
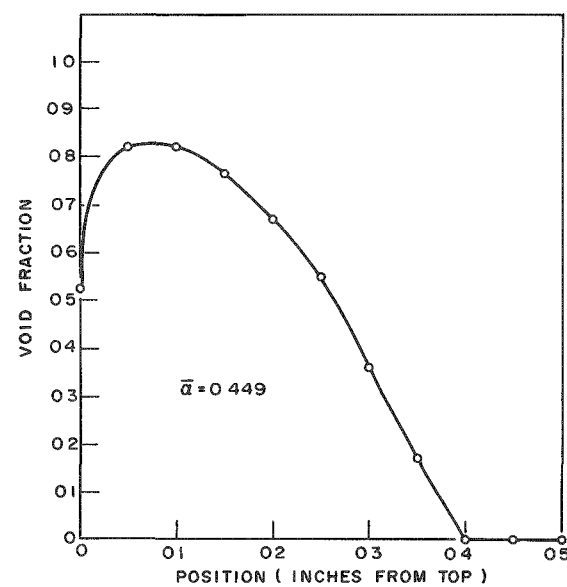
Figure 6.16 Vertical Void Fraction
Distribution for Run
No. 1-C-.5-1,
Position B
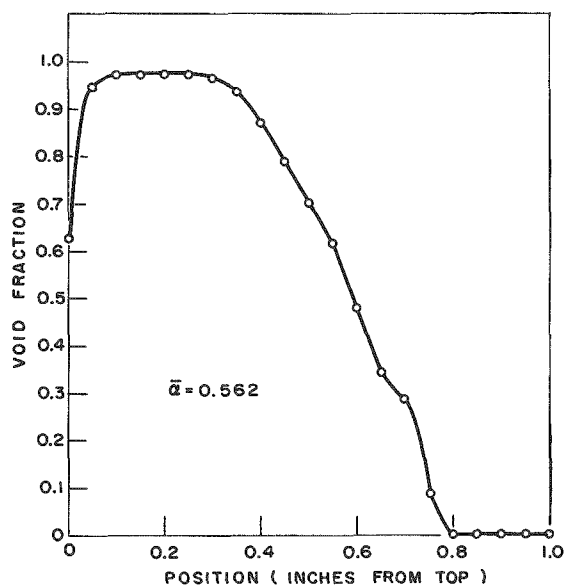
Figure 6.17 Vertical Void Fraction
Distribution for Run
No. 1-C-.5-6,
Position A
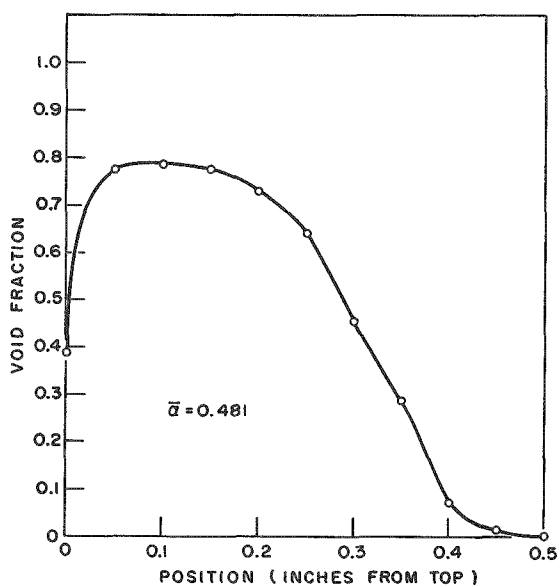
Figure 6.18 Vertical Void Fraction
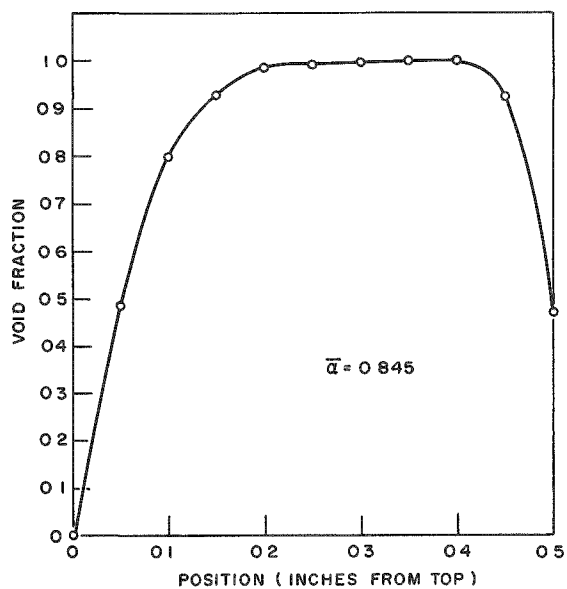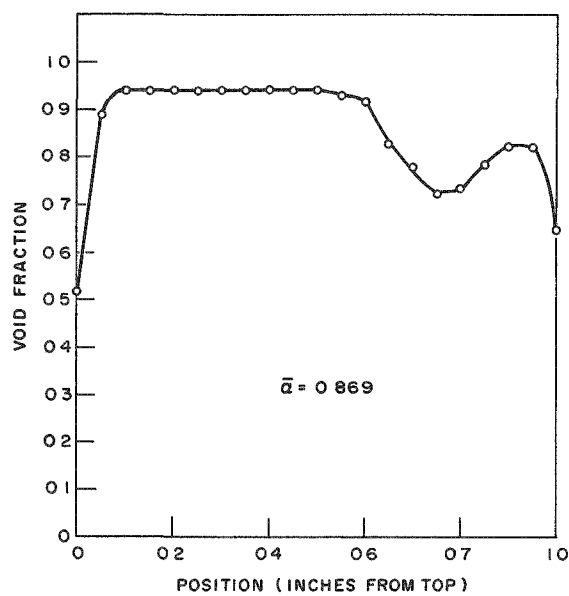Distribution for Run
No. 1-C-.5-6,
Position B
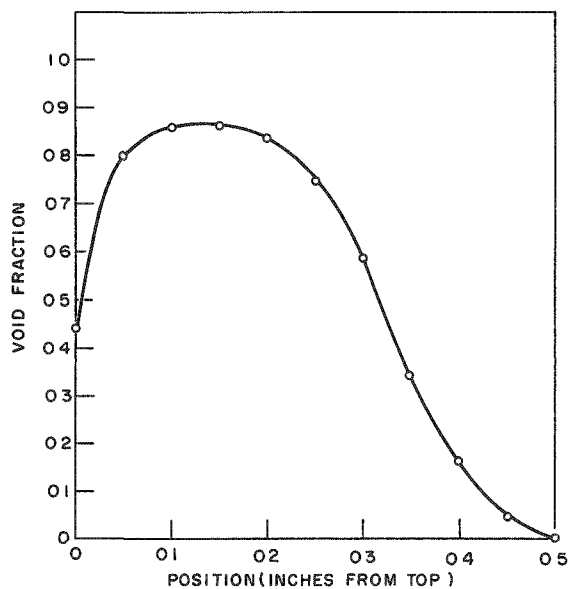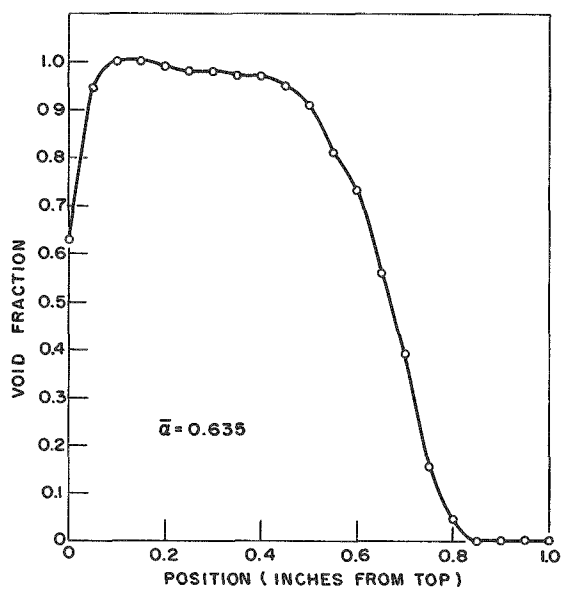

Figure 6.19 Vertical Void Fraction
Distribution for Run
No. 1-C-.5-10,
Position A
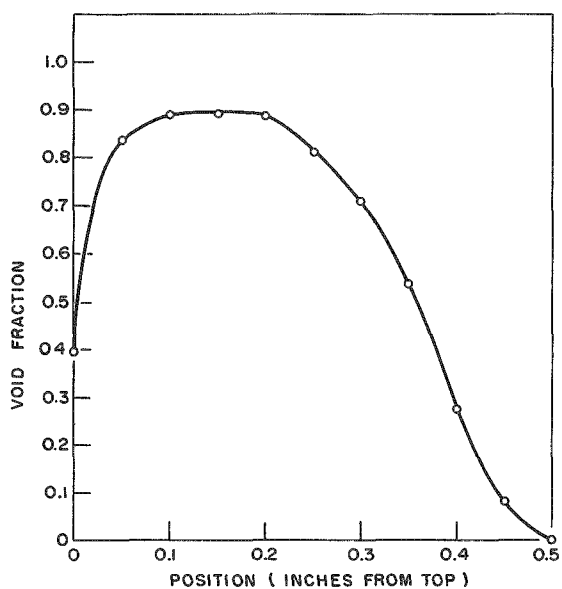
Figure 6.20 Vertical Void Fraction
Distribution for Run
No. 1-C-.5-10,
Position B

which are presented in Figures 6.21 through 6.26. It is evident from these photographs that a wide range of flow patterns are included in this study.

3. Correlation of Volume Fraction Data

The results of this study of volume fraction do not show any separation of the data, as was reported by Bergelin and Gazely[10] due to difference flow mechanisms and different flow patterns.

The void fraction results are presented in Figure 6.27 for the uniform cross section channels in terms of the parameter χ. A curve representing the data is shown and the Lockhart-Martinelli curve is shown for comparison. It can be noted from Figure 6.27 that the values of the void volume fraction are higher than the Martinelli-Lockhart correlation. This corresponds to values of liquid volume fraction being below the Martinelli-Lockhart curve. This trend is also evident in the data which has been reported by other investigators for a variety of fluid systems and measuring techniques.

In studying the relationship between the gas volume fraction and the various flow parameters, it was concluded that any correlation which was valid for the flow in uniform cross section channels should apply equally well to flow where a sudden change in cross section occurs, if the flow is allowed to return to its normal configuration. The void fraction data before and after the expansions and contractions are shown in Figures 6.28 through 6.29. The data are presented with the curve which is based on the uniform channel data. The data for the one inch section were omitted in these figures because the flow patterns were influenced by the exit conditions in the region where the data were obtained.

All of the data are presented for the expansions, contractions and uniform sections in Figure 6.30.
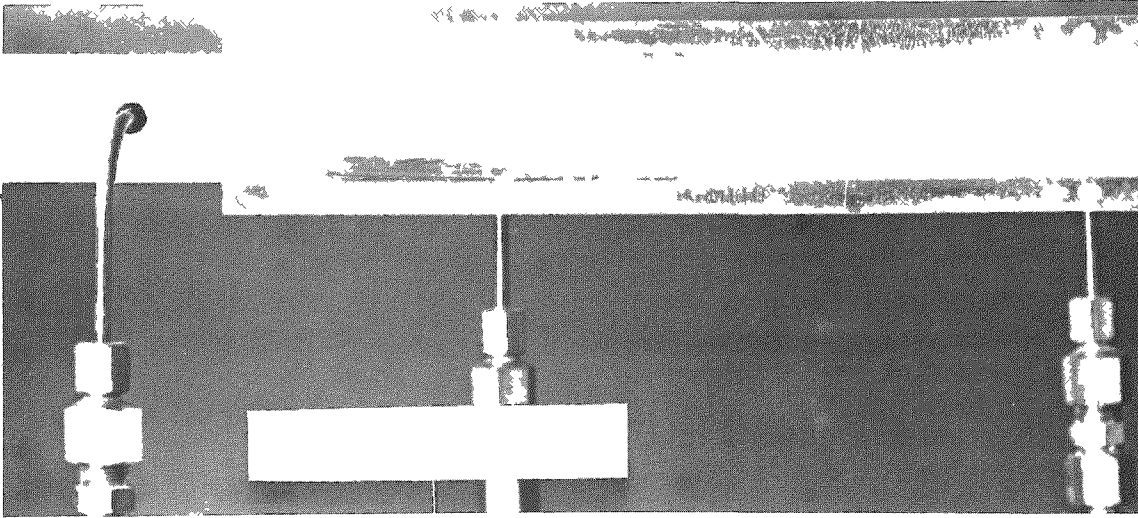
Figure 6.21   Photograph of Flow Pattern for Run No. .5-E-1-1
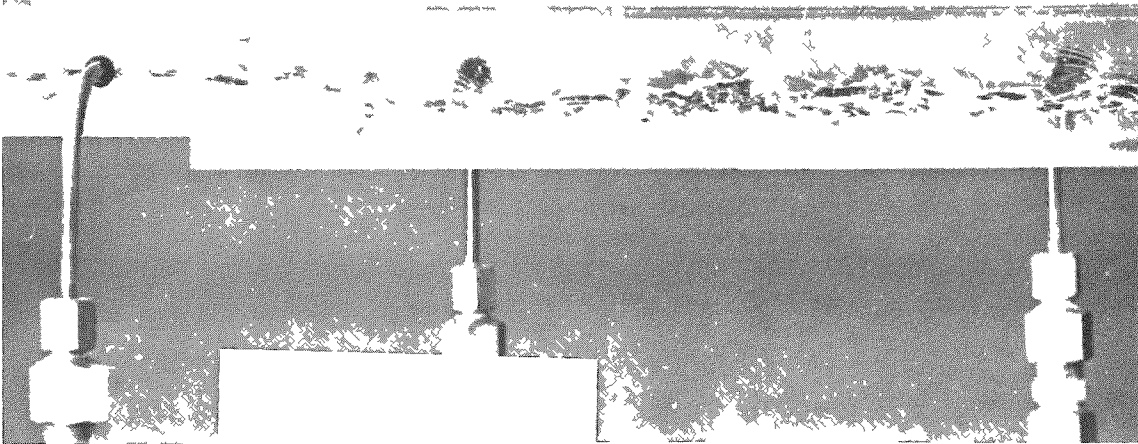
Figure 6.22   Photograph of Flow Pattern for Run No. .5-E-1-4
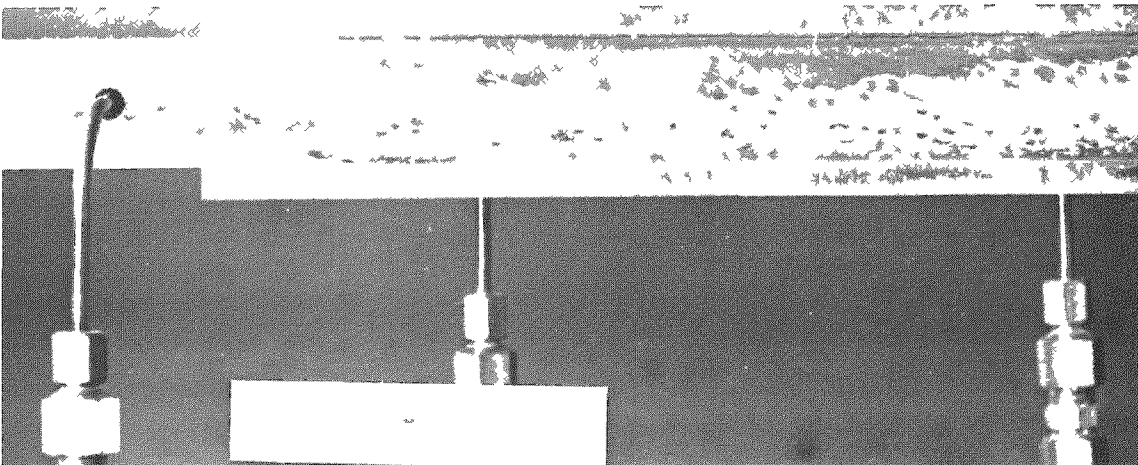
Figure 6.23   Photograph of Flow Pattern for Run No. .5-E-1-9
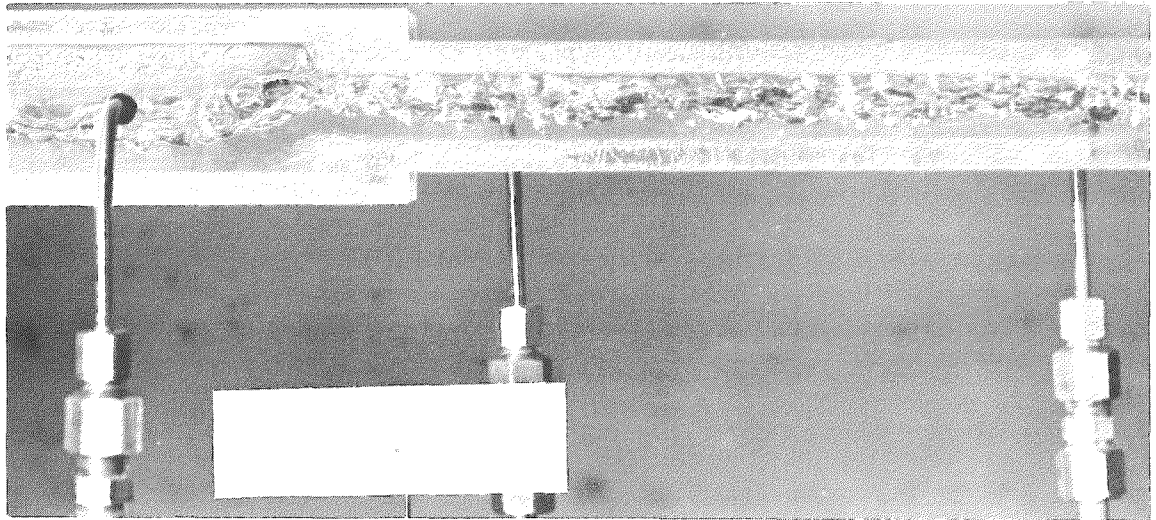
Figure 6.24 Photograph of Flow Pattern for Run No. 1-C-.5-1
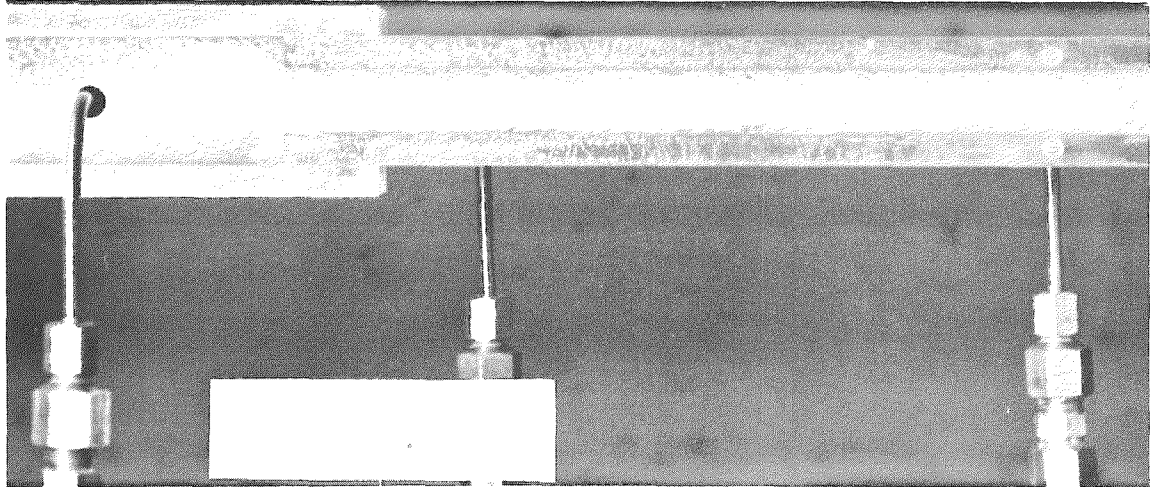
Figure 6.25 Photograph of Flow Pattern for Run No. 1-C-.5-6
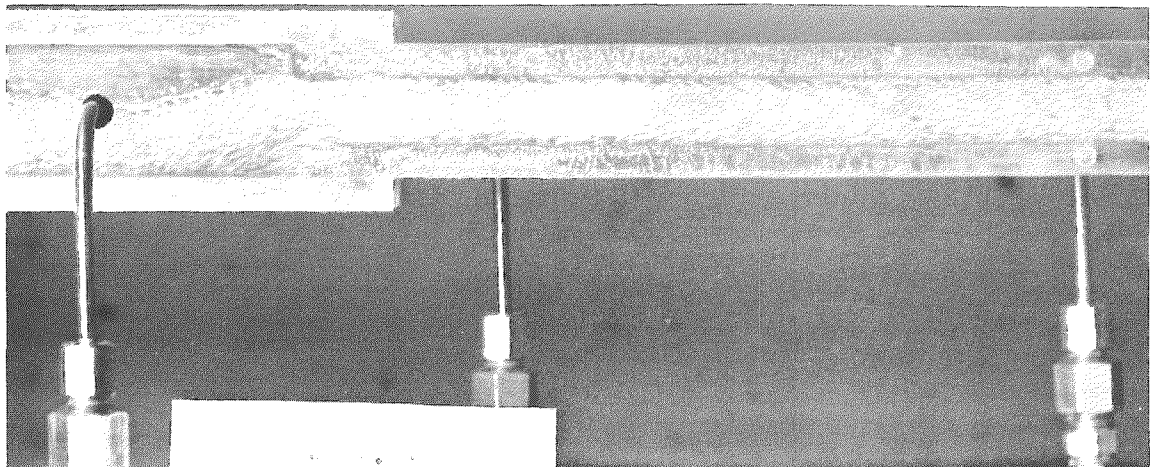
Figure 6.26 Photograph of Flow Pattern for Run No. 1-C-.5-10

78
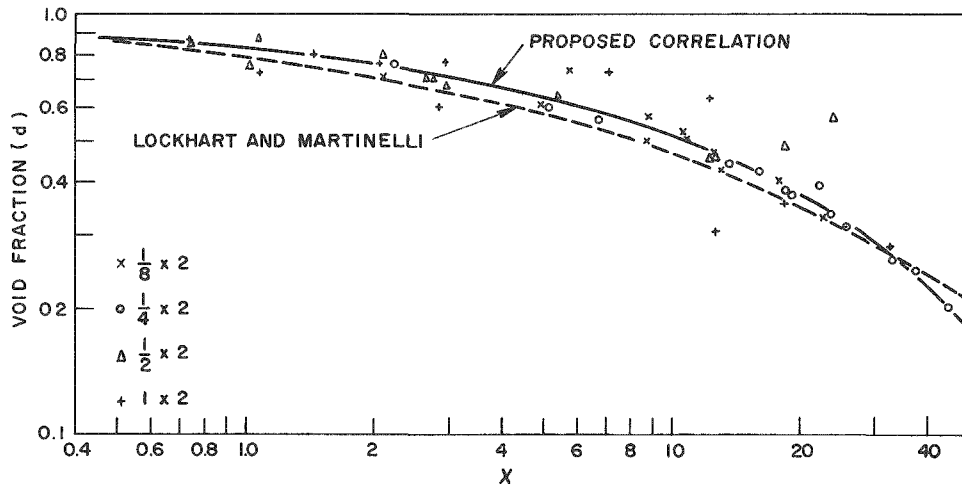
Figure 6.27 Void Fraction Correlation for Constant
Cross Section Channels
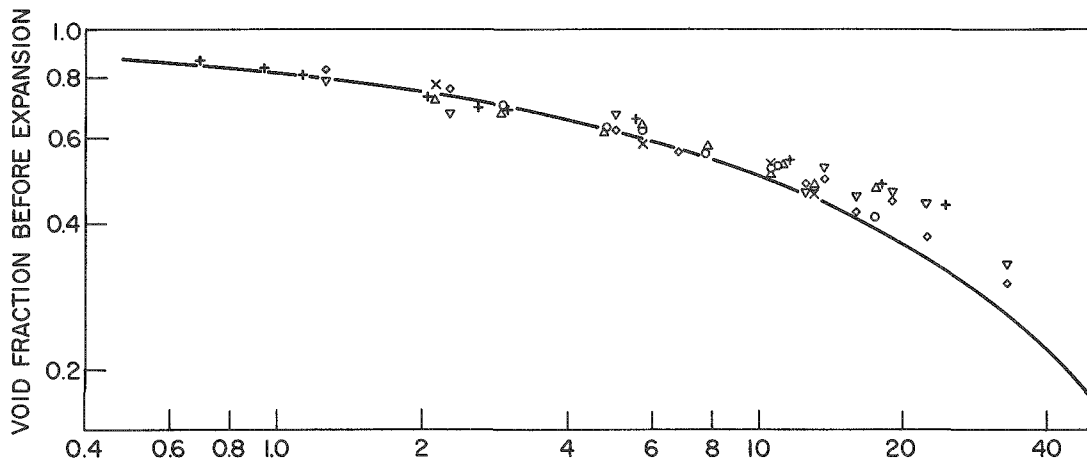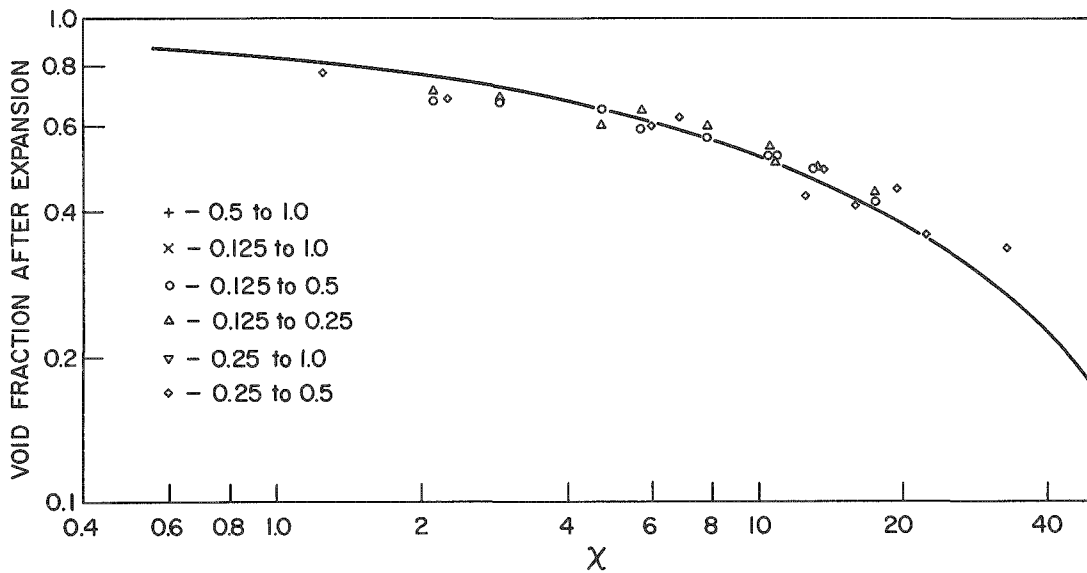
Figure 6.28 Correlation of Void Fraction Before
and After an Expansion
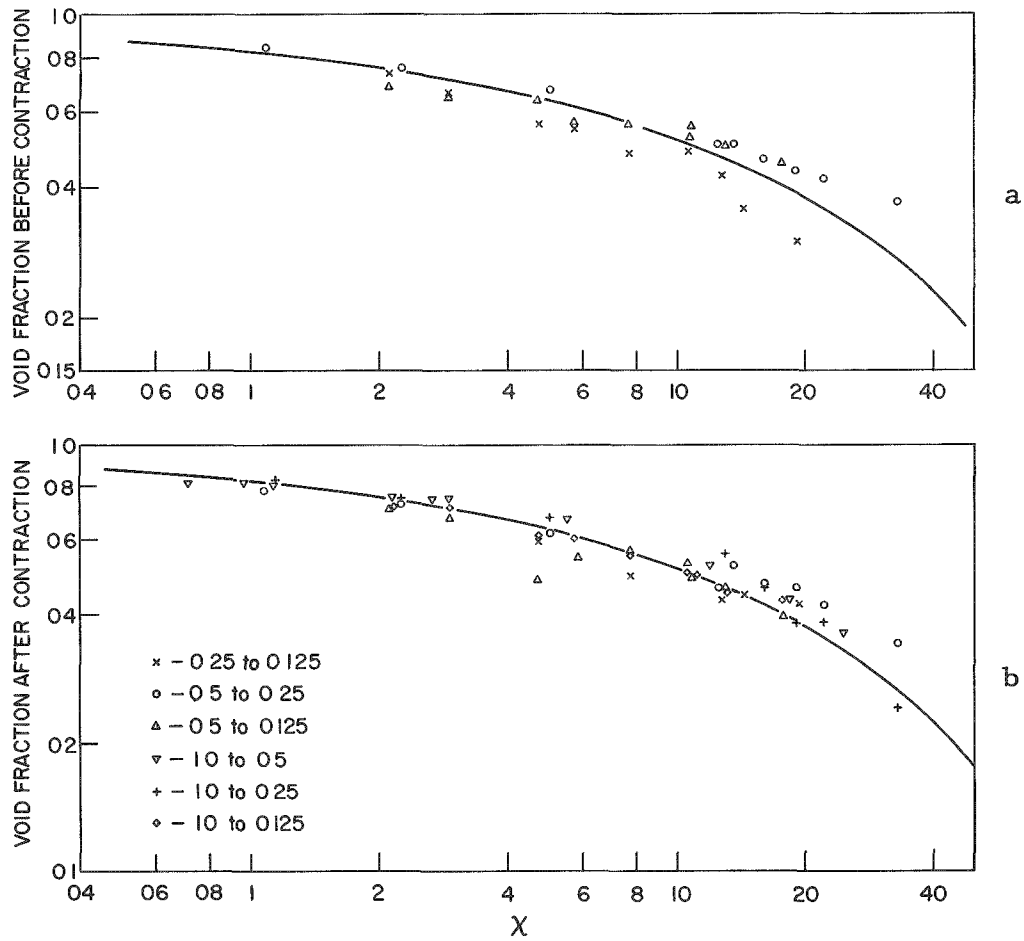
Figure 6.29 Correlation of Void Fraction Before
and After a Contraction
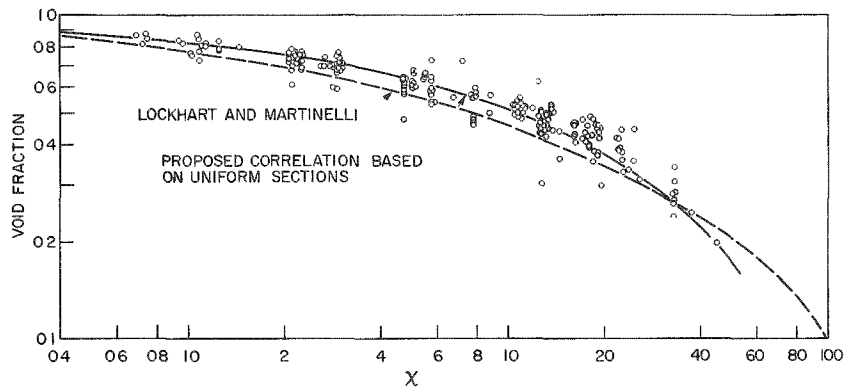
Figure 6.30 Proposed Void Fraction Correlation for
Horizontal Flow

While the void fraction far removed from a disturbance is un-affected by the disturbance, the local effect may be severe. Based upon the data taken for the expansion runs, the following empirical relationship was found to exist between the voids and the other flow parameters:

$$\alpha_B = \alpha_A \left[1 + A\frac{(1-\sigma)^{3/2}}{x^{1/2}} \right] \qquad (6.2)$$

Where

α_A - volume fraction 2 inches before expansion

α_B - volume fraction 2 inches after expansion

σ - area ratio

x - quality

A - 0.05

The average value of the per cent difference between the measured value of α_B and that predicted by the equation (6.2) is 5.1 per cent for the fifty-six runs studied. The comparison of measured and predicted values of the void fraction after an expansion is shown in Figure 6.31. The data on which this correlation is based are shown in Table 6.6.

The variation of volume fraction with position along the channel for various flow rate and area combinations is shown in Figures 6.32 to 6.37. The reproducibility of this data is shown by Figure 6.38 where the data are presented for reruns at the same flow rates and void fraction determinations at the same positions. The difference between the runs and the reruns is due to a number of different effects. These include the inability to reproduce the flow conditions exactly, the errors in the analysis of the strip chart records, and errors in the positioning of the traversing mechanism.

The results of this study indicate that the use of the traversing technique with a radiation source-detector system yields results for
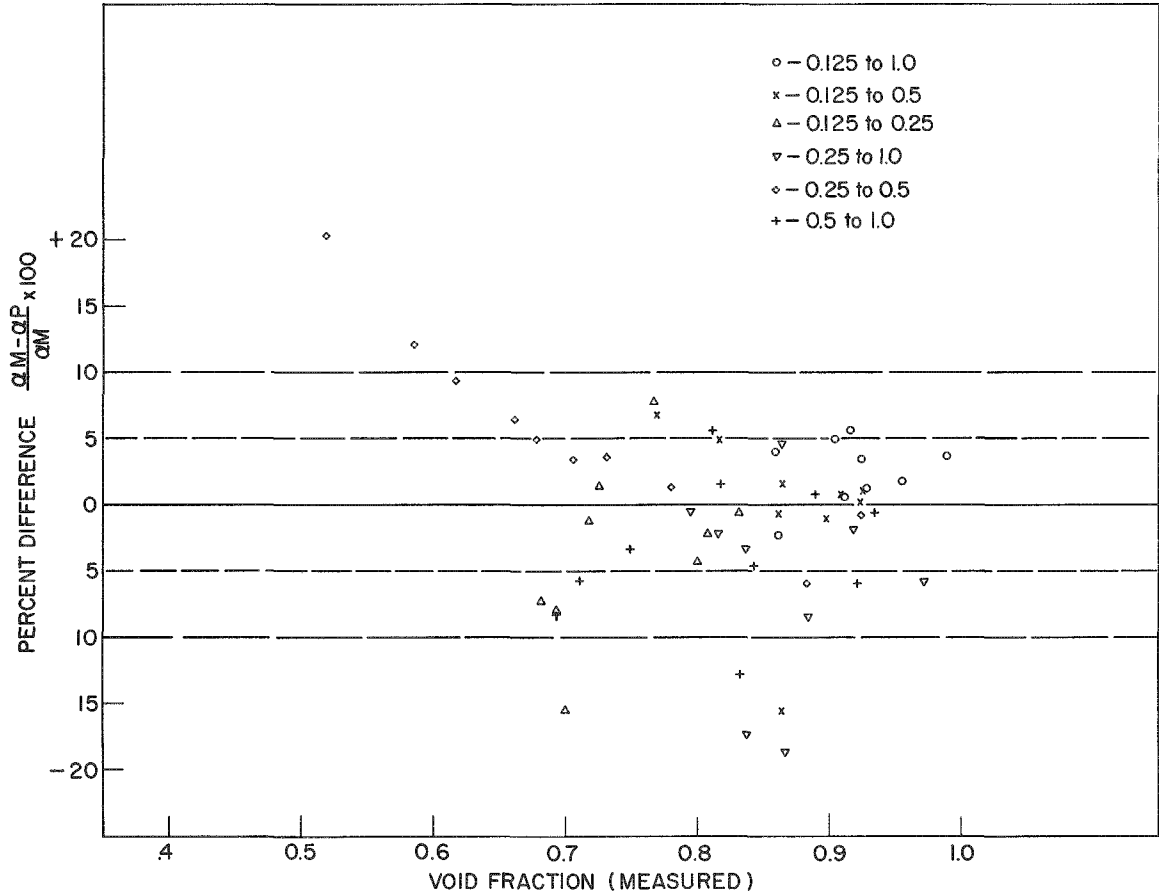
Figure 6.31 Comparison of Measured and Predicted Void
Fraction After an Abrupt Expansion
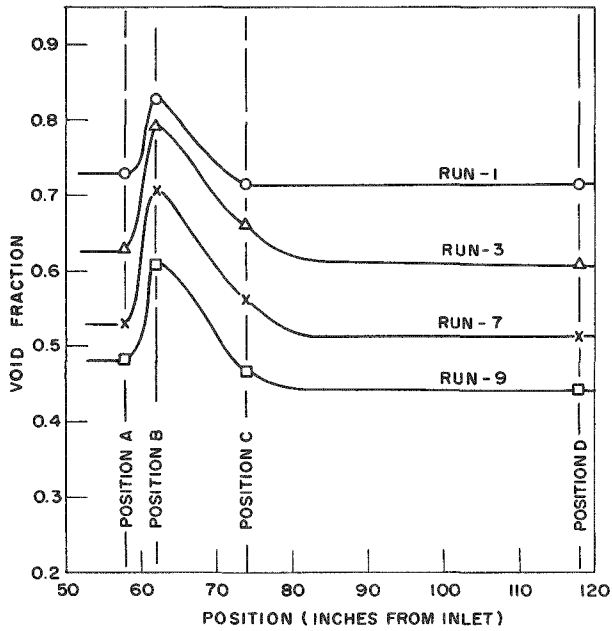
Figure 6.32 Voids vs. Position for
1/8 to 1/4 Expansions

82
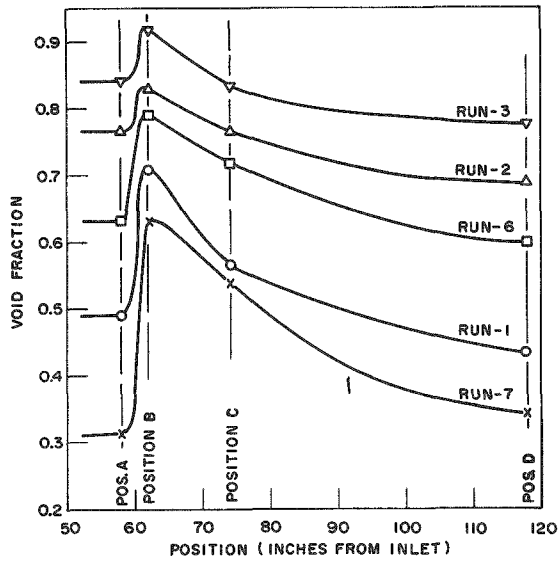
Figure 6.33 Voids vs. Position
for 1/4 to 1/2
Expansions
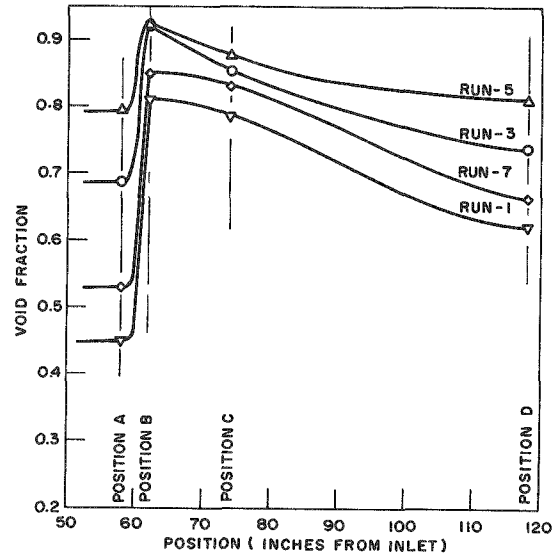
Figure 6.34 Voids vs. Position
for 1/4 to 1
Expansions
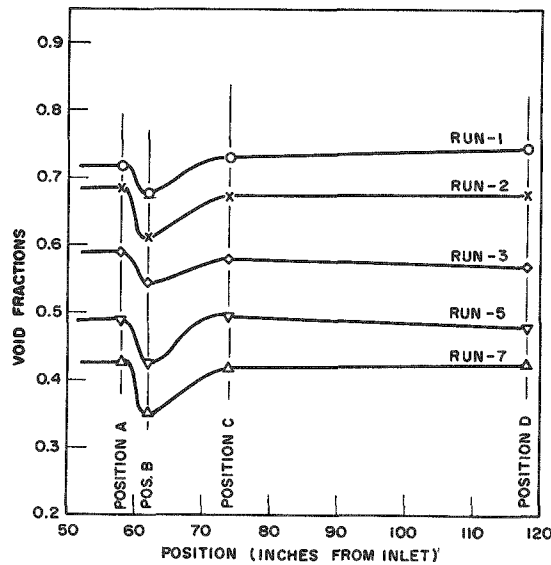
Figure 6.35 Voids vs. Position
for 1/4 to 1/8
Contractions
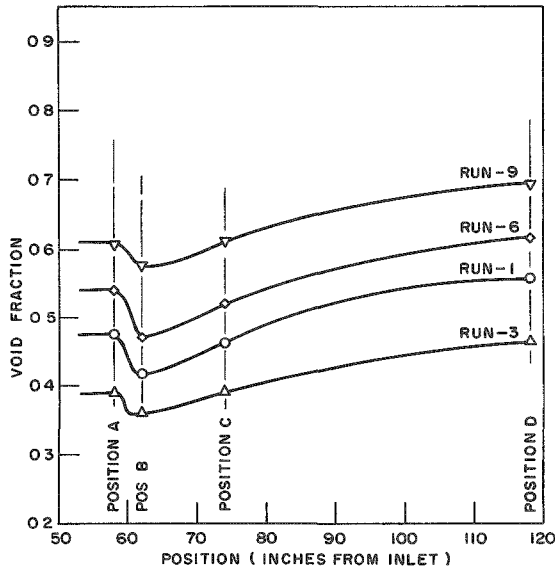
Figure 6.36 Voids vs. Position for 1/8 to 1/2 Contractions
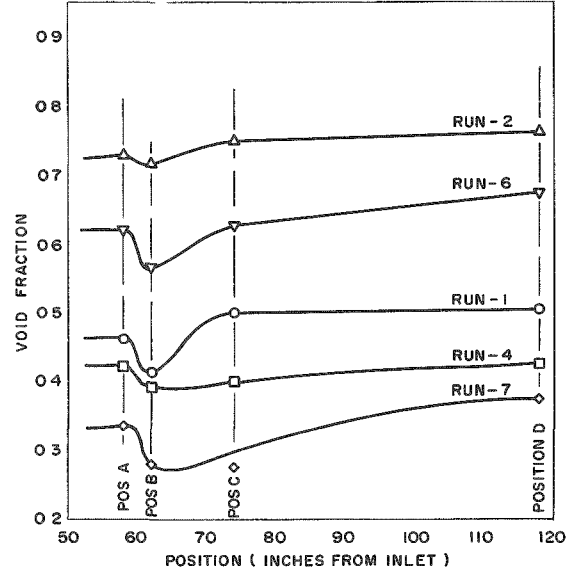
Figure 6.37 Voids vs. Position for 1/2 to 1/4 Contractions
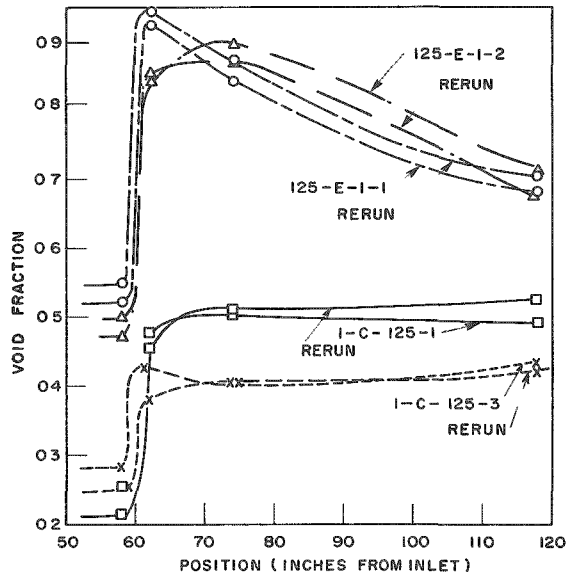
Figure 6.38 Comparison of Void Runs and Reruns under Identical Flow Conditions

the local volume fractions of each phase which are in agreement with those reported by most other investigators for the average volume fraction over a length of a test section.

The results of the distribution study over the cross section compare favorably with the flow patterns shown in the photographs.

The effect of a sudden expansion on the local void distribution in the region of the flow area change has been correlated in terms of the quality and the channel geometry. It has also been shown that the local void fraction in a region removed from any disturbances is not strongly influenced by the conditions for up stream.

Chapter VII

SLIP RATIO INVESTIGATION

The study of the relationship which exists between the phases in a two-phase system can be approached by a consideration of the conservation of mass equations of each phase.

$$W_g = \rho_g V_g A_g \tag{7.1}$$

$$W_\ell = \rho_\ell V_\ell A_\ell \tag{7.2}$$

From the definition of the quality and void fraction, (7.1) and (7.2) become

$$W_g = \rho_g V_g A_T(\alpha) \tag{7.3}$$

$$W_\ell = \rho_\ell V_\ell A_T(1 - \alpha) \tag{7.4}$$

Taking the ratio and solving for V_g/V_ℓ it is found that

$$\frac{V_g}{V_\ell} = \left(\frac{x}{1 - x}\right)\left(\frac{1 - \alpha}{\alpha}\right)\frac{\rho_\ell}{\rho_g} \tag{7.5}$$

This ratio is defined as the slip ratio.

From the correlation of the void fraction data, it was shown that the void fraction is a function of the quality and the physical properties of the fluids. In this study the same fluids, air and water, were used in all of the tests. The variation in air density was taken into account through the pressure variations. From equation (7.5) it would appear that the slip ratio should depend only on the quality and the physical properties of the materials.

In this case the horizontal flow differs from what would be expected for vertical flow due to the effect of the buoyancy of the vapor phase. In vertical flow, the slip depends upon the velocity of the liquid, or some equivalent parameter, i.e., mass flow rate, weight flow rate, etc. This becomes apparent from examining the behavior of a single bubble in vertical flow. At very low flow rates, and at a given quality, the velocity of the bubble will be approximately that of a bubble in still water. For this case the slip ratio is extremely large.

As the velocity of the liquid increases the slip ratio will decrease and the buoyancy forces will become less significant in comparison to the inertial and viscous forces. A study of the effect of flow parameters on slip has been carried out by Petrick.[15] Hoopes[45] considered the problem of slip in two phase flow in an annulus by considering the relationship between the kinetic energy with slip to the kinetic energy with homogeneous flow as a function of quality. The relative velocity of the bubbles with respect to the water was studied by Behringer.[46] Studies on the slip ratio in vertical natural circulation boiling were conducted by Cook.[22] Lottes and Flinn[47] report on studies of vertical flow with boiling which indicate that the slip ratio depends on pressure and liquid velocity.

In this work, which was conducted essentially at atmospheric pressure, the effect of pressure on the slip ratio could not be determined. Equation 7.5 and the correlation for void fraction indicate that the slip should depend on the quality for the system studied.

Using equation (7.5) the slip ratio was calculated for the experimental runs and the result is shown in Figure 7.1. Based on this data it is proposed that the slip ratio can be represented by the equation

$$S = 37 x^{1/2} \tag{7.6}$$

The data shown in Figure 7.1 are presented in Table 7.1, 7.2 and 7.3.
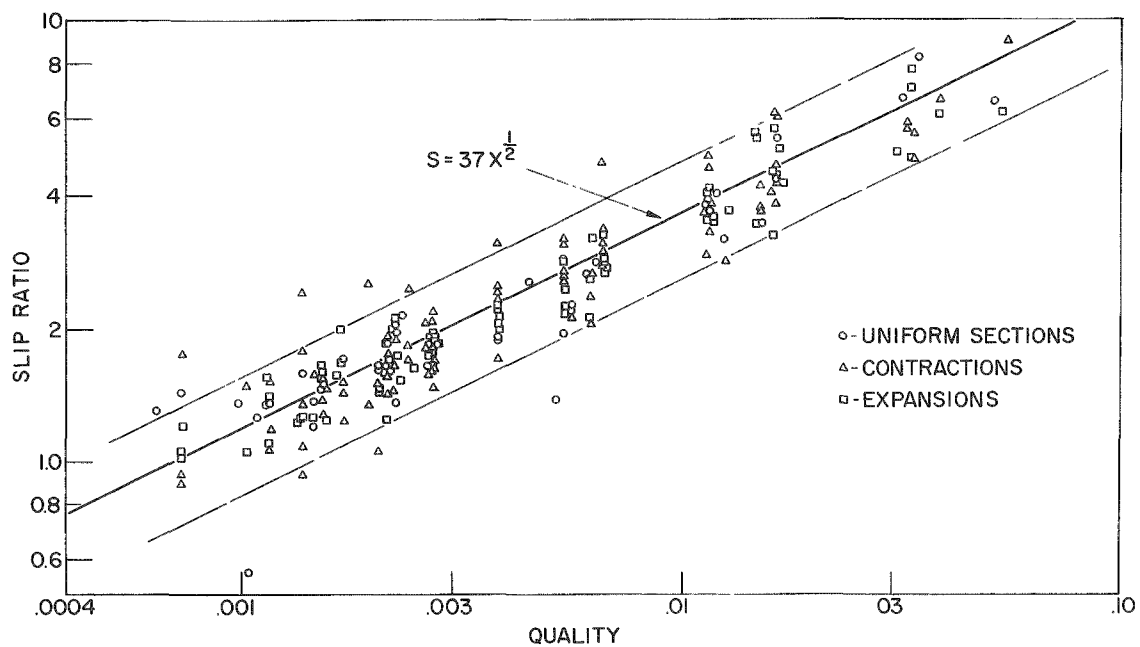
Figure 7.1 Correlation of Slip Ratio
as a Function of Quality

TABLE 7.1

SLIP RATIO - QUALITY DATA - UNIFORM SECTIONS

1/2 x 2 in. Section			1/4 x 2 in. Section			1/8 x 2 in. Section		
Run No.	Quality	Slip Ratio	Run No.	Quality	Slip Ratio	Run No.	Quality	Slip Ratio
1	0.0319	6.85	1	0.00224	1.99	1	0.00271	1.67
2	0.0113	3.86	2	0.00448	2.59	2	0.00382	1.92
3	0.00146	1.20	3	0.0153	3.51	3	0.00540	1.99
4	0.00232	2.14	4	0.00116	1.34	4	0.00151	1.47
5	0.0167	5.50	5	0.00170	1.71	5	0.00214	1.86
6	0.0517	6.70	6	0.00604	2.69	6	0.00267	1.67
7	0.0348	8.41	7	0.00073	1.43	7	0.00113	1.36
8	0.00224	2.02	8	0.00138	1.59	8	0.00224	1.37
9	0.0120	4.11	9	0.00204	1.66	9	0.00387	1.91
10	0.00103	0.56	10	0.00064	1.31	10	0.0064	2.89
11	0.0127	3.41	11	0.00108	1.26	11	0.0116	3.76
12	0.00563	2.22	12	0.00518	1.34	12	0.0164	4.40
			13	0.00098	1.35			
			14	0.00145	1.37			

TABLE 7.2

SLIP RATIO - QUALITY DATA FOR CONTRACTIONS

1-C-.25

Quality	Slip Ratio$_B$
0.00116	1.51
0.0017	1.51
0.0062	2.71
0.0022	1.45
0.0328	5.97
0.0151	4.26
0.0021	1.67
0.00073	1.76
0.00138	1.78

1-C-.5

Quality	Slip Ratio$_B$
0.00238	1.82
0.039	6.83
0.0553	9.2
0.0160	4.1
0.0127	2.77
0.00562	2.16
0.00103	1.49
0.00146	1.58
0.0327	5.8
0.0113	2.95

.5-C-.125

Quality	Slip Ratio$_A$	Slip Ratio$_B$
0.00265	1.63	1.57
0.00214	1.42	1.58
0.00152	1.38	1.28
0.00271	1.48	1.83
0.00382	1.71	2.47
0.00541	2.68	3.25
0.00662	4.83	2.81
0.0116	5.0	4.72
0.0164	6.25	6.2

.5-C-.25

Quality	Slip Ratio$_A$	Slip Ratio$_B$
0.00222	1.92	1.66
0.0151	3.74	3.72
0.0344	5.68	4.97
0.00116	1.06	1.19
0.00170	1.23	1.42
0.00621	2.07	2.38
0.00073	0.89	0.94
0.00138	0.93	1.35
0.00204	1.04	1.50

1-C-.125

Quality	Slip Ratio$_B$
0.00261	2.08
0.00214	1.94
0.00152	1.50
0.00271	2.1
0.00382	2.51
0.00540	2.75
0.00662	3.16
0.0116	3.78
0.0164	4.75
0.00261	1.80
0.00214	1.74
0.00152	1.55

.25-C-.125

Quality	Slip Ratio$_B$	Slip Ratio$_A$
0.0164	4.31	3.77
0.0116	3.76	3.35
0.00662	3.77	3.03
0.0054	3.42	2.59
0.00382	3.18	2.36
0.00271	2.19	1.62
0.0024	2.46	1.70
0.00193	2.57	1.34
0.00137	2.42	1.08

TABLE 7.3

SLIP RATIO - QUALITY DATA FOR EXPANSIONS

.125-E-.25			.25-E-.5			.125-E-1	
Quality	Slip Ratio$_A$	Slip Ratio$_B$	Quality	Slip Ratio$_A$	Slip Ratio$_B$	Quality	Slip Ratio$_A$
0.0164	4.39	5.20	0.00222	1.76	2.24	0.00265	1.85
0.0116	3.94	4.05	0.0149	3.5	5.5	0.00214	1.83
0.00662	2.92	3.40	0.0334	4.9	7.9	0.00151	1.66
0.00540	2.19	2.29	0.00116	1.4	1.56	0.00271	1.72
0.00382	2.06	2.02	0.00169	1.69	2.0	0.00389	2.16
0.00271	1.89	1.69	0.00616	2.66	3.25	0.00537	2.94
0.00266	1.76	1.93	0.00073	1.2	1.07	0.00658	2.83
0.00214	1.66	1.72	0.00138	1.27	1.28	0.0114	3.54
0.00152	1.23	1.49	0.00205	1.49	1.66	0.0161	3.3
						0.00265	1.58
						0.00214	1.60

.125-E-.5			.25-E-1		.5-E-1	
Quality	Slip Ratio$_A$	Slip Ratio$_B$	Quality	Slip Ratio$_A$	Quality	Slip Ratio$_A$
0.00266	1.80	1.84	0.00116	1.10	0.0388	6.26
0.00212	1.76	1.24	0.0017	1.53	0.0164	4.56
0.00152	1.58	1.54	0.0062	2.14	0.054	6.32
0.00271	1.88	1.91	0.00223	2.0	0.00245	1.62
0.00382	2.27	2.2	0.0334	7.20	0.00104	1.05
0.00540	2.49	2.9	0.0148	5.7	0.0129	3.75
0.00660	2.82	2.72	0.00206	1.44	0.00565	2.24
0.0116	3.62	4.23	0.00073	1.02	0.0114	3.58
0.0163	4.47	5.8	0.00138	1.23	0.00147	1.26
					0.032	5.13

Chapter VIII

TWO-PHASE PRESSURE DROPS

1. Introduction

A correlation for the data on two-phase pressure drops which has been widely used is that presented by Lockhart and Martinelli. The parameter ϕ is defined by the relationship

$$\left(\frac{\Delta P}{\Delta \ell}\right)_{TP} = \phi_\ell^2 \left(\frac{\Delta P}{\Delta \ell}\right)_\ell \tag{8.1}$$

or

$$\left(\frac{\Delta P}{\Delta \ell}\right)_{TP} = \phi_g^2 \left(\frac{\Delta P}{\Delta \ell}\right)_g \quad . \tag{8.2}$$

The study further divides the problem into four flow mechanisms depending upon whether the phases flowing separately in the pipe would be flowing in laminar or turbulent flow. The following listing defines these mechanisms

	t-t	v-t	t-v	v-v
Re_{gp}	>2000	>2000	<1000	<1000
$Re_{\ell p}$	>2000	<1000	>2000	<1000

These divisions are arbitrary and it has been shown that a phase may be flowing turbulently at Reynolds' Numbers much less than 2000, but no new boundaries for these regions have been presented. This correlation would indicate that the pressure drop is not dependent on the flow pattern which exists, but only on the pseudo-Reynolds' Numbers of each phase. In defense of the correlation, it should be stated that the assumptions under which it was developed, omit some of the flow patterns, but it has been extended and applied to all patterns. In the correlation, the parameter ϕ is presented in terms of a second parameter χ which is defined as

$$\chi^2 = \frac{\left(\frac{\Delta P}{\Delta \ell}\right)_\ell}{\left(\frac{\Delta P}{\Delta \ell}\right)_g} \tag{8.3}$$

where the pressure gradients for the single phases are computed on the basis of each phase flowing at its own weight flow rate in the pipe.

In connection with the calculation of χ for this study, the pressure gradients were calculated on the basis of Fanning's equation.

$$\left(\frac{\Delta P}{\Delta \ell}\right)_\ell = \frac{f_\ell \, \rho_\ell \, W_\ell^2}{D_e \, 2g \, A^2} \tag{8.4}$$

$$\left(\frac{\Delta P}{\Delta \ell}\right)_g = \frac{f_g \, \rho_g \, W_g^2}{D_e \, 2g \, A^2} \tag{8.5}$$

It was assumed that in the range of variables of interest, the friction factor could be represented by Blasius equation for turbulent flow

$$f = \frac{C}{N_{Re}^m} \tag{8.6}$$

The exponent m was found to be 0.25 from friction factors calculated for the flow of water in the channels as is shown in Figure 8.1.

Taking the ratio of (8.4) and (8.5) and substituting in (8.6) yields

$$\frac{\frac{\Delta P}{\Delta \ell} \, \ell}{\frac{\Delta P}{\Delta \ell} \, g} = \left(\frac{W_\ell}{W_g}\right)^{1.75} \left(\frac{\mu_\ell}{\mu_g}\right)^{0.25} \left(\frac{\rho_g}{\rho_\ell}\right) \tag{8.7}$$

Introducing the quality and solving for the parameter χ produces

$$\chi = \left(\frac{1-x}{x}\right)^{0.875} \left(\frac{\rho_g}{\rho_\ell}\right)^{0.5} \left(\frac{\mu_\ell}{\mu_g}\right)^{0.125} \tag{8.8}$$

This relationship was used to calculate all of the values of χ for the comparison of the data with the Lockhart-Martinelli results.

2. Analysis and Correlation of Data

Pressure drop data were recorded at a variety of flow rates for the 1/8-, 1/4- and 1/2-inch by 2-inch test sections. The calculations were based on the pressure drop in the last six feet of the section. It
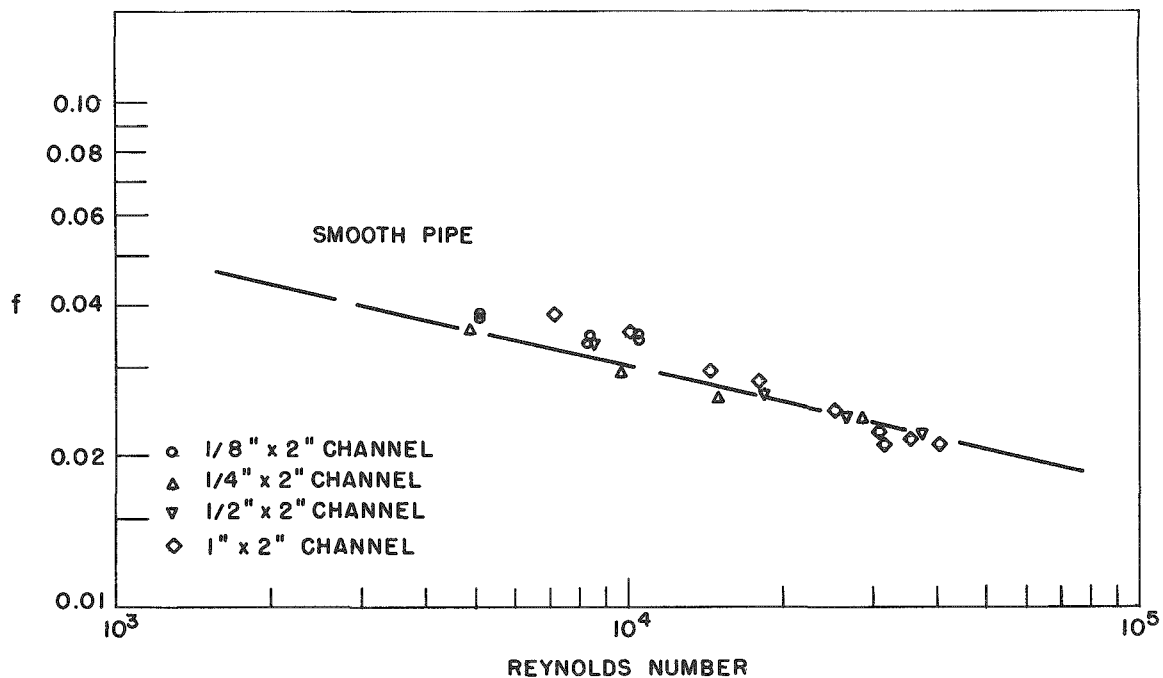
Figure 8.1 Friction Factor vs. Reynold's Number for
Lucite Test Sections
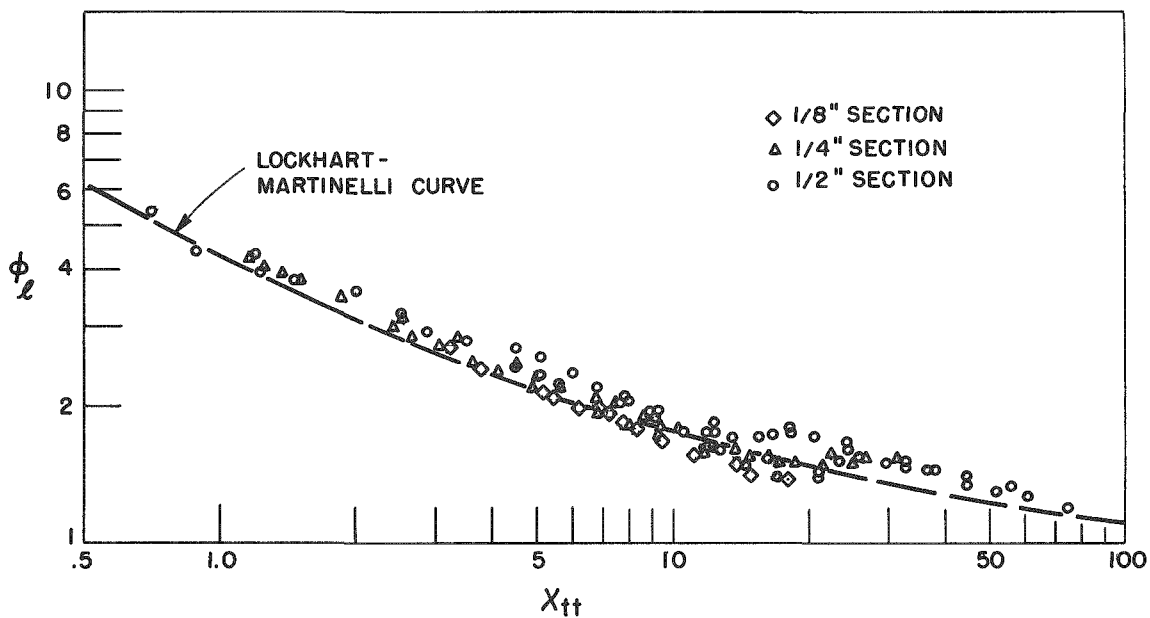
Figure 8.2 Comparison of Pressure Drop Data
with Lockhart-Martinelli Correlation

was felt that the results obtained from the first four feet of the section would be influenced by the mixing section and the transfer from a relatively homogeneous mixture to the various flow patterns.

The data is presented in terms of the $\phi_\ell - \chi_{tt}$ parameters in Figure 8.2. The Lockhart-Martinelli curve is also presented. It is seen that the data fit this curve well, but the measured drop in general are greater than those predicted by the correlation.

It has been suggested by Lottes and Flinn[47] that the increase in pressure drop in two-phase flows results from the increased velocity of the liquid phase, due to the decrease in the flow area. For the local two-phase drop they proposed the following relationship

$$\left(\frac{\Delta P}{\Delta \ell}\right)_{TP} = \frac{1}{(1 - \alpha)^2} \left(\frac{\Delta P}{\Delta \ell}\right)_\ell \tag{8.9}$$

From this assumption they derived a relationship for the pressure drop in a channel with boiling taking place.

It is felt that the assumption that the increase in pressure drop is due to the increase in water velocity only, is incomplete, in that the variation of the effective friction factor with changing velocity should also be included.

It is postulated here that the two-phase pressure drops may be represented by the following equation

$$\left(\frac{\Delta P}{\Delta \ell}\right)_{TP} = \frac{f_{TP}\, \rho_\ell\, V_\ell^2}{D_e\, 2g} \tag{8.10}$$

Assuming that the Blasius equation is also valid, f_{TP} becomes

$$f_{TP} = \frac{C}{N_{Re}^{0.25}} \tag{8.11}$$

Substitution into (8.10) yields

$$\left(\frac{\Delta P}{\Delta \ell}\right)_{TP} = \frac{\rho_\ell^{0.75}\, \mu_\ell^{0.25}}{D_e^{1.25}\, 2g}\, V_\ell^{1.75} \tag{8.12}$$

Correspondingly, a similar equation for the pressure gradient for the liquid flowing alone may be written

$$\left(\frac{\Delta P}{\Delta \ell}\right)_\ell = \frac{\rho_\ell^{0.75} \mu_\ell^{0.25}}{D_{e_0}^{1.25} 2g} V_{\ell_0}^{1.75}$$
(8.13)

The subscript 0 refers to the flow of the liquid alone. The relationship between the velocity of the liquid in the two-phase mixture to the velocity of the liquid flowing alone depends on the ratios of the flow areas as follows

$$\frac{V_\ell}{V_{\ell_0}} = \frac{1}{1 - \alpha}$$
(8.14)

Taking the ratio of 8.12 and 8.13 and substituting in 8.14 yields

$$\frac{\left(\frac{\Delta P}{\Delta \ell}\right)_{TP}}{\left(\frac{\Delta P}{\Delta \ell}\right)_\ell} = \left(\frac{D_e}{D_{e_0}}\right)^{1.25} \left(\frac{1}{1 - \alpha}\right)^{1.75}$$
(8.15)

It can be seen that the manner in which the equivalent diameter for the liquid phase changes will depend upon the type of flow pattern present. Tentatively it is assumed that the equivalent diameter is unchanged. Based on this assumption equation (8.15) reduces to

$$\frac{\left(\frac{\Delta P}{\Delta \ell}\right)_{TP}}{\left(\frac{\Delta P}{\Delta \ell}\right)_\ell} = \left(\frac{1}{1 - \alpha}\right)^{1.75} = \phi_\ell^2$$
(8.16)

The ratio of the pressure gradients or ϕ_ℓ^2 is compared with $(1 - \alpha)$ in Figure 8.3. The data presented are also tabulated in Table 8.1. The data fits the equation (8.16) over most of the range studied. The deviation at the low values of α would indicate that variations in flow patterns may influence the validity of the assumption of the invariance of the equivalent diameter of the liquid phase.

Most of the data falls within ± 20 per cent of the line representing equation (8.16).
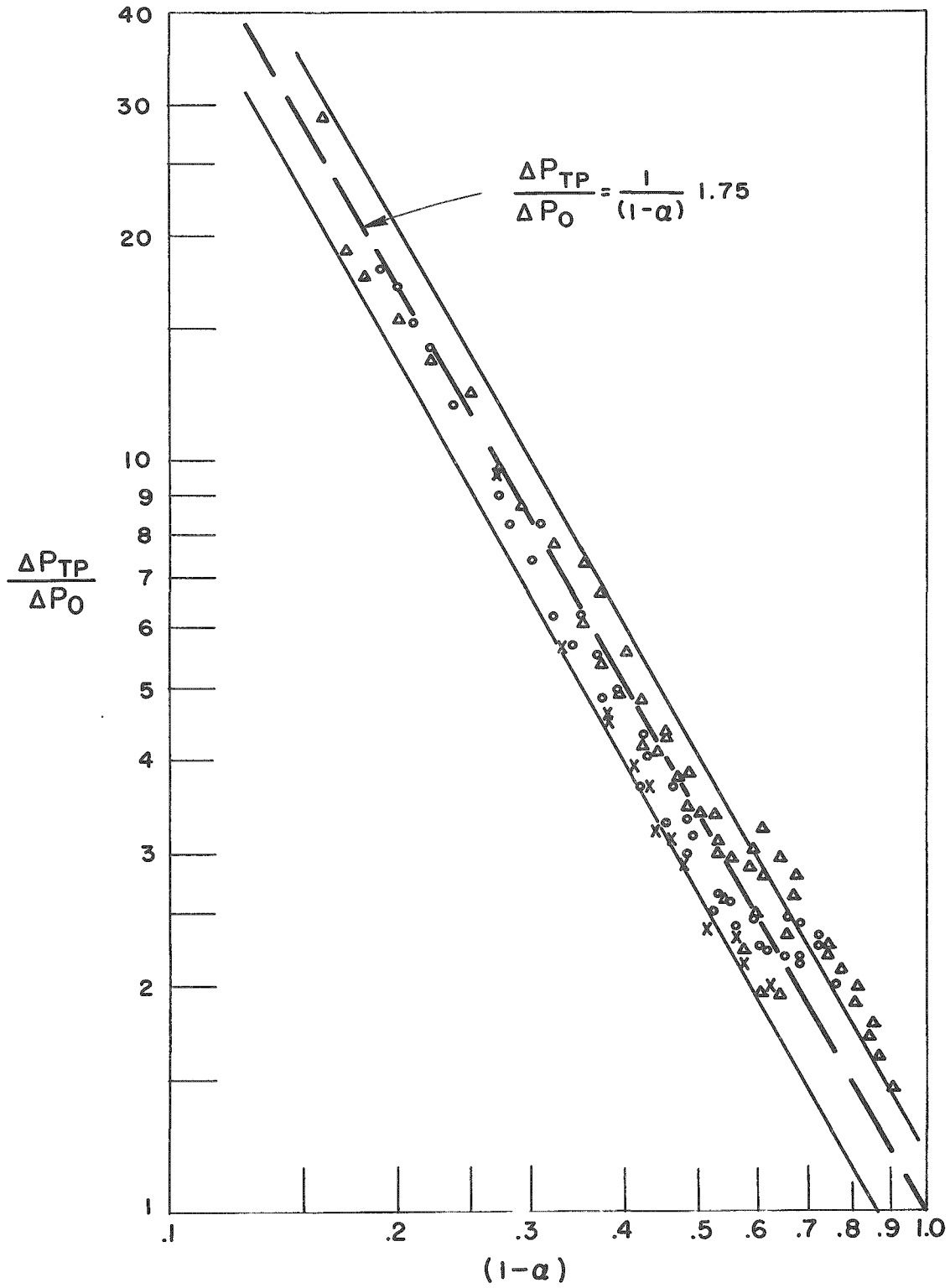
Figure 8.3 Two-Phase Pressure Drop Correlation

TABLE 8.1

TWO-PHASE PRESSURE DROP DATA
1/2 x 2-inch Section

W_ℓ #/sec	Quality	$1 - \alpha$	χ_{tt}	$\Delta P_{TP}/\Delta P_\ell$	ϕ_ℓ
2.65	0.000283	0.90	75	1.47	1.21
2.65	0.000362	0.87	61	1.61	1.27
2.65	0.000434	0.84	52	1.72	1.31
2.65	0.000517	0.81	45	1.85	1.36
2.65	0.000728	0.74	33	2.20	1.48
2.65	0.00103	0.67	24.5	2.66	1.63
2.65	0.00126	0.64	20.7	2.98	1.73
2.65	0.00145	0.60	18.2	3.24	1.80
2.65	0.00162	0.59	16.7	3.07	1.75
2.65	0.00225	0.53	12.5	3.39	1.84
1.88	0.000399	0.85	56	1.79	1.34
1.88	0.000511	0.81	45	2.00	1.41
1.88	0.000612	0.77	38.2	2.12	1.46
1.88	0.000729	0.74	33	2.29	1.51
1.88	0.00103	0.67	24.5	2.81	1.68
1.88	0.00145	0.61	18.2	2.81	1.68
1.88	0.00177	0.58	15.4	2.89	1.70
1.88	0.00204	0.55	13.6	2.96	1.72
1.88	0.00229	0.53	12.3	3.11	1.76
1.88	0.00317	0.48	9.2	3.82	1.95
1.88	0.00379	0.45	7.8	4.37	2.09
1.88	0.00441	0.42	6.8	4.83	2.20
1.18	0.000636	0.76	37	2.08	1.44
1.18	0.000814	0.72	30	2.26	1.50
1.18	0.000975	0.68	25.8	2.43	1.56
1.18	0.00116	0.65	22.3	2.35	1.53
1.18	0.00164	0.59	16.5	2.48	1.57
1.18	0.00231	0.53	12.2	3.00	1.73
1.18	0.00282	0.50	10.3	3.40	1.84
1.18	0.00325	0.47	9.0	3.77	1.94
1.18	0.00364	0.45	8.1	4.33	2.08
1.18	0.00505	0.40	6.0	5.61	2.37
1.18	0.00603	0.37	5.1	6.62	2.57
1.18	0.00703	0.35	4.5	7.30	2.70

TABLE 8.1 (Cont'd.)

W_ℓ #/sec	Quality	$1 - \alpha$	χ_{tt}	$\Delta P_{TP}/\Delta P_\ell$	ϕ_ℓ
0.61	0.00123	0.64	21	1.95	1.40
0.61	0.00157	0.60	17	1.96	1.40
0.61	0.00189	0.56	14.6	2.23	1.49
0.61	0.00225	0.54	12.6	2.59	1.61
0.61	0.00316	0.48	9.2	3.48	1.87
0.61	0.00387	0.44	7.7	4.10	2.02
0.61	0.00448	0.42	6.7	4.20	2.05
0.61	0.00546	0.39	5.6	4.91	2.22
0.61	0.00629	0.37	4.95	5.36	2.32
0.61	0.00705	0.35	4.5	6.07	2.46
0.61	0.00933	0.32	3.5	7.77	2.79
0.61	0.0117	0.29	2.87	8.66	2.94
0.61	0.0136	0.27	2.5	9.73	3.12
0.61	0.0172	0.25	2.0	12.25	3.50
0.61	0.0244	0.22	1.47	13.57	3.68
0.61	0.0300	0.20	1.22	15.45	3.93
0.61	0.0348	0.18	1.07	17.77	4.21
0.61	0.0426	0.17	0.89	19.11	4.37
0.61	0.0552	0.16	0.70	29.02	5.38

1/4 x 2-inch Section

W_ℓ #/sec	Quality	$1 - \alpha$	χ_{tt}	$\Delta P_{TP}/\Delta P_\ell$	ϕ_ℓ
0.305	0.00246	0.52	11.6	2.54	1.59
0.305	0.00317	0.48	9.2	3.0	1.73
0.305	0.00378	0.45	7.9	3.28	1.81
0.305	0.00450	0.42	6.7	3.70	1.92
0.305	0.00634	0.37	4.9	4.85	2.20
0.305	0.00776	0.34	4.1	5.64	2.37
0.305	0.00897	0.32	3.6	6.20	2.49
0.305	0.0109	0.30	3.0	7.36	2.71
0.305	0.0126	0.28	2.67	8.13	2.85
0.305	0.0141	0.27	2.4	9.0	3.00
0.305	0.0191	0.24	1.84	11.8	3.44
0.305	0.0238	0.22	1.5	14.1	3.76
0.305	0.0266	0.21	1.37	15.4	3.92
0.305	0.0296	0.20	1.24	17.0	4.12
0.305	0.0318	0.19	1.16	18.1	4.24

TABLE 8.1 (Cont'd.)

W_ℓ #/sec	Quality	$1 - \alpha$	χ_{tt}	$\Delta P_{TP}/\Delta P_\ell$	ϕ_ℓ
0.61	0.00123	0.64	21	2.14	1.47
0.61	0.00157	0.60	17	2.26	1.51
0.61	0.00189	0.56	14.6	2.41	1.55
0.61	0.00224	0.53	12.5	2.66	1.63
0.61	0.00316	0.48	9.2	3.34	1.83
0.61	0.00448	0.42	6.7	4.30	2.08
0.61	0.00546	0.39	5.6	4.90	2.22
0.61	0.00629	0.37	4.95	5.47	2.34
0.61	0.00705	0.35	4.5	6.20	2.49
0.61	0.00976	0.31	3.35	8.12	2.85
0.96	0.00078	0.72	31	2.34	1.53
0.96	0.0010	0.68	25	2.20	1.48
0.96	0.0012	0.65	21.5	2.18	1.48
0.96	0.00143	0.61	18.5	2.24	1.50
0.96	0.00201	0.55	13.8	2.59	1.61
0.96	0.00284	0.49	10.2	3.19	1.79
0.96	0.00347	0.46	8.5	3.66	1.91
0.96	0.00400	0.43	7.4	4.04	2.01
1.18	0.000634	0.76	37.5	2.02	1.42
1.18	0.000814	0.72	30	2.27	1.51
1.18	0.000975	0.68	25.7	2.43	1.56
1.18	0.00116	0.65	22.3	2.48	1.58
1.18	0.00164	0.59	16.5	2.47	1.57

1/8 x 2-inch Section

W_ℓ #/sec	Quality	$1 - \alpha$	χ_{tt}	$\Delta P_{TP}/\Delta P_\ell$	ϕ_ℓ
0.302	0.00322	0.48	9.4	2.9	1.70
0.302	0.00454	0.43	7.1	3.68	1.92
0.302	0.0064	0.38	5.2	4.54	2.13
0.302	0.0092	0.33	3.8	5.64	2.37
0.302	0.0116	0.30	3.2	7.2	2.68
0.302	0.0164	0.27	2.5	9.55	3.09
0.505	0.00192	0.57	14.8	2.14	1.46
0.505	0.00271	0.51	11.0	2.40	1.55
0.505	0.00382	0.46	8.25	3.14	1.77
0.505	0.00550	0.41	6.17	3.92	1.98
0.505	0.0066	0.38	5.4	4.52	2.12
0.64	0.00152	0.61	17.8	2.0	1.41
0.64	0.00214	0.56	13.9	2.32	1.52
0.64	0.00266	0.52	11.7	2.59	1.61
0.64	0.00434	0.44	7.7	3.23	1.80

In their work on flow in rough tubes Chisholm and Laird[14] found that relationships similar to (8.16) correlated the pressure drop data for smooth tubes and galvanized tubes, but were less successful in correlating the results for sand roughened pipes.

Chapter IX

PRESSURE CHANGE DUE TO AN ABRUPT CONTRACTION OR
EXPANSION

1. Introduction

The ability to calculate the effect of a sudden change in the
flow area on the pressure in a two-phase flow system is necessary to
make possible the prediction of the performance of such a system. To
date this problem has received no attention, although the corresponding
problem in single-phase flow has been studied extensively. The Borda-
Carnot relationship is presented in most texts on fluid mechanics. A
comprehensive treatment of this problem has been presented by London
and Kays[48] for a variety of flow channel configurations for incompressible
ible flow. The problem of a sudden expansion with compressible flow
was studied by Joyner[49] and the results are presented in tabular form
in his report.

2. Single-Phase Contraction Study

In conjunction with the two-phase pressure drop study, a series
of test runs were conducted with water only. The variation of static
pressure with position for some of these runs is presented in Fig-
ures 9.1 and 9.2. Since all channels were two-inches wide, it was
convenient to designate them by the vertical spacing. The designation
.25-C-.125, for example, indicates a contraction from 2 by 0.25 inch
channel to a 2 by 0.125 inch channel. From the pressure profiles, the
pressure drop across the contraction was determined graphically by
extrapolation to the change in cross section on the curves. Because
the compressibility of the water is negligible, the increase in the
velocity head depends only on the area ratio and is given by:

$$\Delta KE = \frac{V^2}{2g}(1 - \sigma^2) \quad , \tag{9.1}$$

where V is the velocity in the smaller section, and σ is the ratio of
the area after the contraction to the area before the contraction.
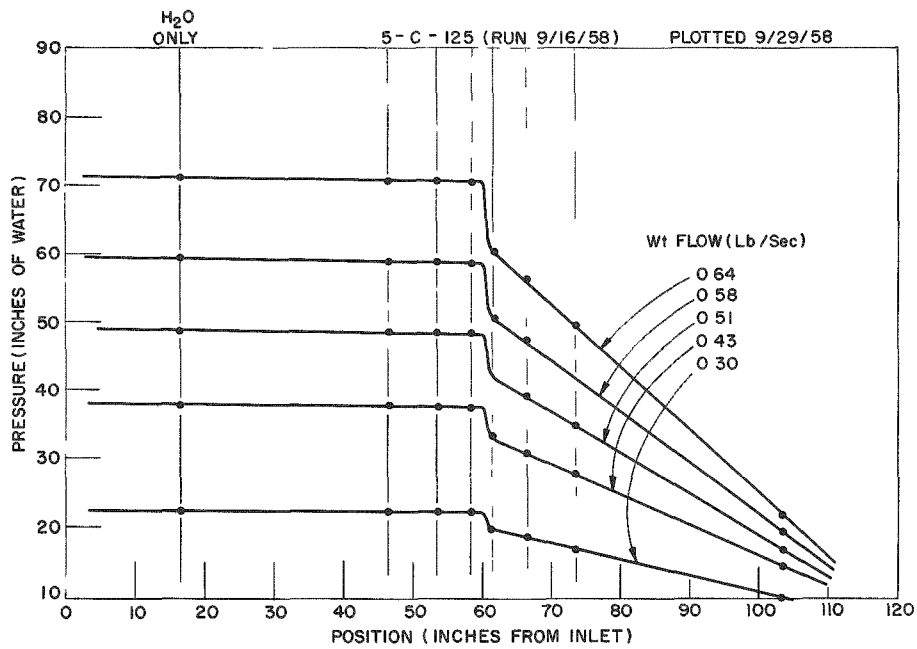
Figure 9.1 Pressure as a Function of Position
for Single-Phase Contraction with
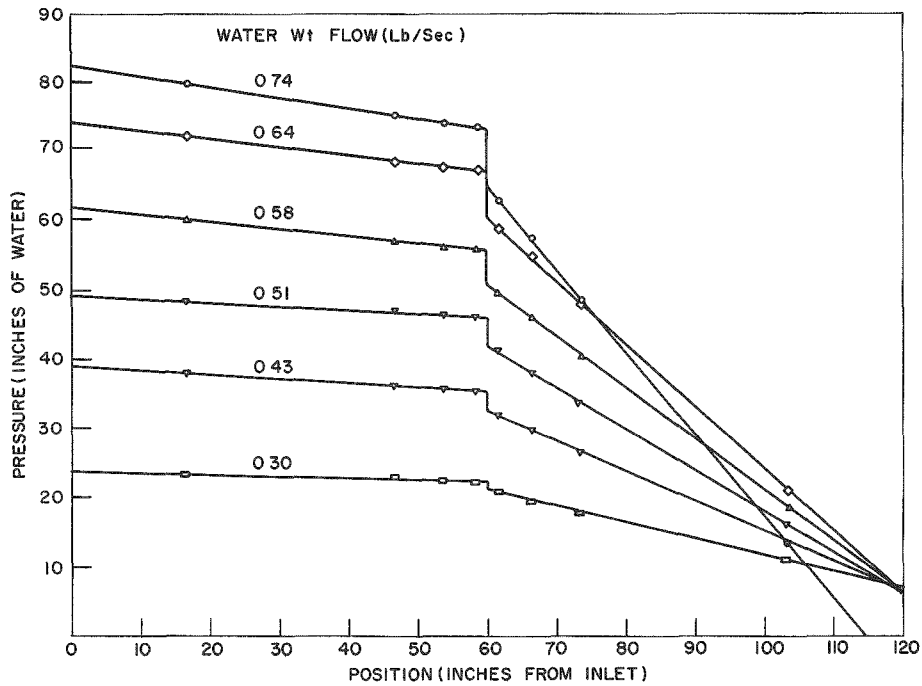Area-Ratio of One-Fourth

Figure 9.2 Pressure as a Function of Position
for Single-Phase Contraction with
an Area-Ratio of One-Half

The actual head loss is the difference between the pressure drop across the contraction and the increase in velocity head. The relationship between the pressure drop across the contraction, the change in velocity head, the head loss, and the velocity head for various channel combinations is shown in Figures 9.3 through 9.5.

The loss coefficient is defined as the ratio of the head loss to the velocity head in the small section and is therefore the slope of the curves for Δh_{loss} versus $V^2/2g$. The loss coefficients obtained from these runs were very close to those presented by Kays and London,[48] which are shown in Figure 9.6

3. Two-Phase Contraction Investigation

The effect of a sudden contraction on the pressure for the flow of two-phase mixtures was investigated for area ratios of one-half, one-fourth, and one-eighth. The pressure profile was plotted for each run and the pressure drop across the contraction was obtained, as in the case of the single phase flow. Representative pressure variations are shown in Figures 9.7 through 9.9. The pressure drop between taps 1.5 inches before and 1.5 inches after the contraction were also noted. The pressure drop between these taps is shown in terms of the combination of flow parameters, $G_w^2 x^{1/2}$, in Figures 9.10 through 9.14 for the flow combinations studied. This set of curves includes the pressure drop in the 1.5 inches preceding and following the contraction. A correction was applied to compensate for this, and the corrected curve for the pressure drop across the contraction is also shown in Figures 9.10 through 9.14. These curves are presented together in Figure 9.15. There it was seen that the effect of the variation in area ratio was small and not well defined. It was noted that the loss coefficients for single phase flow in the range of σ from 0.1 to 0.5 varies only from 0.49 to 0.40 for a Reynold's Number of 10,000 for a similar channel geometry as shown by Kays and London.[48] While there is
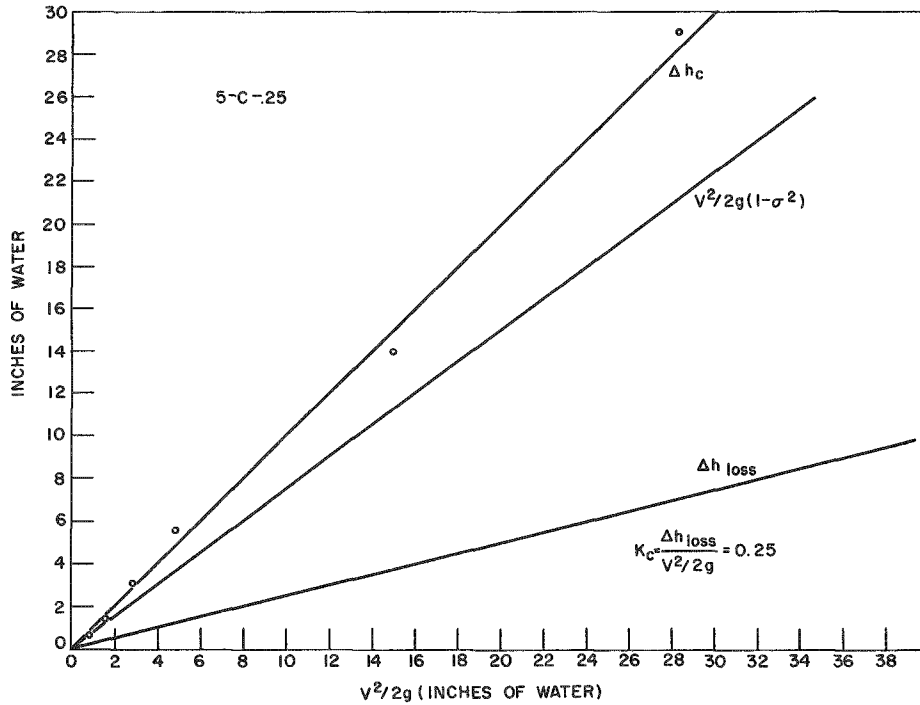
Figure 9.3 Head Loss and Loss Coefficient for One-Half
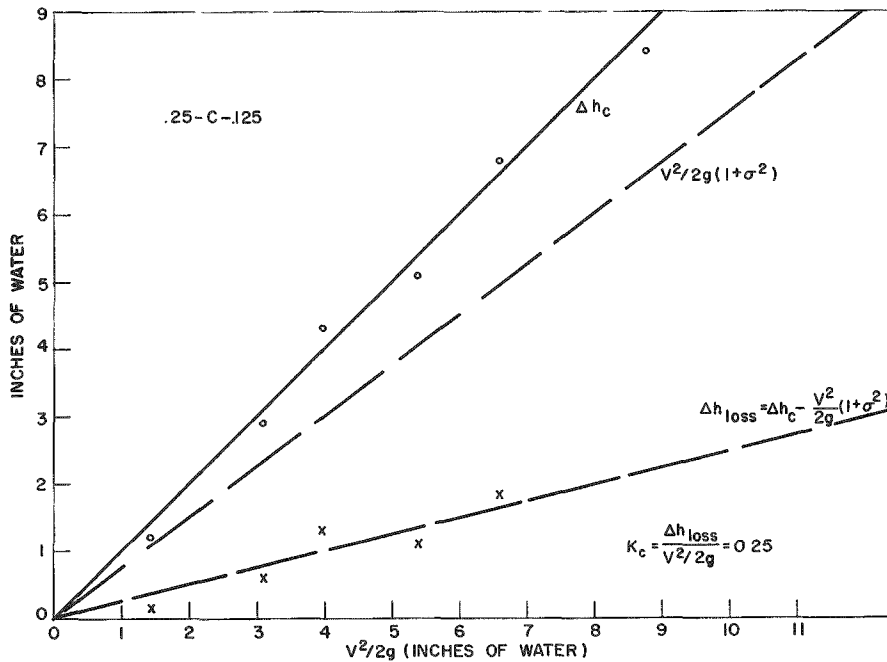to One-Fourth Contraction (Single Phase)

Figure 9.4 Head Loss and Loss Coefficient for One-Fourth
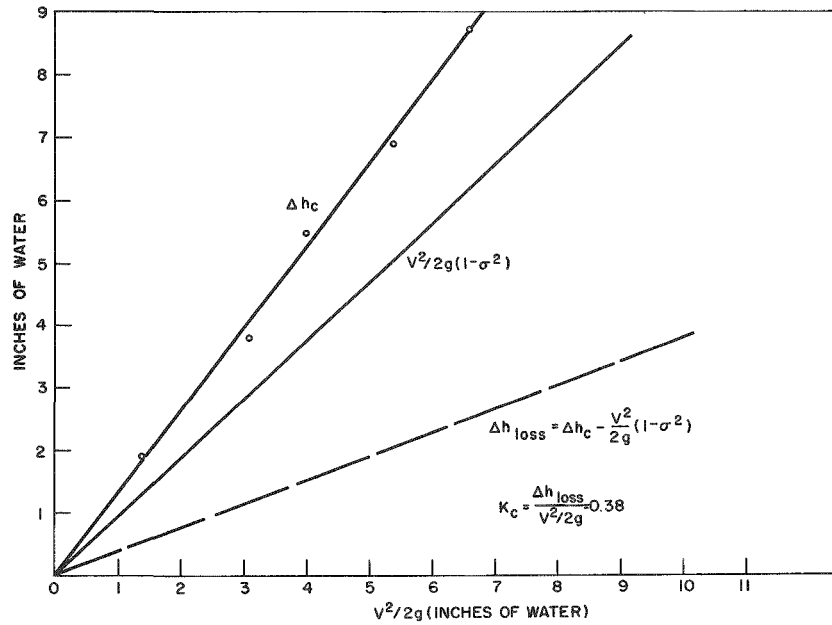to One-Eighth Contraction (Single Phase)

Figure 9.5 Head Loss and Loss Coefficient for One-Half to
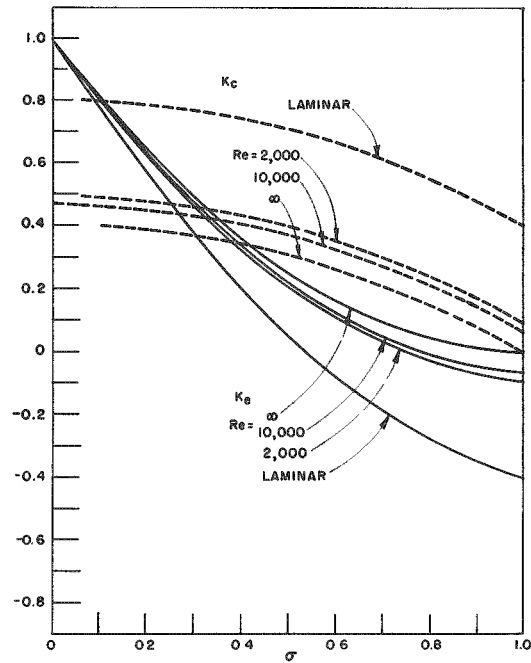One-Eighth Contraction (Single Phase)

Figure 9.6 Single Phase Loss Coefficients obtained by
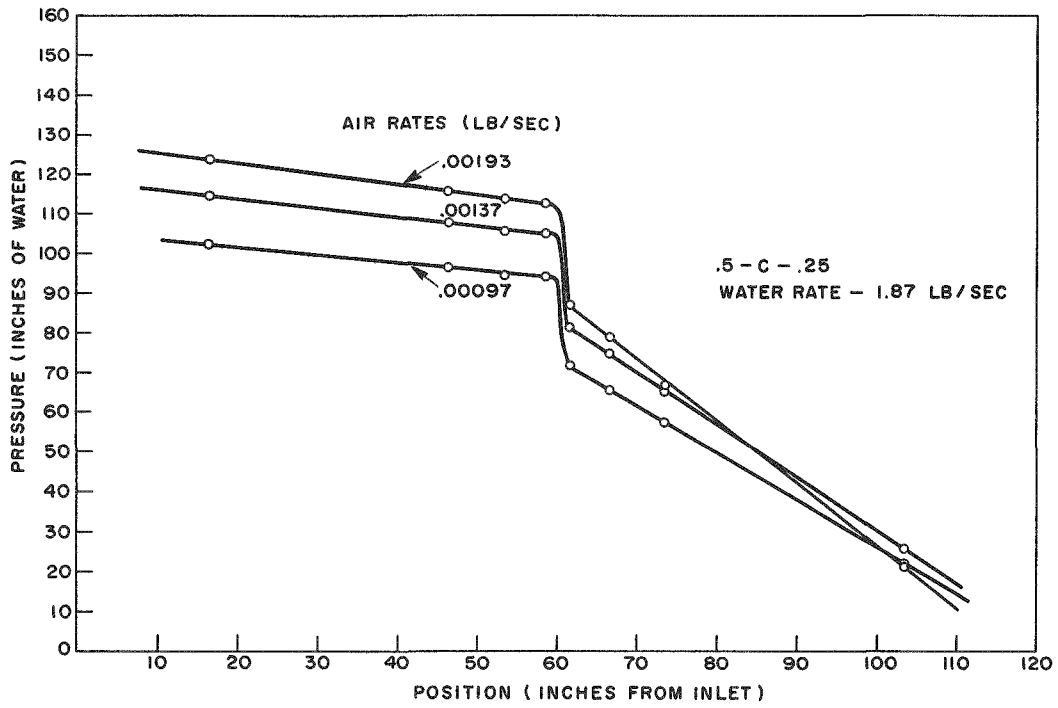Kays and London

Figure 9.7 Pressure Profile for Two-Phase Flow
Through Contraction ($\sigma = 1/2$).

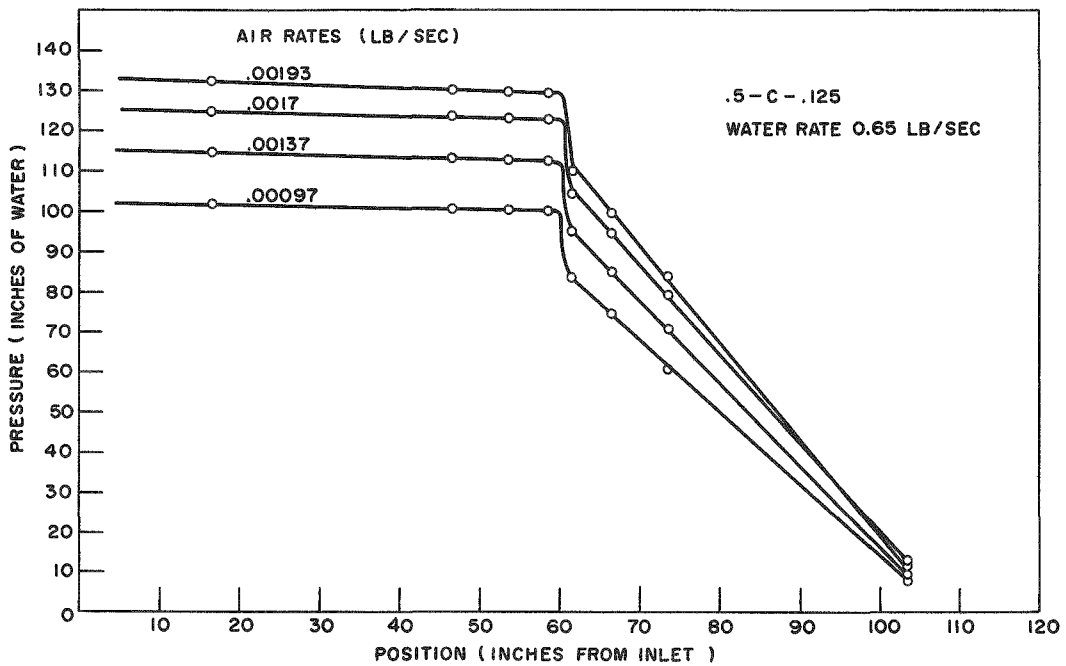Figure 9.8 Pressure Profile for Two-Phase Flow
Through Contraction ($\sigma = 1/4$)
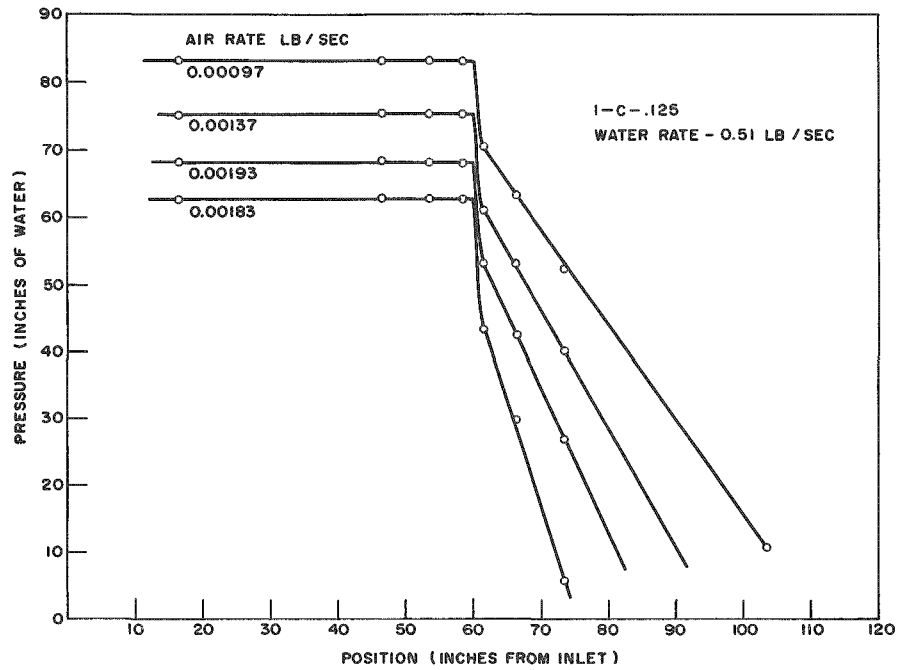
Figure 9.9   Pressure Profile for Two-Phase Flow
Through Contraction (σ = 1/8)

Figure 9.10   Correlation for Two-Phase Pressure Drop
across a Contraction (.25-C-.125)

Figure 9.11 Correlation for Two-Phase Pressure Drop
across a Contraction (.5-C-.125)

Figure 9.12 Correlation for Two-Phase Pressure Drop
(.5-C-.25)

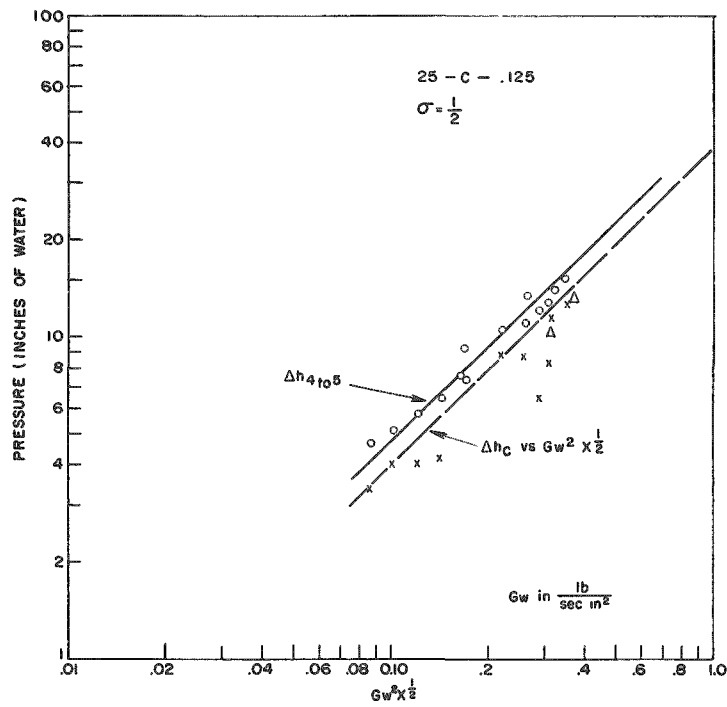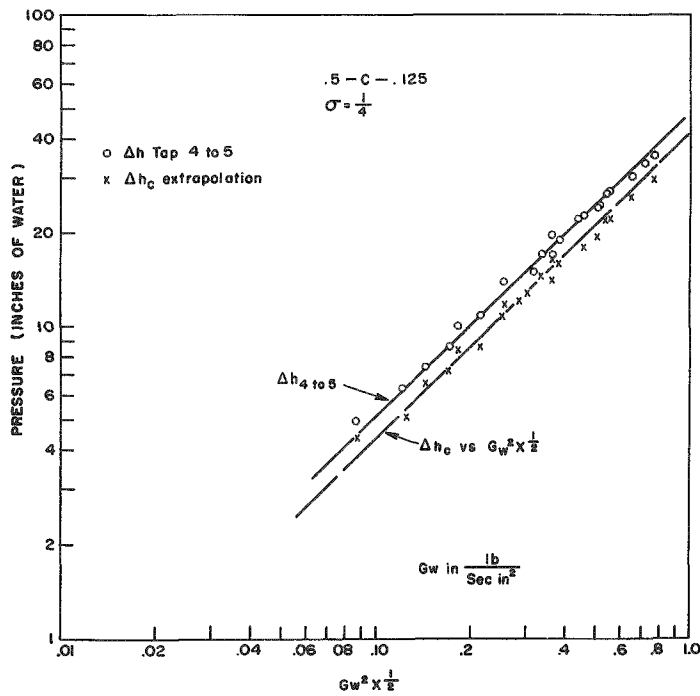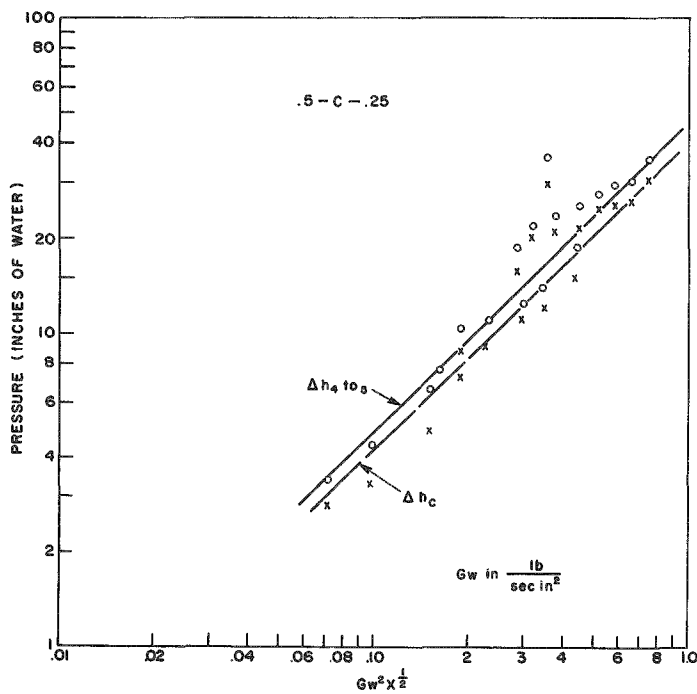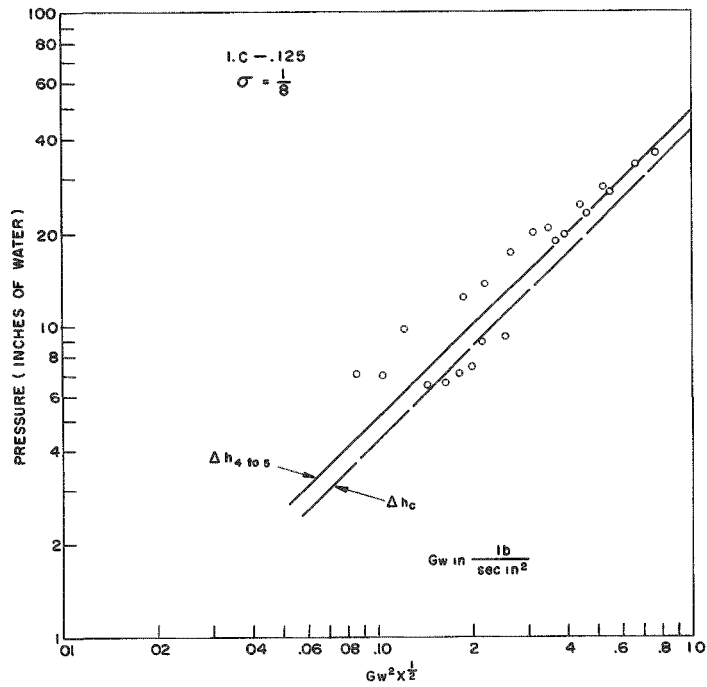Figure 9.13 Correlation for Two-Phase Pressure Drop across a Contraction (1-C-.125)
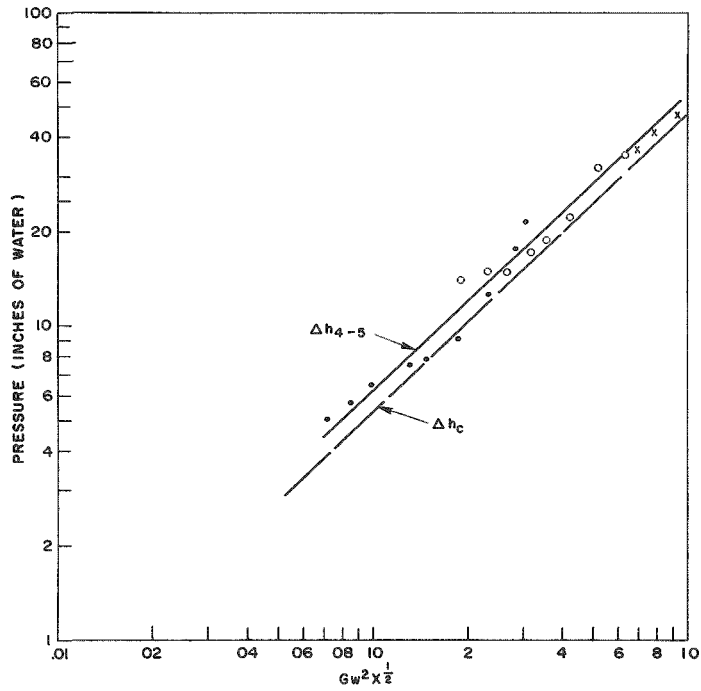

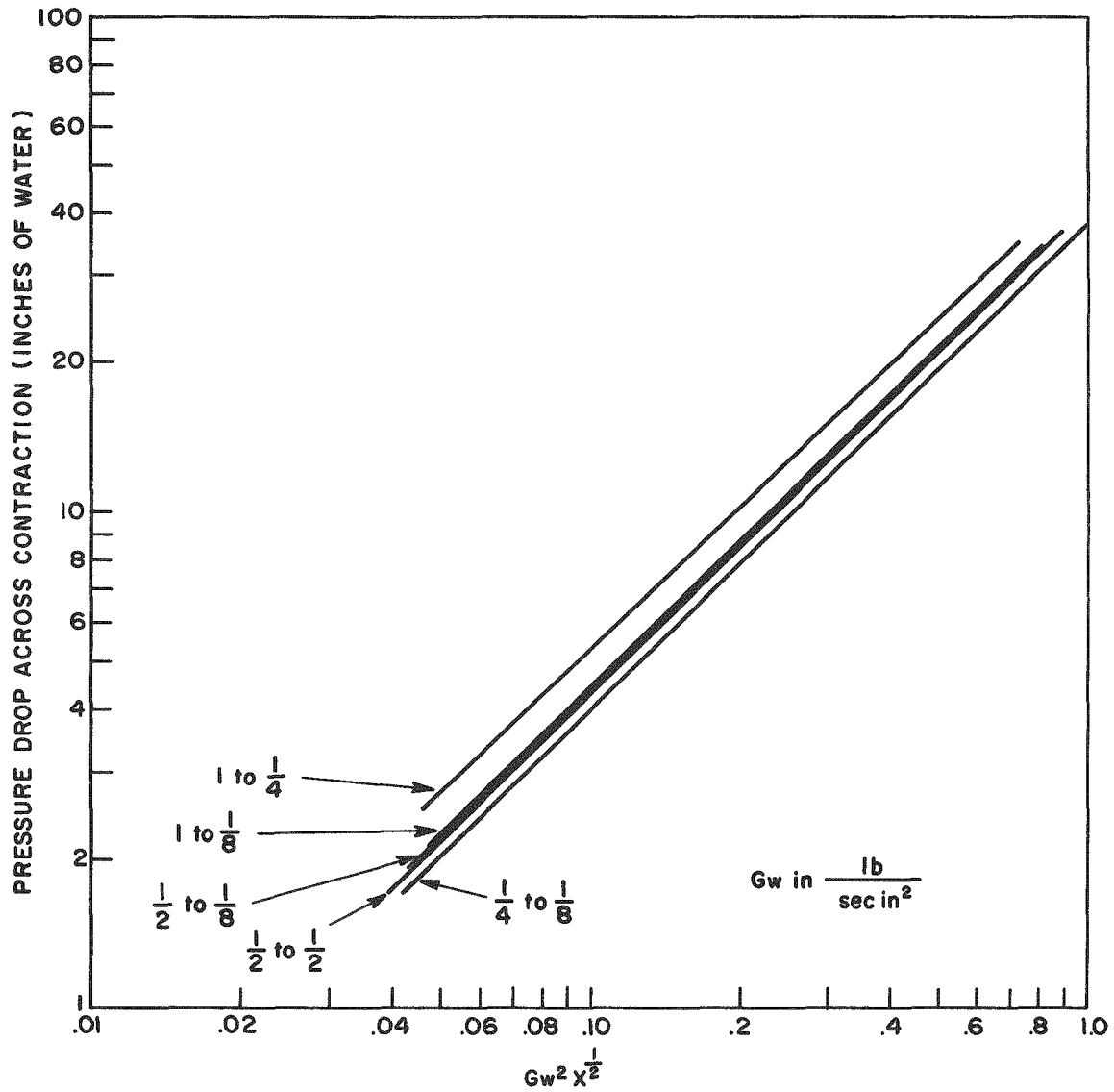Figure 9.14 Correlation for Two-Phase Pressure Drop across a Contraction (1-C-.25).

Figure 9.15   Correlation for Two-Phase Pressure Drop
across a Contraction

considerable spread in some of the data, this set of curves does present
a method for the estimation of the pressure drop across the contraction
in terms of parameters, which are usually known for most two-phase
systems.

4. Single-Phase Expansion Study

A series of test runs were made with water only for the expan-
sions. The pressure recovery was determined graphically from the
plot of pressure as a function of position. Typical plots of pressure
profiles are presented in Figures 9.16 and 9.17, for single phase flow.
As the water is incompressible the equation (9.1) may be used as before
to determine the change in kinetic energy across the expansion. The
head loss in this case is the difference between the decrease in kinetic
energy and the pressure recovery across the expansion. The loss coef-
ficient is defined as before, as the head loss divided by the velocity
head in the small section. The determination of the coefficient for chan-
nels with area ratios of $1/2$ and $1/4$ is shown in Figures 9.18 and 9.19.
The values for the single phase loss coefficients are slightly higher
than those presented by Kays and London, as shown in Figure 9.6, for
sections with an infinite aspect ratio.

5. Two-Phase Expansion Investigation

The pressure variation along the channel length following an ex-
pansion was considerably more complex for two-phase flow than that
for two-phase flow across a contraction, or for single phase flow. A
degree of separation was attained immediately after the expansion,
and for many flow rates, a stagnant air pocket was formed at the top
and bottom of the channel. These can be seen in Figures 6.21 and 6.23
and were present in a large number of the runs observed. The irregu-
larity of the pressure profile is shown in Figures 9.20 through 9.23.
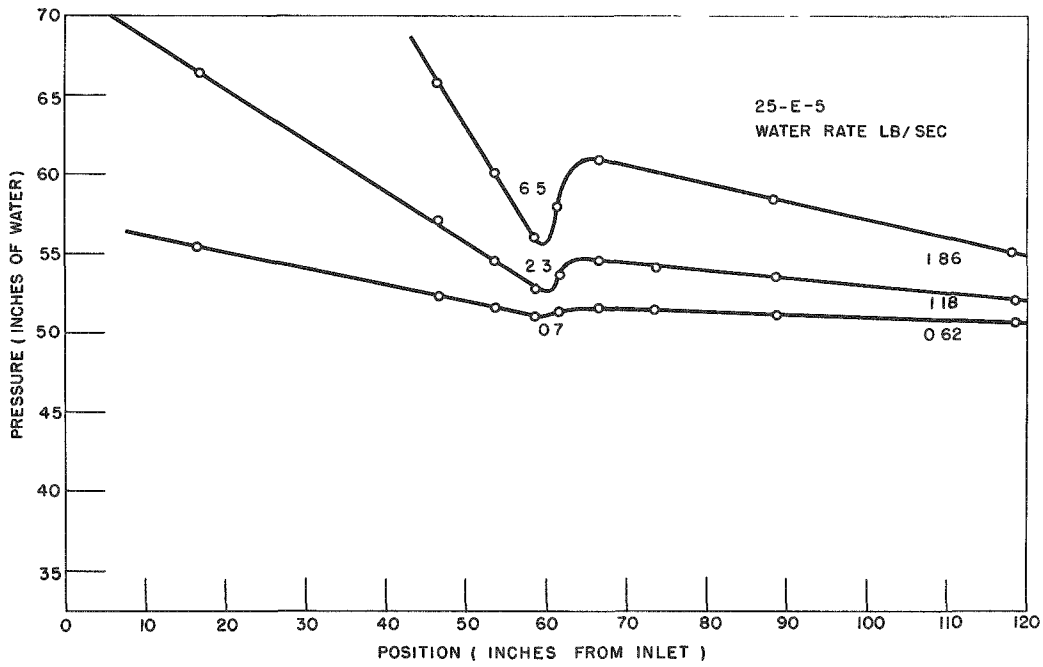
Figure 9.16 Pressure Profile for One-Fourth to One-Half
Expansion, Single Phase
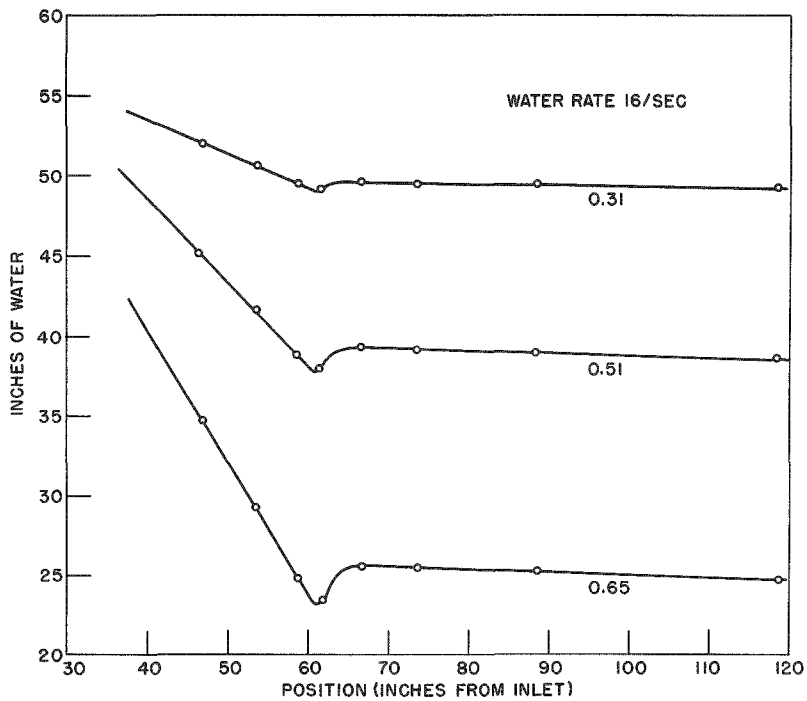
Figure 9.17 Pressure Profile for One-Eighth to
One-Half Expansion, Single Phase
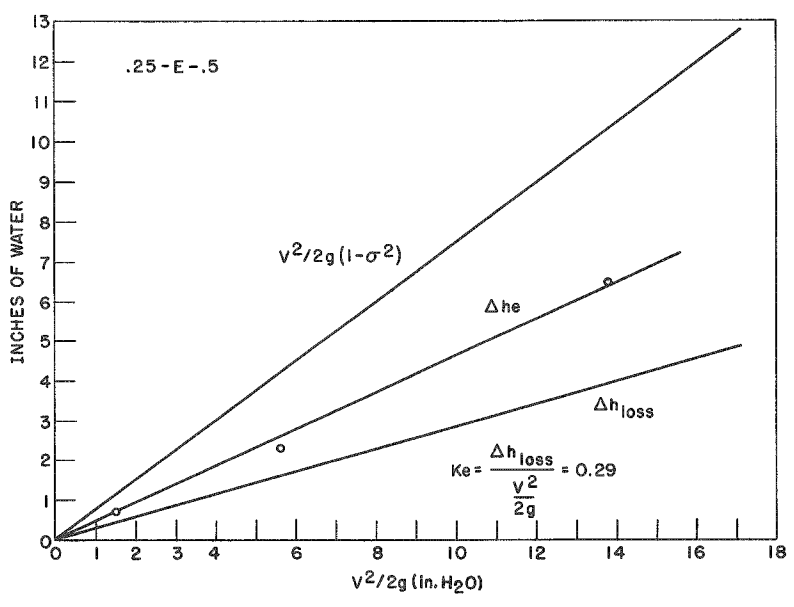
Figure 9.18 Loss Coefficient Determination for
Single-Phase Expansion, (σ = 1/2)
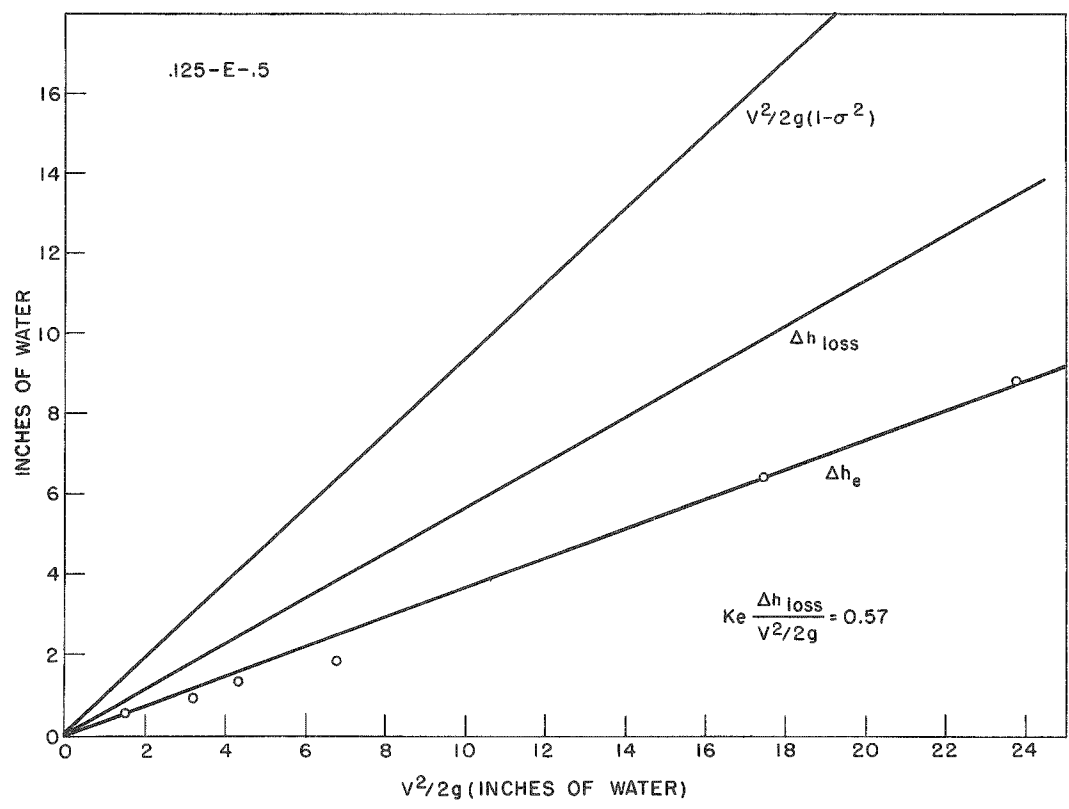
Figure 9.19 Loss Coefficient Determination for Single-Phase
Expansion, (σ = 1/4)
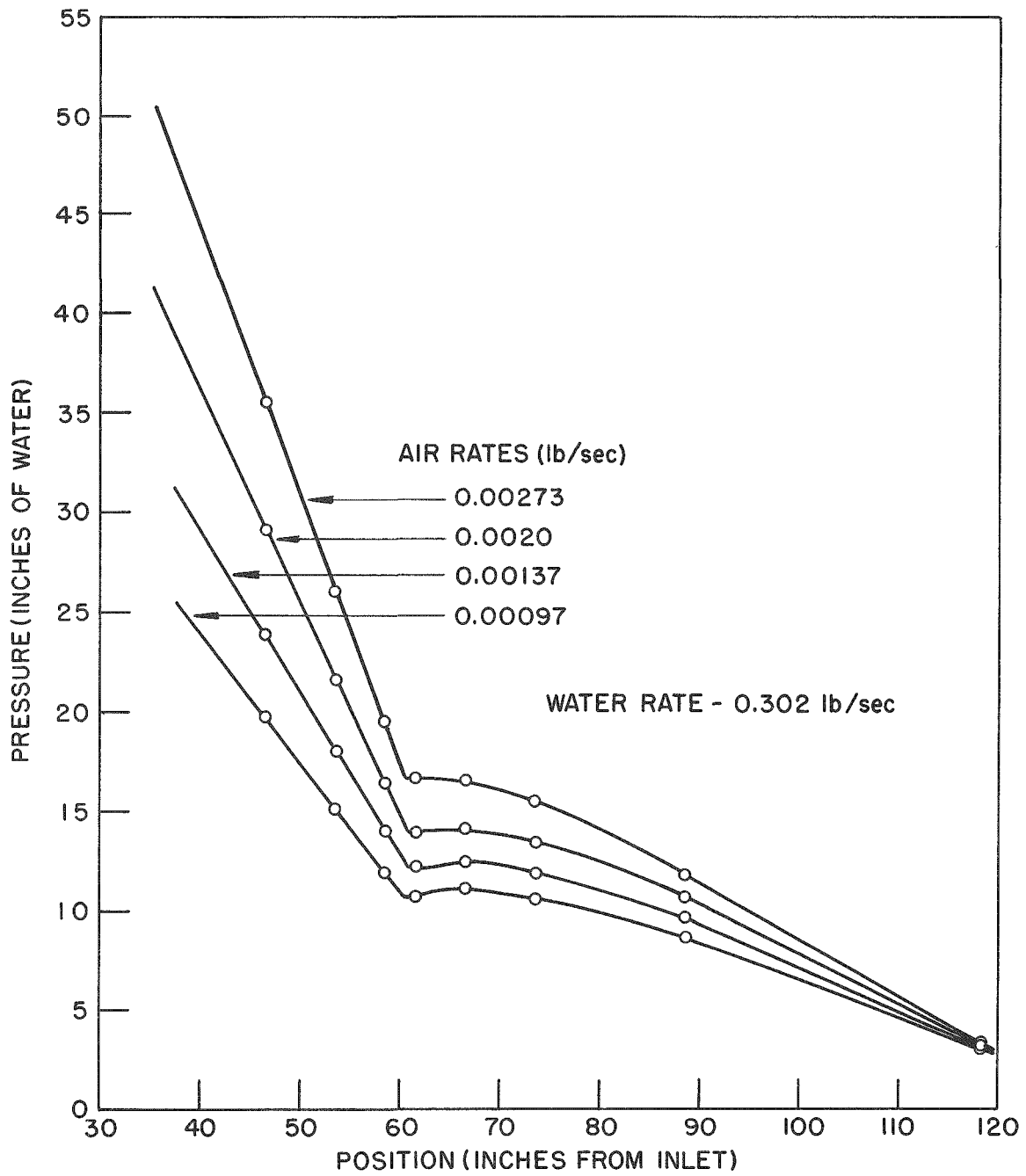
Figure 9.20 Pressure Profile for Two-Phase Expansion (.125-E-.5).
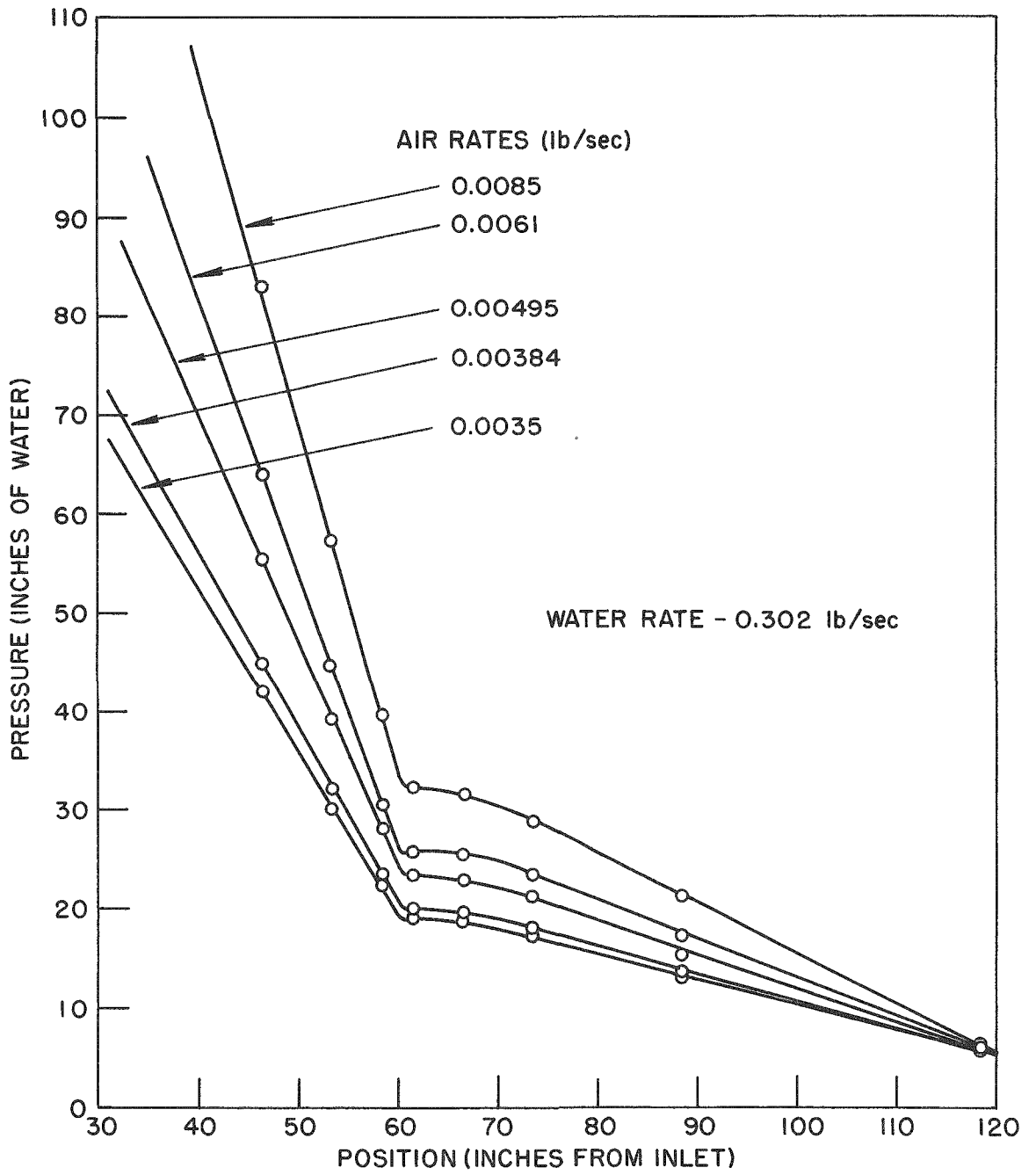
Figure 9.21 Pressure Profile for Two-Phase Expansion (.125-E-.25)

116
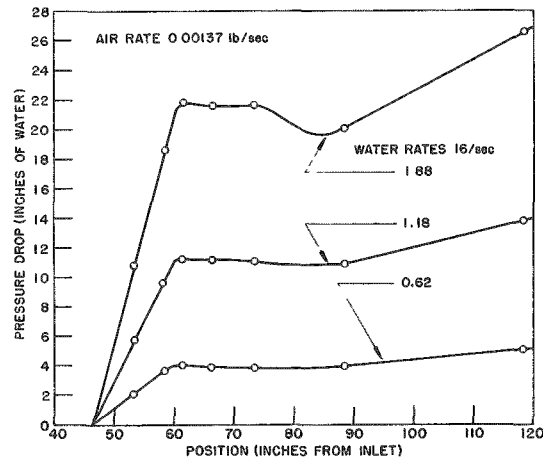
Figure 9.22 Pressure Drop vs. Position for
Two-Phase Flow (.25-E-.5)
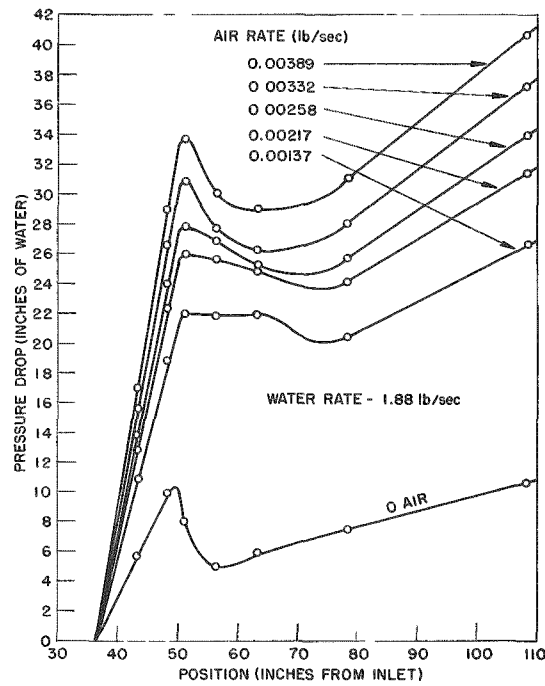
Figure 9.23 Pressure Drop vs. Position for
Two-Phase Flow (.25-E-.5)

The irregularity of the pressure with position made the accurate determination of the pressure recovery extremely difficult. The length over which this recovery takes place was not well defined. The data for the expansion into the sections with one-inch channel spacing were considered as unreliable because the appearance of the flow indicated that the recovery had not taken place in the sixty inches.

The recovery of pressure across the expansion was determined for area ratios of 1/2 and 1/4. The results are shown in Figures 9.24 and 9.25.

6. Loss Determination due to Area Change

The determination of the losses in two-phase flow was made on the basis of the fraction of the change in kinetic energy which was dissipated. The change in kinetic energy was calculated on the basis of average properties of the system:

$$\Delta KE = \rho_m \frac{(V_{2m}^2 - V_{1m}^2)}{2g} \tag{9.2}$$

The mean density was approximated by

$$\rho_m = (1-\alpha)\, \rho_\ell \tag{9.3}$$

On the basis of continuity the velocity was defined by

$$\rho_m V_m\, A = \left(\frac{1}{1-x}\right) \rho_\ell\, V_\ell\, (1-\alpha)\, A \tag{9.4}$$

Using (9.3), equation (9.4) becomes:

$$(1-\alpha)\, \rho_\ell V_m\, A = \frac{\rho_\ell\, V_\ell}{(1-x)}\, (1-\alpha)\, A \tag{9.5}$$

Thus for the atmospheric pressure system studied, where the quality was small in comparison with one, the liquid velocity was approximately the mean velocity. From this, the kinetic energy change was determined by substituting into (9.2), yielding

$$\Delta KE = \frac{\rho_\ell\, (1-\alpha)}{2g} \left(V_{\ell_2}^2 - V_{\ell_1}^2\right) \tag{9.6}$$

118

Figure 9.24 Pressure Recovery for Two-Phase
Expansion (.125-E-.5)
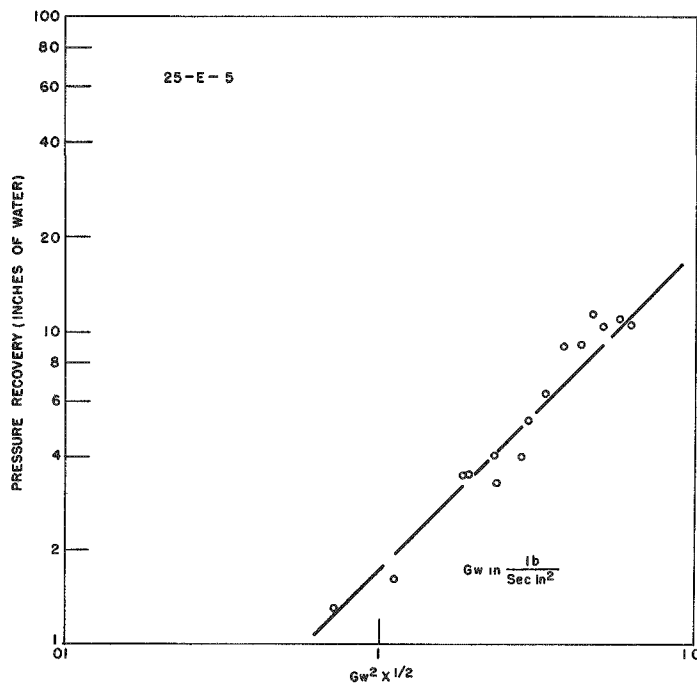
Figure 9.25 Pressure Recovery for Two-Phase Expansion
(.25-E-.5)

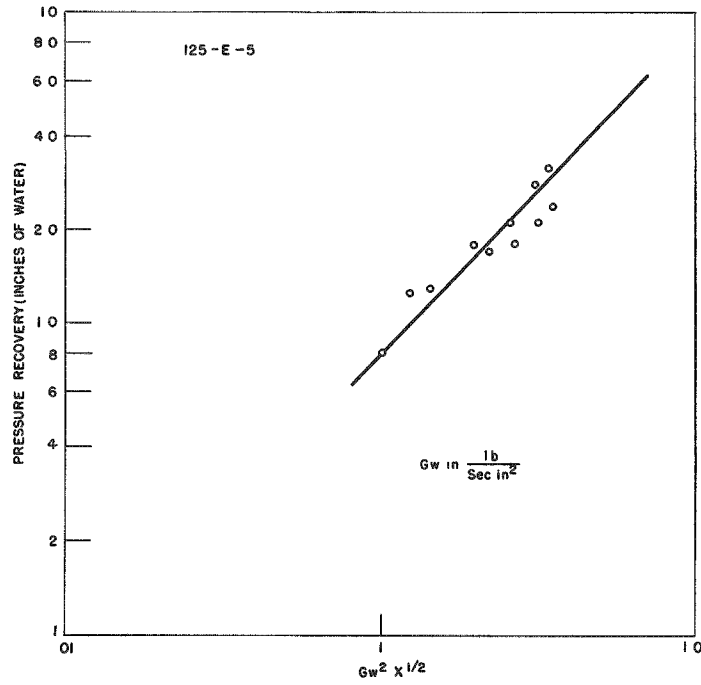This relationship was used in computing the change in kinetic energy for the expansion and contraction runs, and the results are shown in Figure 9.26 plotted against $G_w^2 \, x^{1/2}$.

The change in kinetic energy for the contractions is shown in Figure 9.27 with the line representing the pressure drop across a contraction from Figure 9.15. From Figure 9.27 is seen that the losses, which are the difference between the pressure drop and the increase in kinetic energy, are approximately 20% for the range of variables studied. This is considerably less than the losses in single phase flow where the losses are double this value in the same range of area ratios.

In the analysis of losses due to a contraction in single phase flow, the losses are assumed to be primarily due to the expansion from a "vena contracta" which is formed after the contraction. The examination of the two-phase flow, as is shown in Figures 6.24, 6.25, and 6.26, does not show any well defined "vena contracta" effect. This may account for the lower losses in two-phase flow contractions.

The pressure recovery data for an expansion in two-phase flow are shown in Figure 9.28 where they are compared with the corresponding changes in kinetic energy. The losses in this case are the difference between the kinetic energy change and the pressure recovery. Here the losses are seen to depend strongly on the area-ratio, as is the case in single-phase flow. In Figure 9.29 the ratio of the pressure recovery to the area ratio is compared with the change in kinetic energy. This figure indicates that the fraction of the kinetic energy recovered is equal to the area ratio, σ. Correspondingly, the loss coefficient, defined as the fraction of the change of kinetic energy lost, is equal to $(1-\sigma)$ for the area ratios studied.

Figure 9.26 Kinetic Energy Change Due to an
Abrupt Change in Cross Section
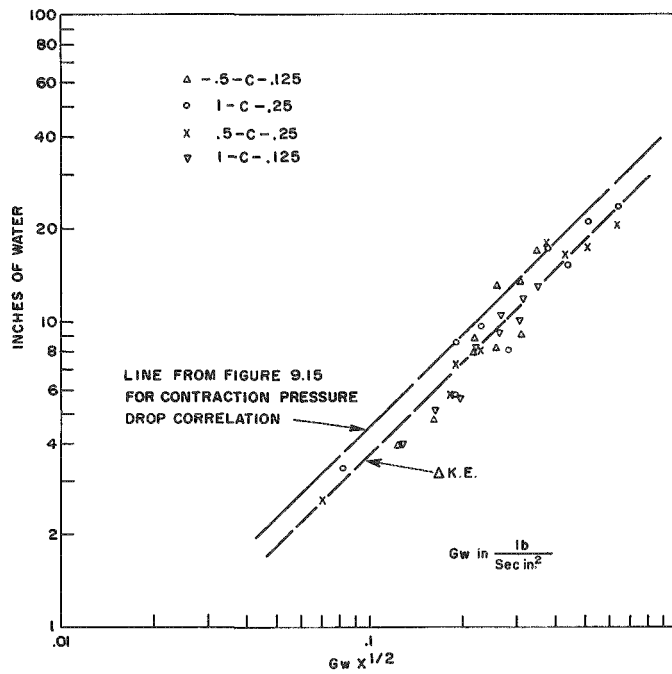
Figure 9.27 Kinetic Energy Increase for Two-Phase
Contractions Compared with Contraction
Pressure Drop
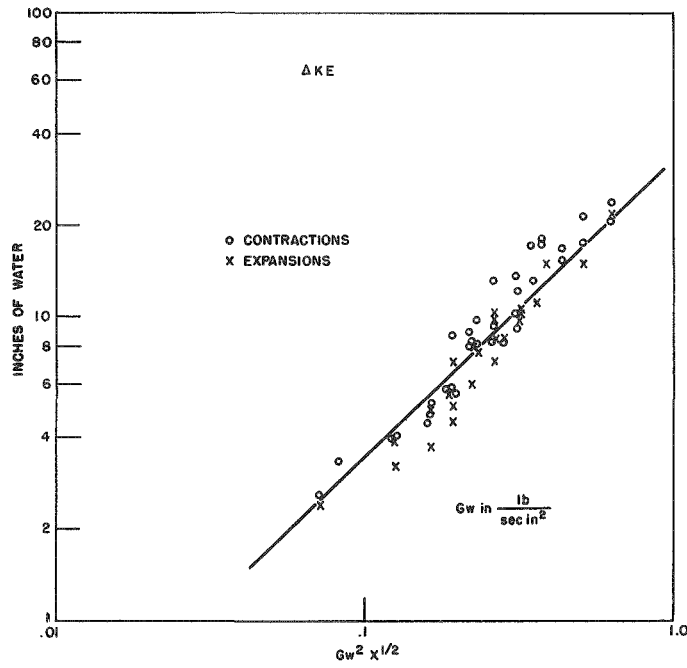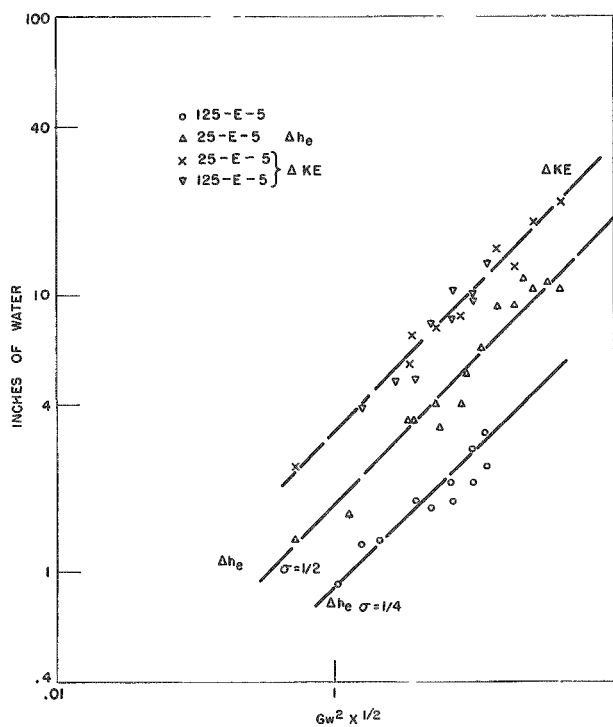
Figure 9.28 Comparison of Pressure Recovery with
Loss of Kinetic Energy for a Two-Phase
Expansion
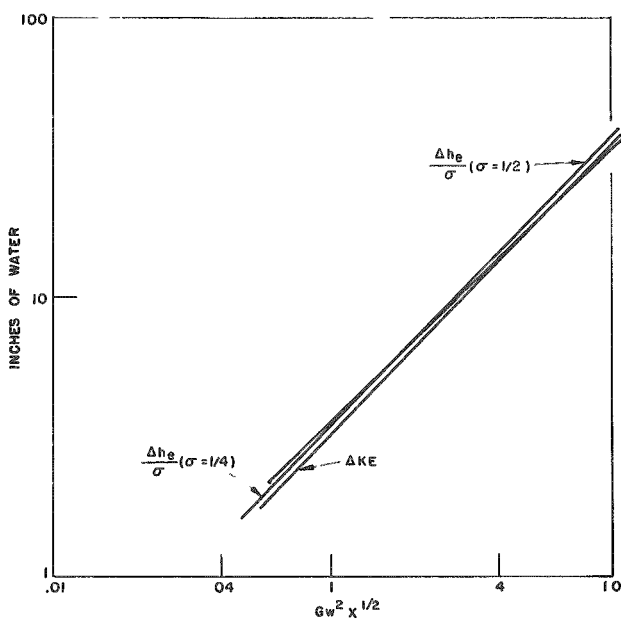
Figure 9.29 Comparison of Change in Kinetic Energy
with the Ratio of the Pressure Recovery
to the Area-Ratio for Two-Phase Expansions

Chapter X
RESULTS AND CONCLUSIONS

1. Summary of Results

The results of the individual phases of this investigation are presented in the following listing.

 a. Mockup Evaluation of Gamma-Ray Attenuation Void Measuring Techniques.

The lucite mockup results shows that the attenuation techniques can be used to obtain dependable values for the volume fraction of each phase. The traversing technique is less sensitive to errors due to preferential void distributions, such as annular flow than the "one-shot" method. The traversing technique also permits the investigation of the void distribution over the cross section.

 b. Flow Pattern Study.

The flow pattern regions were mapped in terms of the weight flow of each phase for three aspect ratios. These flow pattern correlations are in general agreement with those presented in the literature, as was noted in Chapter V.

 c. Vapor Volume Fraction Investigation.

The traversing technique with a gamma-ray source-detector system was used to study the void fraction in the case of uniform sections, expansions and contractions for a variety of combinations of flows and geometry. The void fraction correlation for the uniform sections was applicable to both the expansion and contraction data. A correlation was also presented to permit calculation of the effect of a sudden expansion on the void fraction in the region of the expansion.

 d. Slip Ratio Results

The ratio of the gas velocity to the liquid velocity was calculated for the test runs where void data were available. It was found that the data were correlated by the equation

$$S = 37 \, x^{1/2} \tag{7.6}$$

The slip data were obtained from uniform sections, as well as expansions and contractions.

e.   Two-Phase Pressure Drops

The data for two-phase pressure drops are presented in terms of the Lockhart-Martinelli correlation and are seen to fall slightly higher than the curve which Lockhart and Martinelli propose. An expression is derived, based on the assumption that the increase in pressure drop for two-phase flows is primarily due to the increased velocity of the liquid phase. It was found that the equation

$$\frac{\left(\frac{\Delta P}{\Delta \ell}\right)_{TP}}{\left(\frac{\Delta P}{\Delta \ell}\right)_{\ell}} = \left(\frac{1}{1-\alpha}\right)^{1.75} \tag{8.16}$$

would correlate the data to within $\pm 20\%$ over most of the range studied.

f.   Pressure Drops due to an Abrupt Change in Area

The pressure drop across a contraction in both single-phase and two-phase flow was studied. The results of tests runs with water gave results which compare well with those in the literature. The two-phase pressure drops were compared with the change in kinetic energy due to the contraction. The energy losses are approximately 20% of the change in kinetic energy in the range of area ratios studied, and are not strongly dependent on the area ratio.

The pressure recovery across an expansion was studied for both single-phase and two-phase flows. The single phase loss coefficients are slightly higher than those presented in the literature for rectangular sections with an infinite aspect ratio. The two-phase pressure recovery was compared to the changes in kinetic energy due to the area change. It was found that the fraction of the kinetic energy recovered was proportional to the area-ratio. The per cent of the kinetic energy change which is lost is therefore one minus the area-ratio.

2. Conclusions

In this study correlations have been presented which will enable the designer to predict the effect of an abrupt change in flow area on the behavior of a horizontal, two-phase, two-component flow system. The relationships between the flow parameters and the local volume fraction has been established, and compared with the results obtained by other investigators for the mean volume fraction.

A method for estimating the energy loss due to a sudden area change has been presented. This correlation shows that large errors may result from predicting these losses on the basis of single phase studies.

The large pressure drops associated with two-phase flow are shown to depend on the increase in the velocity of the liquid phase, due to the decrease in the liquid flow area. It is shown that effect of the increased liquid velocity on the "friction factor" for the liquid phase is also significant. A relationship which predicts the ratio of two-phase to single-phase pressure drops is derived, based on the effects just mentioned. This relationship is supported by the experimental data.

The flow pattern regions were mapped in terms of the weight flow rate of each phase. It was shown that the aspect ratio of the rectangular channels was also a significant parameter in the consideration of flow patterns.

For the horizontal flows it was shown that the slip ratio is a function of the quality of the two-phase mixture. The validity of an analysis based on a "homogeneous" flow model will therefore also depend on the quality.

The utility of the void measuring technique has been shown, through a study making use of lucite mockups of the flow patterns. The distribution of each phase over the cross section of the channel has also been studied.

The flow pattern study made it necessary to use transparent test sections, and therefore the test sections were constructed of lucite. This limited the pressure in the test section, so that all of the tests were conducted essentially at atmospheric pressure. An extensive study is needed to determine the effect of pressure on the correlations presented in this report. The extension of this study to include higher pressures would probably improve some of the correlations because the effects of pressure drops on the density of the vapor phase would be much less significant. It is hoped that the results and correlations obtained from this investigation will indicate an approach to be followed in future studies.

BIBLIOGRAPHY

1. Rateau, A., "Experimental Researches on the Flow of Steam through Nozzles and Orifices to which is added a Note on the Flow of Hot Water," A. Constable and Co., Ltd., London, 1905.

2. Benjamin, M. W., and Miller, J. G.,"The Flow of Saturated Water through Throttling Orifices," Trans. Am. Soc. Mech. Engrs. Vol. 63, 419, 1941.

3. McAdams, W. H., Woods, W. K., and Heroman, L. C., Jr., "Vaporization inside Horizontal Tubes - II - Benzene-Oil Mixtures," Trans. Am. Soc. Mech. Engrs., Vol. 64, 193, 1942.

4. Martinelli, R. C., Boelter, L. M. K., Taylor, T. H. M., Thomsen, E. G., and Morrin, E. H., "Isothermal Pressure Drop for Two-Phase Two-Component Flow in a Horizontal Pipe," Trans. Am. Soc. Mech. Engrs., Vol. 66, 139, 1944.

5. Martinelli, R. C., Putnam, J. A., and Lockhart, R. W., "Two-Phase, Two-Component Flow in the Viscous Region," Trans. Am. Inst. Chem. Engrs., Vol. 42, 681, 1946.

6. Lockhart, R. W. and Martinelli, R. C., "Proposed Correlation of Data for Isothermal Two-Phase, Two-Component Flow in Pipes," Chem. Engr. Progress, Vol. 45, 39, 1949.

7. Martinelli, R. C. and Nelson, D. B., "Prediction of Pressure Drop during Forced Circulation Boiling of Water," Trans. Am. Soc. Mech. Engrs., Vol. 70, 695, 1948.

8. Johnson, H. A., and Abou-Sabe, A. H. A., "Heat Transfer and Pressure Drop for Turbulent Flow of Air-Water Mixtures in a Horizontal Pipe," Trans. Am. Soc. Mech. Engrs. Vol. 74, 977-987, 1952.

9. Alves, G. E., "Co-Current Liquid Gas Flow in a Pipe-Line Contactor," Chem. Eng. Progress, Vol. 50, 449, 1954.

10. Bergelin, O. P. and Gazely, C., Jr., "Co-Current Gas-Liquid Flow - I - Flow in Horizontal Tubes," Heat Transfer and Fluid Mechanics Institute, Berkeley, California Meeting (published by ASME), 5-18, 1949.

11. Gazely, C., Jr., "Co-Current Gas-Liquid Flow - III - Interfacial Shear and Stability," Heat Transfer and Fluid Mechanics Institute, Berkeley, California Meeting (published by ASME), 29, 1949.

12. Levy, S., "Theory of Pressure Drop and Heat Transfer for Two-Phase Two-Component Annular Flow in Pipes," Ohio State University. Engr. Exp. Station Bull. No. 149, Proceedings of the Second Midwestern Conference on Fluid Mechanics, 337, 1952.

13. Linning, D. L., "The Adiabatic Flow of Evaporating Fluids in Pipes of Uniform Bore," Inst. Mech. Engrs., London Proceedings B., Vol. IB, No. 2, 1952.

14. Chisholm, D., and Laird, A. D. K., "Two-Phase Flow in Rough Tubes," ASME Paper No. 57-SA-11.

15. Petrick, M. P., "Two-Phase Air-Water Flow Phenomena," ANL-5787. (1958).

16. Isbin, H. S., Moen, R. H., and Mosher, D. R., "Two-Phase Pressure Drops," AECU 2994, 1954.

17. Masnovi, Reno; "Literature Survey of Two-Phase Fluid Flow," WAPD-TH-360, (1958).

18. Griffith, P., Clark, J. A., and Rohsenow, W. M., "Void Volumes in Subcooled Boiling Systems," Office of Naval Research, N5 ori-07894-TR-12 (1958).

19. McManus, H. N., Jr., "An Experimental Investigation of Film Characteristics in Horizontal Annular Two-Phase Flow," ASME Paper No. 57-A-144, (1957).

20. Isbin, H. S., Sher, N. C., Eddy, K. C., "Void Fractions in Two-Phase steam-Water Flow," Journal A.I.Ch.E. (March 1957).

21. Egen, R. A., Dingee, D. A., and Chastain, J. W., "Vapor Formation and Behavior in Boiling Heat Transfer," BMI-1163.

22. Cook, W. H., "Boiling Density in Vertical Rectangular Multichannel Sections with Natural Circulation," ANL-5621, (1956).

23. Untermyer, S., "Portable Thulium X-Ray Unit," Nucleonics, Vol 12, No. 5 (May 1954).

24. Hooker, H. H., and Popper, G. F., "A Gamma-Ray Attenuation Method for Void Fraction Determination in Steam-Water Mixtures," ANL-5766 (1958).

25. Richardson, M. and Kitzes, A. S., "Evaluation of Gamma-Ray Attenuation Techniques for Measuring the Density and Homogeneity of Thorium Oxide Slurries Circulating at 300° C," CF-57-10-61, 1957.

26. Berman, A. I. and Harris, J. N., Rev. Sci.Inst. 25, 21, (1954).

27. Grace, H. P., and Lapple, C. E., "Discharge Coefficients of Small - Diameter Orifices and Flow Nozzles," Trans. Am. Soc. Mech. Engrs., July 1951.

28. Schneider, F. N., White, P. D., and Huntington, R. L., "Some Aspects of Two-Phase Fluid Flow Through Pipelines," presented at Fall Meeting of Petr. Branch, Am. Inst. Mining and Met. Engrs., Dallas, Texas, Oct. 19-21, 1953.

29. Kosterim, S. I., "An Investigation of the Influence of the Diameter and the Attitude of a Pipe on the Hydraulic Resistances and on the Structure of Flow of a Gas-Liquid Mixture," Izvestiia - Akademiia Nauk SSSR - Otdelenie Teknicheskie Nauk, 1864, July-Dec. 1949.

30. Fried, L., "Pressure Drop and Heat Transfer for Two-Phase Two-Component Flow," Chem. Eng. Progress Symposium Series No. 9, Vol. 5, Heat Transfer - Research Studies for 1954 published by Am. Inst. Chem. Engrs., 47, 1954.

31. Krasiakova, L. I., "Some Characteristic Flows of a Two-Phase Mixture in a Horizontal Pipe, "Zhurnal Technicheskoi Fiziki, Vol. 22, No. 4, 656, 1952.

32. Baker, O., "Design of Pipelines for the Simultaneous Flow of Oil and Gas," The Oil and Gas Journal, July 26, 1954.

33. Jenkins, R., "Two-Phase Two-Component Flow of Air and Water," M.S. Thesis, Univ. of Delaware, 1947.

34. Galegar, W. C., Stovall, W. B., and Huntington, R. L., "More Data on Two-Phase Vertical Flow," Petroleum Refiner, Vol. 33, No. 11, 208-211, 1954.

35. Reichart, H. L., Jr., "The Flow of Fluids in Two Phases through a Horizontal Pipe," B.S. Thesis, Mass. Inst. Tech. 1934.

36. Frazier, A. W., "Pressure Drop in Two-Phase Fluid Flow," B.S. Thesis, Carnegie Inst. of Tech. 1942.

37. Thomsen, E. G., "Pressure Drop Accompanying Two-Component Flow in a Closed Conduit with Various Liquids and Air," M.S. Thesis, Univ. of California (1941).

38. Taylor, T. H. M., "Pressure Drop Accompanying Isothermal Two-Component, Two-Phase Flow in a Horizontal Glass Pipe," M.S. Thesis, Univ. of California (1942).

39. Lockhart, R. W., "Isothermal Pressure Drop for Two-Phase, Two-Component, Viscous - Viscous Flow in a Tube at Various Angles to the Horizontal," M.S. Thesis, Univ. of California (1945).

40. Lockhart, R. W., "An Analysis of Isothermal Two-Phase, Two-Component Flow Data," Mech. Eng. Thesis, Univ. of California (1946).

41. McElwee, F. D., "Behavior of Two-Phase, Two-Component Flow in Tubes," M.S. Thesis, Univ. of California (1947).

42. Dengler, C. E., "Heat Transfer and Pressure Drop for Evaporation of Water in a Vertical Tube," Ph.D. Thesis, Mass. Inst. Tech. (1952).

43. Isbin, H. S., Sher, N. C., and Eccy, K. C., "Void Fractions in Two-Phase Steam-Water Flow," A.l.Ch.E. Journal, Vol. 3, No. 1 (1957).

44. Marchaterre, J. F., "Effect of Pressure on Boiling Density in Multiple Rectangular Channels," ANL-5522.

45. Hoopes, W. H., "Flow of Steam-Water Mixtures in a Heated Annulus and through Orifices," Am. Inst. Chem. Engrs. Journal, Vol. 3, No. 2 (1957).

46. Behringer, P., "Velocity in Rise of Steam Bubbles in Boiler Tubes," Verein Deutscher Inginieure, Forschungsheft 365 B, 4, 1934.

47. Lottes, P. A. and Flinn, W. S., "A Method of Analysis of Natural Circulation Boiling Systems," Nuclear Science and Engineering, Vol. I, No. 6, 1956.

48. Kays, W. M. and London, A. L., "Compact Heat Exchangers," The National Press, Palo Alto, California, 1955.

49. Joyner, Upshur T., "Charts of Pressure, Density and Temperature Changes at an Abrupt Increase in Cross-Sectional Area of Flow of Compressible Air" N.A.C.A. A.R.R. No. L4L19.